PROBABILISTIC SEISMIC DEMAND ASSESSMENT OF STEEL FRAMES WITH SHAPE MEMORY ALLOY CONNECTIONS

A Dissertation
Presented to
The Academic Faculty

By

BERK TAFTALI

In Partial Fulfillment
Of the Requirements for the Degree
Doctor of Philosophy in Civil Engineering

Georgia Institute of Technology

August, 2007

PROBABILISTIC SEISMIC DEMAND ASSESSMENT OF STEEL FRAMES WITH SHAPE MEMORY ALLOY CONNECTIONS

Approved by:

Dr. Bruce R. Ellingwood, Co-Advisor
School of Civil and Environmental Engineering
Georgia Institute of Technology

Dr. Reginald DesRoches, Co-Advisor
School of Civil and Environmental Engineering
Georgia Institute of Technology

Dr. Roberto T. Leon
School of Civil and Environmental Engineering
Georgia Institute of Technology

Dr. Donald W. White
School of Civil and Environmental Engineering
Georgia Institute of Technology

Dr. Steven P. French
College of Architecture
Georgia Institute of Technology

Date Approved: July 3, 2007

To my family, present and future...

ACKNOWLEDGEMENTS

Finally, the single unedited part of my thesis... It appears in the first pages, but it was the last to be written, and as always, in the last minute. It is meant to acknowledge all these wonderful people who made it possible for me to reach to the end of this journey.

So where do I start? I think it is in order for me to say that I will always be indebted to Dr. Erhan Karaesmen, who was instrumental in me getting accepted to Columbia University's masters program in engineering mechanics. My stubbornness on applying only to masters programs almost cost me the chance to study at the US if it was not for his strong recommendation letters and last minute e-mails. You cannot blame me, though. I was young, naive, and afraid of commitment. Nothing much changed in the past years, except that I am not that young any more. Also, my gratitude goes to all my professors at M.E.T.U, who provided me with an excellent background so that I would not struggle in my graduate level classes as much as I did through my undergraduate years.

Dr. Hilmi Lus, whom I met at Columbia, is the reason I got interested in earthquake engineering at the first place. He not only thought me my first class in structural dynamics, but also became my main source of advice, both on academics and life in the Big Apple. My gratitude goes to him for helping me without even knowing me. He was not very pleased when I decided to leave Columbia for Georgia Tech, and after all these years, I cannot stop wondering how my life would be had I stayed at Columbia.

Then came my Atlanta years... Dr. Reginald DesRoches, whom I like to express my deepest gratitude, is the reason I came to Georgia Tech. He encouraged me to send my application even though it was a month past the deadline, somehow got it accepted by the department, and offered me the chance to work with him. During my four year tenure at Georgia Tech (and even at the last two years that I was at the sunshine state), he always supported me in every way possible. If I ever decide to go into academia, he will be the model I would follow when dealing with my students.

I was so excited when I got the e-mail from Dr. DesRoches telling me that I got accepted, I did not pay attention to the last sentence: “By the way, you will be co-advised by Dr. Bruce Ellingwood”. Almost six years passed, and each passing day I realize how lucky I was to have the chance to work with Dr. Ellingwood. I came to admire his wealth of knowledge, professionalism and dedication for excellence. His enthusiasm for research was contagious, it was simply too difficult for me to resist. Dr. DesRoches, Dr. Ellingwood, I will never be able to pay you back for all you did for me. This dissertation would have not been possible without your guidance and support.

I would also like to express my thanks to Dr. Robert Morris, whom I work under now for Computers and Structures. His support and encouragement during the last couple of months made it possible for me to complete this dissertation. I am grateful for the members of my reading committee, Dr. Roberto Leon, Dr. Donald White, and Dr. Stephen French, who spent time to revise this document, and made it look even better. Your comments were extremely helpful and constructive.

During my time at Atlanta, I made several very good friends that I know I will keep through the rest of my life. My thanks go to my office mate Dr. Ozan Cem Celik whose meticulous approach to classes and research partially rubbed on me and made my life easier on the long run. Soon to be Dr. Ahmet Citipitioglu, whom I spent countless hours procrastinating at the coffee house or talking about latest gadgets, also deserves to be acknowledged here for showing me there is more to life than to study. Dr. Ozgur Kurc not only always managed to find time for my questions on anything and everything, but also got me my first real job. I cherish all the discussions we had with Dr. Kursat Kinali, from modeling of connections to politics and soccer, and of course, girls. Special thanks are in order to soon to be Dr. Murat Eroz. Without him helping me, I would not have kept my sanity during the week of my defense. Even the pages you are reading now are submitted by him. My friends, I now realize that the only times I enjoyed myself at hot and humid Atlanta were when I was with you. I hope that our paths will cross again, hopefully not too far in the future...

Finally, a couple words to my family. Mom, dad, thanks for being patient with me. You have always supported me, unconditionally, from thousands of miles away. I can only hope to be a son that you can be proud of. A special thank you goes to Ms. Ayse Asli Sonmez, whom has never stopped believing in me even at times I stopped believing in myself. For all the times you have told me “Go get’em, Tiger”, I guess I finally did...

TABLE OF CONTENTS

LIST OF TABLES

LIST OF FIGURES

LIST OF ABBREVIATIONS

A^f	Austenite finish temperature.
AISC	American Institute of Steel Construction.
A^s	Austenite start temperature.
ATC	Applied Technology Council.
BS	Base shear.
CDF	Cumulative distribution function.
CEN	Comite Europeen de Normalisation.
CJP	Complete joint penetration.
CR	Connection rotation.
CUREE	California Universities for Research in Earthquake Engineering.
DM	Demand measure.
FEMA	Federal Emergency Management Agency.
FR	Fully restrained.
FS	Full-strength.
g	Gravitational acceleration.
CBO	International Conference of Building Officials.
ICC	International Code Counsil.
IDA	Incremental dynamic analysis.
IM	Intensity measure.
ISDA	Inter-story drift angle.
LFRS	Lateral force resisting system.
LS	Limit state.

MAF	Mean annual frequency.
MANSIDE	Memory Alloys for New Seismic Isolation and Energy Dissipation Devices.
M^f	Martensite finish temperature.
M^s	Martensite start temperature.
NHE	Normalized hysteretic energy.
NIST	National Institute of Standards and Technology.
Ni-Ti	Nickel-Titanium.
NiTiNOL	Nickel Titanium Naval Ordnance Laboratory.
N-S	North-South.
NSPA	Nonlinear static pushover analysis.
NTHA	Nonlinear time history analysis.
OMF	Ordinary moment frame.
OpenSees	Open System for Earthquake Engineering Simulation.
PBE	Performance-based engineering.
PGA	Peak ground acceleration.
PR	Partially restrained.
PS	Partial-strength.
PSDA	Probabilistic seismic demand analysis.
RBS	Reduced beam section.
R_c	Hardness of the Rockwell C scale.
rCR	Residual connection rotation.
RDA	Roof drift angle.
rISDA	Residual inter-story drift angle.
R_w	Force reduction factor.
S_a	Spectral acceleration.

SAC	Partnership of the Structural Engineers Association of California (SEAOC), the Applied Technology Council (ATC), and the California Universities for Research in Earthquake Engineering (CUREE).
SCWB	Strong column weak beam.
SEAOC	Structural Engineers Association of California.
SMA	Shape memory alloy.
SMRF	Steel moment resisting frame.
UBC	Uniform Building Code.
USGS	United States Geological Survey.
WSMF	Welded steel moment frame.

SUMMARY

Shape Memory Alloys (SMAs) exhibit the ability to undergo large deformations but can recover permanent strains via heating (shape memory effect) or when stress is removed (superelastic effect). This study evaluates the comparative seismic performance of steel moment resisting frames (SMRFs) with innovative beam-to-column connections that use SMA bars as connecting elements.

The performance evaluation studies are based on two types of SMA beam-to-column connections: (1) superelastic SMA connections with recentering capability; (2) martensitic SMA connections with high energy dissipation capacity. Fiber models for these SMA connections are implemented in the OpenSees finite element framework, and are verified against data from full-scale experimental tests that were performed on a prototype SMA connection in previous research at Georgia Tech. Three- and nine-story model buildings with partially restrained (PR) moment frames are selected from the SAC Phase II Project as case studies. Nonlinear time history analyses on these model buildings, with and without SMA connections, are conducted using suites of ground acceleration records from the SAC Phase II project that represent different seismic hazard levels. The effects of SMA connections on peak and residual inter-story drift angles, connection rotations, and normalized dissipated hysteretic energy demands and the sensitivity of the demand measures to variations in SMA connection design are quantified.

The seismic demands on the model buildings with conventional PR and selected SMA connections are evaluated in a probabilistic framework. The resulting seismic demand

relationships are used to assess the effectiveness of the SMA connections in enhancing the building performance over a range of demand levels. The results of this performance evaluation show that the SMA connections are most effective in controlling structural response under high levels of seismic intensity leading to large deformation demands. In particular, the energy dissipating SMA connections are effective in reducing maximum deformation demands, while the recentering SMA connections are more suitable for controlling residual deformations in the structure.

CHAPTER 1

INTRODUCTION

1.1. Motivation

Prior to the Northridge, California earthquake of January 17, 1994, fully restrained (FR) welded steel moment frames (WSMFs) were thought to be a superior seismic lateral force resisting system (LFRS). Following the extensive damage to the connections of WSMFs observed following the Northridge earthquake, this superiority came into question (FEMA, 1995; Maison and Bonowitz, 1999). The Federal Emergency Management Agency (FEMA) formed the SAC Joint Venture of the Structural Engineers Association of California (SEAOC), the Applied Technology Council (ATC), and California Universities for Research in Earthquake Engineering (CUREE). The goal of Phase I of the SAC Steel Project was to perform studies on the seismic performance of steel moment resisting frame buildings (SMRFs) and to develop recommendations for their design, repair and retrofit. Experimental and analytical work continued in Phase II of the project, with the ultimate goal of developing reliable seismic design criteria for SMRFs.

Modern earthquake-resistant design is based on the principle that a structural system must possess sufficient strength, ductility and energy absorption capabilities to adequately dissipate the energy of rare earthquakes by means of inelastic mechanisms without becoming unstable under gravity effects. Many pre-Northridge FR welded connection details were found to be susceptible to brittle failure (Maison et al., 1996), violating this principle. Subsequent analyses of ductile SMRF structures designed by pre-Northridge codes revealed that their performance was likely to be unacceptable for rare

seismic events (Gupta and Krawinkler, 1999; 2000a). As a result, numerous alternative connection details have been proposed in recent years for the design and retrofit of SMRFs in areas of moderate to high seismicity. Some of the proposed moment connection details were designed to avoid weld fracture by concentrating inelastic deformation in the beams away from the welds (Chen et al., 1996; 1997; 2001; Civjan et al., 2001). Properly detailed partially restrained (PR) connections were also considered as an alternative to FR moment-resistant connections, which are difficult and expensive to construct. As a part of the SAC Steel Project, the performance of various types of bolted PR connections also was investigated. Although the bolted connections were found to be a viable alternative to FR connections, attributes such as low initial rotational stiffness and pinched hysteresis behavior tempered their performance (Swanson and Leon, 2000).

Current design philosophy (FEMA, 2000f; ICC, 2003) allows damage under strong earthquakes, but requires the structure to be ductile enough to sustain large plastic deformations without collapse. Passive control methods such as seismic base isolation and energy dissipation reduce or eliminate plastic deformations by promoting favorable behavior of special devices added to the structural system. Current passive control technologies have their own limitations, such as problems related to aging and durability (e.g. rubber components), maintenance (e.g. devices based on fluid viscosity), installation and/or replacement after strong events (e.g. devices based on steel yielding), and variable performance depending on temperature (e.g. polymer-based devices). The increasingly demanding performance requirements have led to the development of innovative devices utilizing new materials.

Shape memory alloys (SMAs) are a class of alloys that show the potential to eliminate many of the limitations associated with current passive control technologies. SMAs have the ability to undergo large strains (~6-8%) while recovering their initial configuration at the end of the deformation process, with minimal residual deformation. This is achieved by means of a solid-to-solid phase transformation, which can be either stress or temperature induced. Their successful integration in a steel connection offers a PR, partial-strength (PS) connection with stable hysteresis, high hysteretic damping, good ductility, and the possibility of re-centering capability (Ocel et al., 2004).

Structural codes and design guidelines in the United States are moving towards adoption of performance-based design approaches (Ellingwood, 1998; Hamburger, 1998). Performance-based engineering (PBE) includes the concept that designs should be capable of satisfying various performance objectives, under a spectrum of design ground motions ranging from minor to severe. The “performance level” is defined as the acceptable level of damage, and the condition that the performance level not be exceeded for a specific earthquake hazard is termed a “performance objective”. Within this context, the prediction of seismic performance of a structure is affected by a large number of complicating factors. Furthermore, due to inherent randomness in ground shaking, lack of knowledge in the precise definition of the structure’s characteristics, and inability to model the actual behavior accurately, estimation of seismic performance entails significant uncertainty.

One way of depicting such uncertainties in performance of existing and new structures is utilization of probabilistic seismic demand relationships of SMRFs. A properly constructed probabilistic seismic demand curve offers a concise way to summarize the uncertainties

in performance across a range of ground motion characteristics and intensity levels. This dissertation presents the results of a probabilistic seismic demand assessment of steel frames with PR connections utilizing SMAs.

1.2. Objectives and Scope

The objective of this dissertation is to evaluate the performance of frames with PR connections utilizing SMAs using a probabilistic framework. To achieve this objective, the following tasks are performed:

- Develop a connection model that can represent the hysteretic moment-rotation behavior of a SMA connection accurately, and implement that model into a nonlinear dynamic finite element platform in such a way that it will promote parametric studies and provide guidance for future research.

- Quantify the effects of SMA connections on selected demand measures and examine the sensitivity of these demand measures to variations in SMA connection design for several steel frames subjected to earthquake records representing different levels of seismic hazard.

- Develop probabilistic seismic demand relationships to quantify the benefits of SMA connections on reducing seismic demands while accounting for the uncertainties in performance across a range of intensity levels.

1.3. Organization and Outline

This dissertation is composed of seven chapters, an appendix and a list of references at the end. The present chapter has provided the motivation and laid out the objectives and the scope of the proposed research. A broad review and critical assessment of state-of-the-art for the behavior and modeling of steel beam-to-column connections and SMRFs, and performance assessment of steel structures are provided in Chapter 2. SMAs as

connection elements are also introduced in Chapter 2, along with a review on their cyclic properties and applications in the field of seismic protection of structures. In Chapter 3, a description of the two PR frames that are investigated as case studies and the ground acceleration records utilized for evaluation of seismic demands are identified. Two passive control systems that utilize SMA connections that are implemented in these structures and the basic design philosophy behind the selection of these systems are presented.

A thorough description of the analytical modeling approach is given in Chapter 4. The implementation of a material model for SMAs, a moment-rotation response model for degrading PR connections, and a fiber connection model for SMA connections are presented. The details of necessary extensions to the finite element platform used, OpenSees, are deferred to Appendix A. Also in this chapter are the description of the finite element models developed for the two PR frames and the assumptions made in modeling of individual components and the seismic loads. In Chapter 5, the effects of SMA connections on selected demand measures are quantified deterministically for the two PR frames subjected to earthquake records representing different levels of seismic hazard. The sensitivities of the demand statistics to variations in SMA connection design and PR connection failures are also presented. Chapter 6 presents a probabilistic seismic demand analysis (PSDA), which summarizes the uncertainties in frame performance across a range of seismic intensity levels concisely and quantifies the benefits of SMA connections in reducing seismic demands. Finally, the main conclusions of this dissertation and suggestions for future research are presented in Chapter 7.

CHAPTER 2

REVIEW AND CRITICAL ASSESSMENT OF THE STATE OF THE ART

2.1. Cyclic Behavior and Modeling of Steel Beam-to-Column Connections

Steel beam-to-column connections can be classified by three main characteristics that can be obtained from the moment-rotation curve: stiffness, strength, and ductility. Considering stiffness, connections are classified as fully restrained (FR), partially restrained (PR), or simple (pinned). Considering strength, connections are classified as either full-strength (FS) or partial-strength (PS), depending on whether they are capable of transferring the full plastic moment of the beams. Finally, considering the plastic deformation capacity, connections are classified as brittle or ductile (Swanson and Leon, 2000).

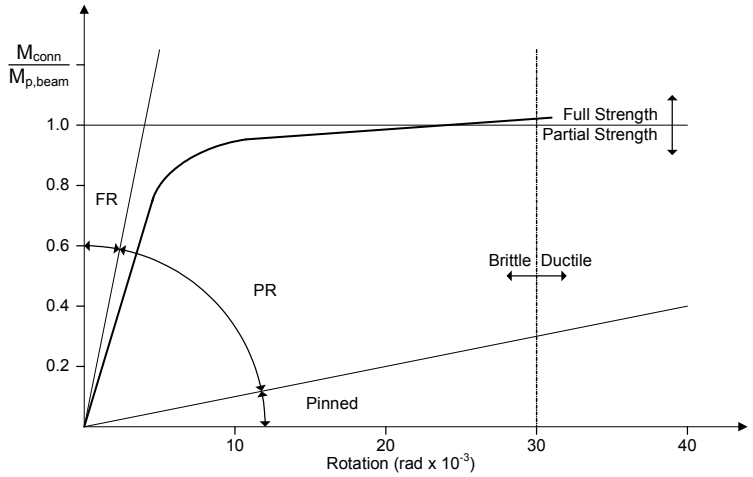

Figure 2.1 Classification of beam-to-column connections (reproduced from Swanson and Leon, 2000).

The following sections review the experimental work on the cyclic behavior of steel beam-to-column connections and methods of modeling the connection moment-rotation response.

2.1.1. Fully Restrained Connections

Observation of damage sustained by the buildings in the 1994 Northridge earthquake indicated that brittle fractures initiated within the connections at very low levels of seismic demand (Youssef et al., 1995). Contrary to the belief that such SMRF connections were capable of developing large plastic rotations without significant deterioration of stiffness and strength, these connections failed to permit either the beam to yield in flexure or the column panel zone to yield in shear due to the brittle nature of the connection failure.

In these FS, FR connections, the flanges of the steel girders were welded to the column flanges using complete joint penetration (CJP) and the shear tabs were welded to the column flanges and welded or bolted to the girder webs. Typically, but not always, fractures initiated at the CJP weld between the beam bottom flange and column flange, and progressed along a number of different paths depending on the individual joint conditions (Youssef et al., 1995). Once such fractures occurred, the beam-to-column connection lost much of its flexural rigidity and strength. Cyclic loading tests of pre-Northridge beam-column subassemblages also revealed that even the specimens made of the same material with the same connection detail exhibited highly variable stiffness, strength and energy dissipation capacities before fracture (Yang and Popov, 1995). Some connections failed in less than two cycles whereas others were able to withstand up to four or more, leading to the conclusion that the capacity of such connections in a building could wary widely from one to another. A wide range of phenomena have been

documented as having contributed to the fractures in these connections, such as the use of weld metal with insufficient notch toughness, discontinuities leading to stress concentrations on CJP welds, and insufficient quality control (Youssef et al., 1995).

Experimental research performed on the behavior of welded FR connections both before and after the 1994 Northridge earthquake (FEMA, 2000a; Leon, 1997; among others) have demonstrated that their drawbacks are mainly due to the connection geometry and to the fact that the whole lateral resistance of the structural system is concentrated in relatively few connections[1]. The problems due to connection geometry impose large strain demands in critical parts of the connection, leading to weld fracture, resulting in low rotational ductility in the connection and overall poor seismic performance of the LFRS. Similarly, heavy girder sections are required as a consequence of fully restrained construction, which leads to large connection forces and intensifies the strain concentration problem. Poor seismic performance of common welded FR connection details eventually promoted more research on alternative connection types that avoid the aforementioned problems.

2.1.2. Partially Restrained Connections

In phase I of the SAC project, the focus was set on procedures for repairing damaged welded FR connections. A parallel effort was also initiated by the National Institute of Standards and Technology (NIST) and the American Institute of Steel Construction (AISC) to develop retrofit techniques (Gross et al., 1999). One of the SAC research initiatives was to investigate the effectiveness of various types of bolted PR connections as an alternative to FR welded connections.

1. In modern SMRF design, most frequently, only the perimeter frames are designed to be moment-resisting.

2.1.2.1.Experimental Studies

In recent years, many researchers have carried out experimental tests on various types of PR connections and connection components. Some of these studies aimed to provide data for calibration of analytical models while others were focused on understanding the cyclic behavior of PR frames under dynamic loads.

Astaneh-Asl et al. (1989) conducted experimental tests to investigate hysteretic behavior of double angle connections under monotonically increasing cyclic loading. Six specimens on three different beam sections (W16x40, S24x80, and S12x31.8) were tested to failure, and developed considerable moments, performing well up to a connection rotation of 0.025 rad. without fracture. The specimens failed by fracture of bolts in tension and fracture of angles adjacent to the fillets. The development of a gap between the angles and column under tension was also reported for all specimens, which resulted in pinching of the observed hysteretic moment-rotation response.

Azizinamini and Radziminski (1989) evaluated the static and cyclic behavior of connections consisting of top and seat flange angles and double web angles. The moment-rotation behavior was sensitive to several geometrical parameters such as the angle thickness and the gage lengths. Low-cycle fatigue under multiple cycles of large amplitude displacements was also identified as a factor limiting the effectiveness of these connections in contributing to the energy dissipation capacity of a ductile SMRF. Subsequently, Harper and Radziminski (1990) tested thirteen all-bolted and bolted-welded top, seat and web angle connections on different sizes of beams (W8 and W14) under progressively increasing limits of displacement. The tests were terminated after cracking was observed at the flange angles before the point of rupture. Even though the

connections performed in a ductile fashion and stable hysteresis loops were obtained, a pinching effect was observed on the moment-rotation behavior along with major slip on some of the tested specimens.

Bernuzzi et al. (1996) tested quasi-statically a total of 16 PR specimens that consisted of top and seat angle, flush end plate and end plate connections under different loading histories. The cyclic response of the tested PR connections was satisfactory in terms of stiffness, strength and rotational ductility, even though their performance was substantially affected by pinching and slippage. The energy dissipation capacity was also adequate, although it became significant at high rotations which can be associated with high inter-story drift angles outside the interest in seismic design.

Bursi et al. (1996) tested 22 isolated T-stub components with different geometrical and mechanical properties monotonically and quasi-statically. The experimental program was aimed at developing component-based connection models that can simulate not only the envelope of the connection response but also stiffness and strength degradation as well as pinching of the related hysteretic responses. All T-stubs exhibited ductile and stable hysteretic behavior up to fracture caused by low-cycle fatigue.

The shaking table tests conducted on a full-scale one-story, one-bay steel structure by Nader and Astaneh-Asl (1996) showed that the shear responses of FR and PR connections were very similar, but the stiffness of the PR connection in shear was less stable than for the FR connections due to bolt slip and bolt hole enlargements during cyclic loading. Such bolt slips and hole elongations were reported to result in increase in ductility demand (Astaneh-Asl et al., 1989; Astaneh-Asl and Nader, 1990).

In an effort to investigate the behavior of top and bottom angle connections, Shen and Astaneh-Asl (1999) tested a series of bolted angles under cyclic loads. A stable cyclic moment-rotation response was observed with an ultimate strength that was two to three times the yielding capacity and a cyclic ductility ratio of eight to ten. Even though the hysteresis was influenced by bolt slip under severe cyclic loading, it was concluded that a properly designed bolted connection might have high ductility and cyclic energy dissipation capacity since the brittle failure that was observed in welded connections was eliminated.

Kukreti and Abolmaali (1999) tested a range of all bolted top and seat angle connections to investigate the effect of parameters defining the connection geometry on the moment-rotation response. The connections were reported to fail by excessive rotation (around 0.045 rad.), leading to significant loss in the stiffness of the connection. Excessive separation of the top or seat angle from the column flange was also observed at higher load levels, resulting in pinching of the hysteretic moment-rotation response. A wide range of initial stiffnesses and ultimate moment capacities were deemed to be possible by altering the connection geometry.

Faella et al. (2000) tested 28 T-stub assemblages with different geometric parameters under monotonic and cyclic loading. The observed failure mechanisms were different under monotonic and cyclic loading, and varied from specimen to specimen. Stiffness degradation and pinching as well as slip were observed in the specimens tested. The experimental results were used to calibrate an analytical model to simulate the cyclic force-displacement response of bolted T-stubs.

Extensive experimental work was performed during the SAC steel project on the force-displacement relation of PR steel beam-column connections (FEMA, 2000d). The asymmetry of hysteresis loops, progressive strength and/or stiffness degradation, pinching, as well as large variability in energy dissipation capacity due to many possible failure modes were found to be the common factors that affected the performance of the connections tested.

De Matteis et al. (2000) investigated the cyclic and low-cycle fatigue response of top and seat angle connections with and without web angles obtained from two different experimental programs (Mander et al., 1994; Calado et al., 1999), aimed at assessing the feasibility of an analytical model developed by Della Corte et al. (2000). The effect of web angles on the energy dissipation capacity was found to be insignificant due to the major plastic deformation concentration at the flange angles. The cyclic performance of the tested connections was found to be affected mainly by pinching of the hysteretic response.

Green et al. (2004) tested a full-scale composite connection detail under bidirectional cyclic loading. The concrete slab added both strength and stiffness to the connection performance when compared to a similar bare steel counterpart. Pinching of the moment-rotation response was started after 1% drift, and the degradation of the behavior got more severe with the loss of composite action due to local failure of the concrete slab after 1.5% drift.

The experimental behavior of typical PR beam-to-column connections reviewed in this section revealed several behavioral aspects. In the case of monotonic loading, the effect

of nonlinearity in the early stages of the response and kinematic hardening were found to be significant. In the case of cyclic loading, cyclic hardening, low-cycle fatigue phenomena and deterioration of the behavior due to strength and stiffness degradation and pinching were found to be important. Finally, the qualitative shape of the hysteretic moment-rotation response was found to be strongly dependent on the connection geometry and detail, mainly because of the complex interaction between the connection components and the large number of possible failure modes. This eventually led to high uncertainty in the ductility estimates, such as the plastic rotation at which a yield mechanism initiates or at which the connection loses its capacity to support gravity loads.

2.1.2.2.Analytical Studies and Modeling

It is clear that the beam-to-column connection behavior and the way it is modeled are important when the design or performance evaluation of a building frame is based on inelastic demand or the dissipation of the input seismic energy in the connecting elements. In recent years, considerable research has been conducted aimed at developing connection models that can represent the complex cyclic behavior of PR connections, such as strength and stiffness degradation, pinching of the hysteretic response, and low-cycle fatigue.

There are three main approaches to modeling PR moment-rotation behavior, each with its own advantages and limitations. In ascending order of complexity, these methods can be labeled as empirical models that represent the whole connection response with a single rotational spring, mechanical or component models where the connection response is obtained from several axial springs corresponding to the deformable elements of the connection, and finally, detailed finite element models. The most accurate

of the three approaches is the finite element idealization. However, this procedure is computationally expensive and often is not suitable for seismic performance evaluation even with the current advances in computational resources available to the engineer, hence is left out of scope of this study. A review of the work done on empirical and mechanical modeling approaches are presented in the following sections.

2.1.2.2.1.Empirical Models:

Empirical models use mathematical expressions that are developed by fitting curves to available experimental results of connections loaded monotonically and/or cyclically. An improvement on a purely empirical model is obtained by introducing quantities that have well-established physical definitions such as initial stiffness, ultimate moment, etc. to the mathematical expressions.

Early efforts were aimed at representing the monotonic moment-rotation curve (Richard and Abbot, 1975; Frye and Morris, 1975; Kishi and Chen, 1986, 1987, 1990; Kishi et al., 1988; Chen and Kishi, 1989; Abdalla and Chen, 1995; White and Chen, 1996; among others). The extension to behavior under cyclic loading was done by using the monotonic behavior as the backbone curve for cyclic behavior, along with introduction of rules for unloading and reloading. Bilinear, trilinear (Moncarz and Gerstle, 1981), and multilinear (Bernuzzi et al., 1996) hysteretic models were based on piecewise linearization of the moment-rotation curve. Leon and Shin (1995), developed a modified trilinear model for composite connections, taking into account unloading stiffness degradation due to cracking of the concrete slab as well as unsymmetrical stiffness for positive and negative rotation, and calibrated the model using test results. The pinching effects at large

rotations (greater than 0.01 rad.) were not modeled exactly, but simulated with the softening due to degraded unloading stiffness.

Pre-Northridge FR welded connections in moment frames behaved like a PR connection after fracture. Foutch and Shi (1997) proposed a piecewise linear model that can simulate the weld fracture. Gross (1998) developed a similar model considering the weld fracture at only one beam flange, and used it in conjunction with a bilinear panel zone hysteresis model to simulate the behavior of a welded steel connection. Wang and Wen (2000a)) proposed an empirical model based on the Bouc-Wen smooth hysteresis rule (Baber and Wen, 1981) to investigate the effects of connection fracture. The model was able to reproduce asymmetry in hysteresis loops, progressive strength and/or stiffness degradation, pinching, and effect of joint slip. Deng et al. (2000) proposed a hysteretic connection element that incorporated both stiffness and strength degradation and pinching and utilized damage indices that were based on ductility, accumulated plastic deformation and energy dissipation to detect failure of the connection. Finally, Della Corte et al. (2000) developed a mathematical model to represent the cyclic behavior of steel beam-to-column connections, and investigated the effect of connection modeling on the response of single degree-of-freedom systems and steel frames subjected to seismic excitations. Consideration of pinching in the connection modeling affected the ductility demands considerably. Initial stiffness and strength were also influential, whereas the effect of strength degradation due to plastic fatigue in plastic connection rotation demands was statistically insignificant.

The empirical models reviewed in this section were mainly based on fitting mathematical relationships to the actual experimental cyclic behavior of connections. The application of

such models is, therefore, limited to the structural details tested. Most of the reviewed studies dealt with the overall connection behavior and its modeling. This approach does not allow the quantification of the contribution of each component, and, as a consequence, the role played by the geometrical and mechanical parameters.

2.1.2.2.2.Mechanical Models:

Mechanical (also known as component or fiber) models lie somewhere between the empirical and the finite element models. The fundamental approach is based on idealizing the connection as a combination of rigid and deformable springs, and the overall connection behavior is obtained from the axial response of its basic components. The nonlinearity of the response is a consequence of inelastic constitutive laws adopted for its deformable components.

As was the case in empirical modeling approach, early mechanical models were developed for monotonic connection behavior. The necessary parameters to define the properties of the component springs were identified either from experiments (Wales and Rossow, 1983; Tschemmernegg and Humer, 1988; Huber and Tschemmernegg, 1998; Kattner and Crisinel, 2000; Swanson and Leon, 2001), using basic mechanics principles (Tschemmernegg and Querioz, 1996), or from detailed finite element analyses (Nemati et al., 2000). The evaluation of the monotonic moment-rotation curve according to the component method has recently been codified in Eurocode 3 (CEN, 1997) by broadly classifying connection components and their force-deformation characteristics.

The mechanical modeling approach has also been adopted by several researchers to simulate the cyclic behavior of PR connections. Madas and Elnashai (1992) developed a

model of the overall connection response from component contributions, such as seat and top angle, web-to-flange connections and panel zone. The response of each component was obtained from principles of mechanics, and did not require any experimental data. However, the model lacked the capability of simulating any degradation in the connection response as well as predicting the plastic rotation capacity. Elnashai and Elghazouli (1994) improved the model by introducing the effect of bolt slip. De Stefano et al. (1994) utilized a similar approach that did not require any empirical parameter in modeling double-angle connections. The connection was simulated by a series of rigid and deformable beam elements whose constitutive relationships were derived from beam elements subjected to flexure.

Shen and Astaneh-Asl (2000) developed a fiber model by assembling the top-and-bottom angle connection response from the response of bolted-angles under tension and compression. A multilinear approach was employed when modeling the hysteretic behavior of angles. A bolt slip model was added to the angle component to simulate the slip phenomenon under cyclic loading. The model and the assumptions made in developing the parameters were directly derived from the results of previous experimental work of the researches on bolted angle components (Shen and Astaneh-Asl, 1999).

Faella et al. (2000) proposed a model for prediction of the cyclic behavior of bolted T-stub connections using their geometric and mechanical properties and verified it with the results of experimental tests on T-stub assemblages. The model considered three failure modes observed in monotonic loading (flange yielding, bolt fracture and a combination of both), and extended the monotonic model to treat cyclic behavior. Even though most of the model parameters could be theoretically predicted starting from the monotonic force-

deformation relationship, those defining the strength and stiffness degradation were empirical and were determined from experimental data, hence limiting the proposed model to the connection details tested.

Kattner and Crisinel (2000) developed a two-dimensional model based on mechanical approach to simulate the behavior of PR composite joints and compared the response predicted by the model to response observed during tests of several types of composite joints. The types of connections that could be simulated were limited to those for which constitutive relations of the flexible components were available.

Swanson and Leon (2001) used the results of 48 T-stub component tests (Swanson and Leon, 2000) to develop and calibrate a comprehensive monotonic T-stub connection stiffness model, and extended it to simulate the cyclic behavior (Leon and Swanson, 2000). The individual T-stub model accounted for nonlinear material properties, variable tension bolt stiffness, partially plastic hinges in the T-stub flange and variable shear bolt locations in the slip/bearing mechanism, making it accurate enough to use in component connection models.

Calado (2003) developed a component based connection model for cyclic response of top, seat and web angle connections with damage accumulation and shear bolt deformation. The connection components were simulated by beam elements and rigid links. The model required only geometric and mechanical characteristics of the connection and did not require experimental data for its calibration.

Rassati et al. (2004b) proposed two mechanical models with different levels of detail for PR composite connections. The simplified model was based on the argument that the accuracy of the component model depended on considering all deformable components rather than on the ability to model each spring accurately. It utilized simplified (bilinear or trilinear) constitutive models, and neglected shear effects in the connection. The improved model considered more deformable components along with more detailed constitutive models, and had the ability to be used in three-dimensional problems, but was computationally more expensive. Verification against experimental data showed good agreement between the predicted and the observed response.

In general, the mechanical models reviewed in this section provide a reasonably accurate estimation of the connection force-deformation response. Mechanical models that do not depend on any experimental data are particularly useful for predicting the elastic and the post-yield response, starting from the knowledge of geometrical and mechanical properties of the connection detail. However, most of the time, strength and stiffness degradation, as well as the ultimate capacity of the connection, cannot be predicted reliably because modeling such phenomena requires experimental data on the desired connection detail. The main benefit of the mechanical modeling approach is that it allows estimation of changes in the overall connection behavior due to various changes in the connection detail. However, the number of parameters needed to define a model increases with the increased complexity of the connection detail. Even though they can be based on basic mechanics of materials principles, many of the component force-deformation relationships require calibration against data from cyclic tests. Furthermore, the predicted response appears to be sensitive to some parameters such as slip, whose relevant values are not easily predictable.

2.2. Behavior and Modeling of Steel Moment Resisting Frames (SMRFs)

The performance of SMRFs after the unexpected damage to welded FR connections during the 1994 Northridge earthquake has been widely investigated, including pre- and post-Northridge WSMFs as well as alternative framing systems with PR connections.

2.2.1. Fully Restrained Frames

As a part of the system performance evaluation effort of SAC Steel Project, extensive studies on the seismic performance of ductile SMRFs with FR connections were carried out by Gupta and Krawinkler (1999). Analytical models of different levels of detail for 3-, 9-, and 20-story SMRFs located at Los Angeles, Seattle and Boston were subjected to sets of ground motions representing specific hazard levels. Important conclusions drawn from their predicted performance were summarized below:

- Analytical modeling assumptions affected the predicted response significantly for the cases in which a mechanism occurred or the structure was driven into the range of negative post-yield stiffness (Gupta and Krawinkler, 2000b).

- Structures designed according to the strong-column weak-beam (SCWB) concept were susceptible to the formation of plastic hinges at the columns. Considerable plastic deformation occurred in the weak panel zones instead of in the beams, as had been expected.

- Larger than expected inelastic drifts were observed in the code designed SMRF structures even with the fully ductile member behavior assumption. This led to the conclusion that the potential for unacceptable performance was not negligible, especially for rare seismic events.

The aforementioned analytical studies on performance of SMRFs assumed ductile and non-degrading connection behavior regardless of the level of deformation, which has been shown to be inconsistent with experimental data. This led to a separate project (Naeim et al., 2000) in which the sensitivity of predicted response to hysteretic degradation characteristics was investigated. The effects were small for all but very severe ground motions with large plastic rotation demands. A similar study by Foutch and Yun (2002) investigated the effect of modeling assumptions on the predicted response of SMRFs subjected to seismic loads. Six models of different complexities were developed for a 9- and a 20-story FR building with ductile reduced beam section (RBS) and brittle pre-Northridge welded connections, and subjected to ten standard California region and ten near fault ground motion records. The contribution of the gravity frames was considerable, especially for the frames with brittle connections.

Another project on the behavior of SMRFs was concerned with the effect of connection fractures on predicted drift demands (Luco and Cornell, 1998; Luco and Cornell, 2000). It was concluded that for “mild” ground motions (of the 10% in 50 yr. type), the predicted effect of connection fractures was minimal due to lack of high demands to induce fracture on enough connections. Even under “moderate” ground motions (most of the 2% in 50 yr. records), the effect of connection fractures on the median drift demands was relatively small. Only in the records which cause very large story drifts in the ductile frames, connection fractures aggravated the situation, causing even larger predicted drift demands. Song and Ellingwood (1999a, 1999b), who also studied the effect of connection fractures on the global response of four SMRFs, reported similar behavior.

2.2.2. Partially Restrained Frames

The basis for utilizing PR frames in seismic regions is to dissipate the energy imparted to the frame by the earthquake through the ductile response of the connecting elements of the PR beam-to-column connections. An appropriate PR connection should avoid brittle failure modes and provide a plastic rotation capacity that is in compliance with the plastic rotation demand under seismic excitations.

2.2.2.1.Experimental Studies

Considerable experimental work has been conducted on SMRFs with PR connections as an alternative framing system to those of with FR connections. Some of these studies provided data for calibration of analytical models while others were aimed at understanding the comparative behavior of the FR and PR frames under dynamic loading.

Leon and Shin (1995) tested a half-scale, two-story, two-bay steel frame with strong top and seat angle connections under quasi-static cyclic loading. Even though many instances of slip between flange angles and beam flanges were observed, the frame behaved in a ductile fashion up to 3% inter-story drift.

Nader and Astaneh-Asl (1991, 1996) performed a total of 44 shaking table tests on a single-story steel structure with flexible, PR and FR connections using three different base excitations scaled up to a peak ground acceleration (PGA) of 0.5 g. It was concluded that semi-rigid steel frames do not necessarily sustain larger lateral drifts or more damage than rigid frames and a well proportioned PR connection designed to allow

active participation in nonlinear deformation might enhance the dynamic properties of steel frames.

Experimental and analytical work by Elnashai and Elghazouli (1994) on a full-scale one-bay, two-story PR frame with top, seat and web angle connections indicated that PR frames exhibited ductile and stable hysteretic behavior and might be used effectively in earthquake-resistant design. The stiffness and capacity of connections affected the number, location and the extent of plastic hinges developed in frame members. This in turn determined the distribution of local ductility within the frame and influenced the global ductility of the structure. Subsequently, Elnashai et al. (1998) performed monotonic, cyclic and pseudo-dynamic tests on a total of eight (two FR, six PR with top, seat and web angle connections) two-story steel frames to compare the behavior of PR and FR frames. It was concluded that the bolted connection exhibited a ductile and stable hysteresis, favorably affecting the performance of the frames in which they were utilized, and presented a viable alternative to FR weak-beam strong-column design.

The experimental work reviewed in this section demonstrated that the seismic performance of a structure can be significantly enhanced by utilization of PR connections. Due to the period elongation of the frame as well as the higher energy dissipation in the connection, PR frames may attract lower inertial forces and exhibit higher hysteretic damping. However, strength and stiffness degradation, pinching and bolt slip negatively impacted not only the performance of the individual connections, but also the performance of the structural system as a whole.

2.2.2.2.Analytical Studies

Several analytical studies have also been conducted on the seismic response of SMRFs with various types of PR connections.

In an analytical study of a six-story steel frame with composite connections, Shin (1992) demonstrated that the PR frames attracted less story forces which might result in smaller relative story drifts for particular earthquakes than the FR frames. The analysis did not account for panel zone deformations, and the connections were modeled with a trilinear model that only considered degradation in the unloading stiffness. In a similar analytical study, Leon and Shin (1995) reported that a LFRS consisting of PR composite connections showed good seismic performance for ground motions expected in zones of low to moderate seismicity. In particular, the frames with PR composite connections showed equal or better energy dissipation capacity than frames with FR connections, and had fewer problems with local buckling of members.

Two analytical studies were performed in the SAC program to assess the system behavior of frame structures with PR connections. In the first study, Kasai et al. (1999) investigated the effect of PR connection stiffness and strength on the frame seismic performance. The nine SAC pre-Northridge frames (3-, 9-, and 20-story frames for Los Angeles, Seattle, and Boston) were provided with PR connections instead of FR connections, without changing the member designs, and were subjected to sets of ground motions representing specific hazard levels. The yield strength and post-yield stiffness of the frames were directly influenced by the strength and stiffness of the PR connections. The elastic stiffness of the frames was unaffected by the initial stiffness of the PR connections, which was attributed to the higher contributions of beam and column

deformations to the frame displacements than that of the PR connections. Finally, the drift averaged through the frame height was insensitive to connection elastic and post-yield stiffness and yield moment. However, concentration of drift in the form of soft-story behavior was noted for cases with weak connections, leading to the conclusion that an appropriate distribution of connection strength through the height was necessary for acceptable seismic performance.

In the second study (Maison and Kasai, 2000; Maison et al., 2000), the specific objective was to assess the feasibility of designs with PR connections in regions of moderate to high seismicity. Redesigns of the 3-story building in LA and the 9-story building in Seattle were carried out. The seismic design loads were computed according to SMRF provisions with FR connections to allow a direct comparison of designs for PR and FR frames. These studies confirmed that it is possible to design PR structures whose seismic performance is comparable to that of ductile FR structures. However, the high plastic rotation demands sustained under severe events led to the conclusion that use of PR connections in highly seismic regions requires careful deformation-based design to provide the necessary plastic rotation capacity.

Salazar and Haldar (2001) performed an analytical study to quantify the amount of energy dissipation at PR connections, utilizing a smooth, nonlinear moment-rotation relationship. The analytical study reported that PR connections reduced the overall stiffness of the frames, but added a major source of energy dissipation which was found to be comparable to viscous damping. The PR frames considered in this study attracted less base shear. Increasing the stiffness of the connections significantly increased the base shear, but did not always decrease the predicted maximum lateral displacements.

Della Corte et al. (2002) investigated the effect of strength degradation and pinching on the predicted capacity of moment-resisting frames with FR and PR connections. An analytical model that can represent hardening, softening as well as pinching phenomena was used when modeling the connection behavior in a two-bay, five-story frame. Local softening of FR connections affected the system capacity only at high levels of drift demand, whereas pinching of PR connections did not show a general trend.

Analytical work reviewed in this section demonstrated that PR frames can provide similar or better seismic performance than their FR counterparts. The additional flexibility introduced by the PR connections results in elongation of the fundamental period, leading to reduction of the seismic forces experienced by the structure. Furthermore, structural redundancy is increased due to utilization of all connections as a part of the LFRS. Reported lateral displacements are of the same order or smaller as those in their FR counterparts, contradicting the belief that excessive deformations will occur in structures with PR connections, or that the structure will be more susceptible to lateral instability under gravity load.

2.3. Shape Memory Alloys (SMAs)

Shape Memory Alloys (SMAs) are a class of metallic alloys that exhibit the ability to undergo large deformations, but can recover permanent strains either through heating above a certain temperature (known as the shape memory effect) or through removal of the stress (known as the superelastic effect). This is possible because the deformation is accommodated in the form of a solid-to-solid phase transformation in SMAs, instead of formation of intergranular dislocations. Shape memory alloys based on nickel and titanium (Ni-Ti, also commonly known as NiTi-NOL) have provided the most suitable

combination of material properties for most commercial applications (Duerig et al., 1990). Therefore, Ni-Ti based SMA's will be focused on this study[1]. Some properties of Ni-Ti based SMAs are summarized in Table 2.1 and are discussed in the following sections.

Table 2.1 Properties of Ni-Ti SMA compared to typical structural steel (Delemont, 2001).

Property	Ni-Ti SMA		Structural Steel
	Austenite	Martensite	
Physical Properties			
Melting Point	1240 - 1310 ◦ C		1500 ◦ C
Density	6.45 g/cm^3		7.849 g/cm^3
Thermal Conductivity	0.28 W/cm ◦ C	0.14 W/cm ◦ C	0.65 W/cm ◦ C
Coeff. of Thermal Expansion	11.3x10^{-6}/ ◦ C	6.6x10^{-6}/ ◦ C	11.7x10^{-6}/ ◦ C
Mechanical Properties			
Recoverable Elongation	up to 8%		0.2%
Young's Modulus	30-83 GPa	21-41 GPa	200 GPa
Yield Strength	195-690 MPa	70-140 MPa	248-517 MPa
Ultimate Tensile Strength	895-1900 MPa		448-827 MPa
Elongation at Failure	5-50% (typically ~25%)		20%
Poisson's Ratio	0.33		0.27-0.30
Hot Workability	Quite good		Good
Cold Workability	Difficult due to rapid work hardening		Good
Machinability	Difficult, abrasive techniques preferred		Good
Hardness	30-60 R_C		Varies
Weldability	Quite good		Very good
Chemical Properties			
Corrosion Performance	Excellent (similar to stainless steel)		Fair

2.3.1. Phases of SMAs

The SMAs have two stable phases: the high-temperature phase, called austenite and the low-temperature phase, called martensite. In addition, martensite can be in one of two forms: twinned and detwinned, as shown in Figure 2.2. A solid-to-solid phase transformation which occurs between these two phases upon either heating/cooling or

1. It should be assumed that the properties and the applications of SMA discussed in this and the following chapters refer to Ni-Ti based SMAs, unless otherwise stated.

application of stress is the basis for the unique properties of SMAs. Superelasticity and the shape memory effect are the key effects of SMAs associated with the phase transformation.

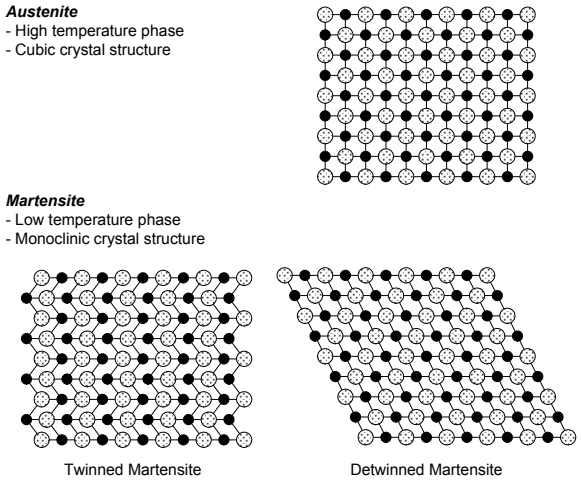

Figure 2.2 Different phases of an SMA

The transformation between austenite and martensite is accompanied by a variety of significant property changes. The martensitic structure can deform by moving twin boundaries while austenite deforms by dislocation generation. As a result, the yield strength of martensite is lower than that of austenite. On the other hand, only a certain amount of martensitic deformation can be accommodated by movement of twin boundaries. Once this is exceeded, the material deforms elastically, eventually yielding a second time, this time by dislocations resulting from plastic flow which make the process irreversible.

At a temperature above the austenite start temperature (A^s), an SMA is stable in its austenitic phase. Upon cooling in the absence of applied load, the material transforms from austenite into twinned (self-accommodated) martensite, without any observable macroscopic shape change. This is because martensitic transformations are displacive transformations where the atoms are rearranged into a new, more stable crystal structure without changing the chemical characteristics. Upon heating the material in the martensitic phase, a reverse phase transformation takes place and as a result the material transforms back to austenite. This heat-induced transformation process is illustrated in Figure 2.3

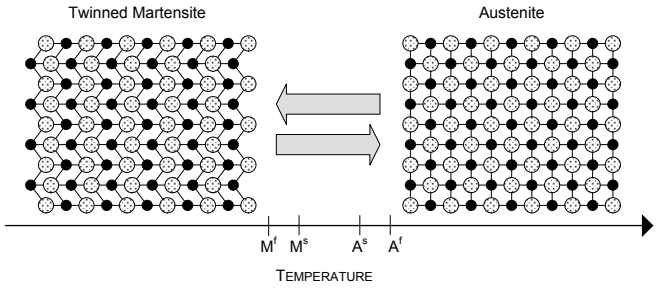

Figure 2.3 Temperature-induced phase transformation of an SMA without mechanical loading.

Four characteristic temperatures defined in Figure 2.3 are of importance: martensitic start temperature (M^s) which is the temperature at which the material starts transforming from austenite to martensite; martensitic finish temperature (M^f), at which the transformation is complete and the material is fully in the martensitic phase; austenite start temperature (A^s) at which the reverse transformation (austenite to martensite) initiates; and austenite finish temperature (A^f) at which the reverse phase transformation is completed and the material is the austenitic phase.

It is also possible to induce a martensitic transformation which leads directly to detwinned martensite. If load is applied in the austenitic phase and the material is cooled, the phase transformation results in detwinned martensite, and reheating the material results in complete shape recovery. The above-described loading path is shown in Figure 2.4. The transformation temperatures in this case strongly depend on the magnitude of the applied load. Higher values of the applied load will lead to higher values of the transformation temperatures. Usually, the presence of stress increases the transformation temperatures in a linear fashion.

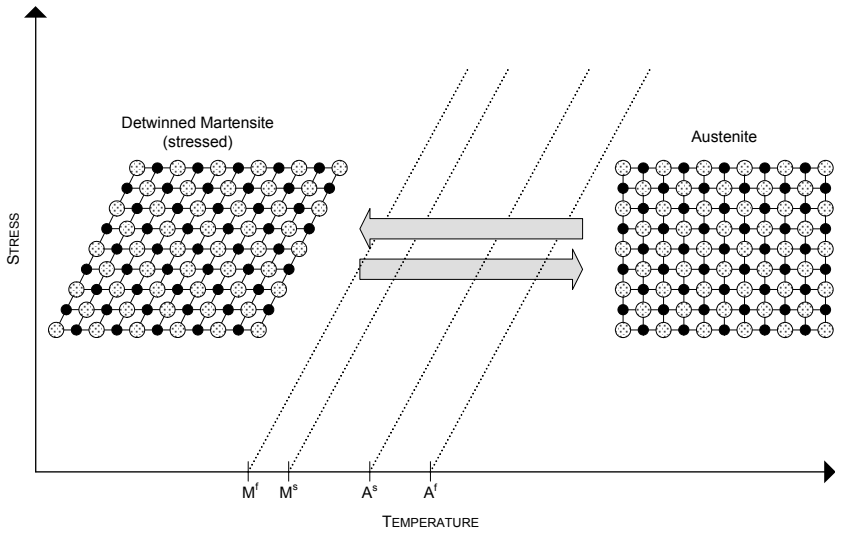

Figure 2.4 Temperature induced phase transformation with applied load

2.3.1.1.Shape Memory Effect

If mechanical load is applied to the material in the twinned martensite state (at a temperature below M^f), the alloy is easily deformed by detwinning to large strains (on the order of 6-8%). Upon release of the load, the material remains deformed. A subsequent

heating of the deformed material to a temperature above A^f results in reverse phase transformation (martensite to austenite) and leads to complete shape recovery, as shown in Figure 2.5. This process is often referred to as the shape memory effect (Duerig et al., 1990).

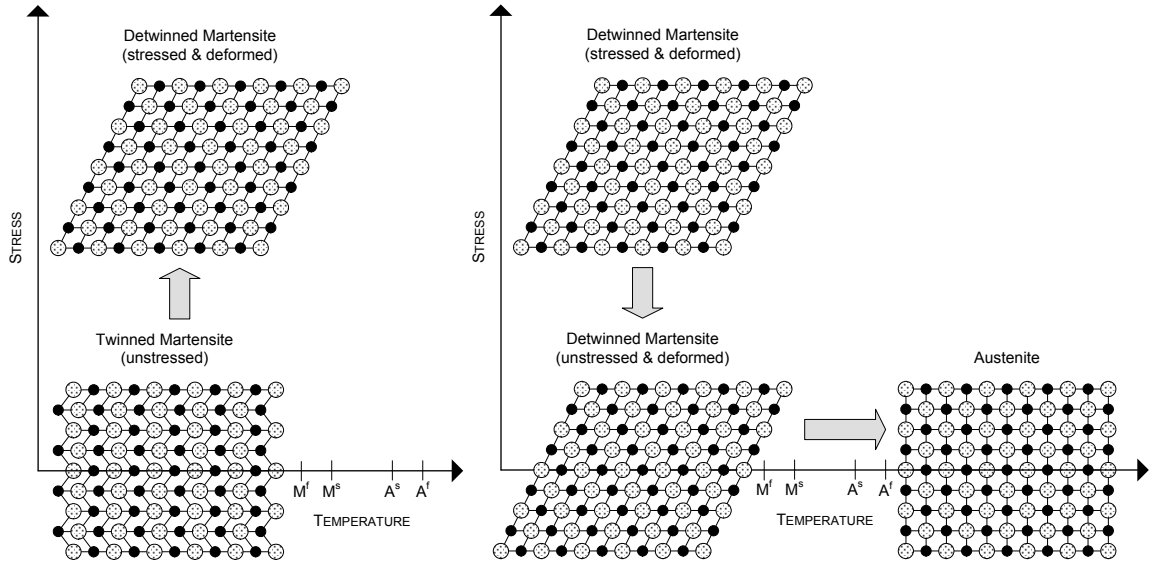

Figure 2.5 Shape memory effect of an SMA

2.3.1.2.Superelasticity

At high temperatures, an SMA exists in its austenitic phase. At a temperature that is slightly above A^f, martensite can be stress-induced. Upon application of load, fully detwinned, stress-induced martensite is obtained and large strains are observed. By removal of the load, the material reverts back to austenite at a lower stress, forming a hysteresis, and shape recovery occurs and without the application of heat. This effect is

known as superelasticity or pseudoelasticity. A loading path demonstrating the superelastic effect and the resulting stress-strain diagram is shown in Figure 2.6.

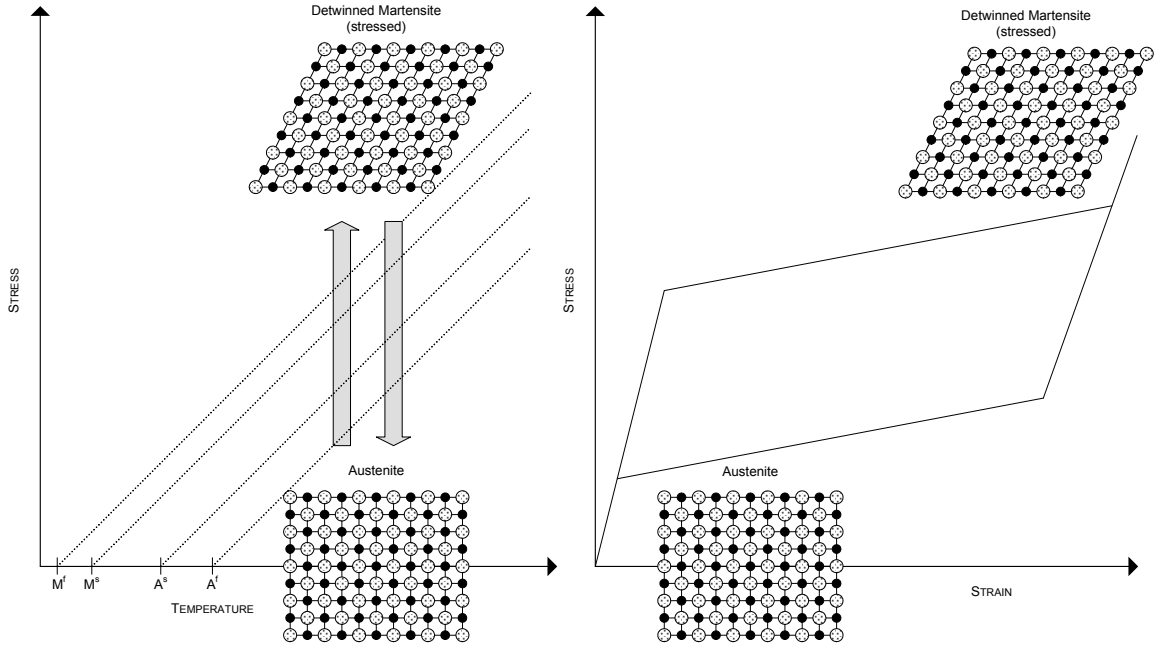

Figure 2.6 Superelastic loading path (left) and stress-strain diagram (right).

Figure 2.7 shows an idealized plot of the stress-strain-temperature relationships in Ni-Ti based SMAs and summarizes the two characteristics, superelasticity and shape memory effect.

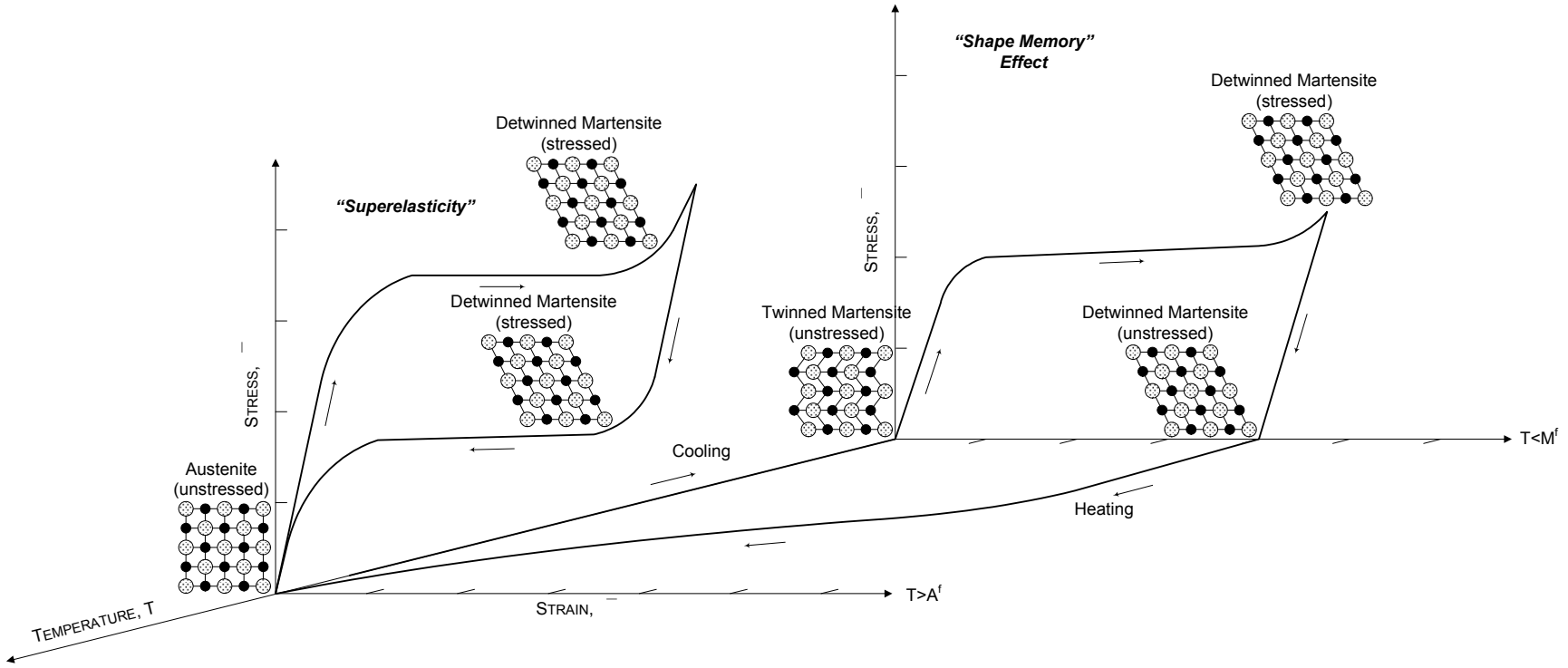

Figure 2.7 Stress-strain-temperature diagram showing superelasticity and shape memory behavior of an SMA.

2.3.2. Cyclic Properties

In recent years, considerable number of experimental studies have been carried out to determine certain characteristics of SMAs such as damping capacity, cyclic performance, and strain rate dependence under seismic actions. These studies stem from the increasing interest in the possibility of using SMA devices in seismic design of new and retrofit of existing structures.

The most comprehensive and up-to-date study on cyclic characteristics of SMAs is the MANSIDE (1998) project. The Ni-Ti class of alloys was highly efficient in providing excellent corrosion and fatigue resistance, superelasticity, large recoverable strains and high hysteretic damping based on cost. However, the study also pointed out some potential drawbacks of the material including the sensitivity of the mechanical behavior to strain rate and ambient temperature, and deterioration of properties with cyclic loading. Material properties of SMAs also sustained significant changes with differences in the chemical composition, cold work, heat treatment, and thermomechanical cycling.

Most of the experimental studies were carried out using SMAs in wire or thin bar form. Experimental data on large diameter SMA bars which would typically be necessary in earthquake engineering applications are scarce. In one of the limited experimental studies, DesRoches and Delemont (2002) investigated the force-deformation and energy dissipation characteristics of a 280 mm long, 25.4 mm diameter superelastic SMA bar. The specimens were loaded under tension at increasing strains from 0.5 to 8% with at a strain rate of 0.10 mm/mm/sec. The SMA bar indicated a loading plateau stress of approximately 450 MPa (65 ksi), an unloading plateau stress of 140-200 MPa (20-29 ksi), a strain hardening stiffness of 7% of the elastic stiffness, and less than 0.25% residual

strain when loaded up to a total strain of 4% (less than 1% residual strain when loaded up to 8%). Furthermore, elastic deformation of fully-transformed martensite after 5-6% strain with nearly 45% of the initial stiffness was observed.

DesRoches et al. (2004) tested Ni-Ti SMA wires and bars to evaluate the effect of bar size and loading history on the strength, energy dissipation capacity and recentering properties in superelastic form. Specimens of various diameters (1.8, 7.1, 12.7, and 25.4 mm) and lengths (152 and 279.4 mm) were subjected to cyclic tension loading up to 6% strain under both quasi-static and dynamic loading. Both the wire and the bar form of the material exhibited very good superelastic behavior with an average residual strain of 0.65%. Even though increasing strain rate deteriorated the energy dissipation capacity, the transformation stress was increased, and the recentering capability was not affected.

McCormic et al. (2005) investigated the effect of mechanical training on cyclic properties of superelastic Ni-Ti SMA wires through a three factor two level full factorial experimental design. A simple mechanical training procedure showed promise to stabilize and adjust the characteristics of the material such as loading plateau stress, equivalent viscous damping, and residual strain for seismic applications.

2.3.3. Innovative Connections with SMAs

The use of SMAs in passive control devices has been extensively studied leading to many innovative applications such as SMA restrainer bars to be used in bridges (DesRoches and Delemont, 2002), SMA bracing systems (Lafortune et al., 2007), and steel beam-to-column connections with SMA connecting elements (Ocel et al., 2004).

Ocel et al. (2004) evaluated the feasibility of a new class of PR connections aimed at improving the system performance by means of providing increased energy dissipating capacity via SMA elements. The proposed connection consisted of four large diameter martensitic SMA bars connecting the beam flange to the column flange and serving as the primary moment transfer mechanism. A steel shear tab was used to transfer the shear forces. Since SMAs in martensitic state are more flexible and weaker than structural steel (see Table 2.1), the proposed connection behaved like a PR, PS connection[1]. Two connection designs were tested quasi-statically using the SAC loading protocol. These SMA connections dissipated the energy through the deformation of the SMA bars, preventing the yielding of the beam and the column. The connection hysteresis was found to be stable up to the 4% drift level with no strength degradation observed. The Ni-Ti SMA bars used in this connection had a unique ability to recover large residual deformations by application of heat (via shape memory effect, see Section 2.3.1.1). A second test was performed using heat-straightened bars in the connection nearly identical hysteretic behavior was observed as in the case of initial testing with no loss in strength, stiffness and no signs of fatigue. However, an additional test performed under dynamic loading showed a decrease in energy dissipation due to strain-rate effects when compared to the quasi-static tests.

An analytical study that investigated a post-tensioned connector system utilizing steel connectors and SMA post-tensioning elements was performed at the University of Arizona (Post-tensioned, 2005). Superelastic SMA elements were utilized to provide the connection with recentering capability. The connectors were detailed to: (1) possess high inherent elastic stiffness in comparison to traditional semi-rigid connections to reduce

1. Further details of the prototype connection are presented in Section 3.4.1.

structural drifts at service loads and low-level seismic events, (2) provide stable hysteretic behavior at moderate seismic events while incurring only modest damage due to the elastic nature of the post-tensioning, and (3) enter their superelastic ranges, hence limit the permanent drifts for seismic events of high return period. Nonlinear dynamic analyses of model structures employing the prototype design showed promising response reduction and self-centering effects.

The analytical and experimental work reviewed in this section has shown that energy dissipation and recentering systems involving SMA elements implemented in beam-to-column connections are potential alternatives for existing PR and FR connections. PR connections utilizing SMAs appear to have the potential to enhance the ductility and the damping capacity of PR connections in steel frames. These ideas will be developed further subsequently.

2.4. Probabilistic Performance Evaluation of SMRFs

The process of predicting the capacity of a structure when subjected to ground accelerations as well as the demands that will actually be experienced entail significant uncertainties. Some of these uncertainties originate from factors that are inherently random (aleatory uncertainty, or randomness) at the scale of understanding (e.g. transformation plateau stress of SMA, earthquake occurrence on a known fault) and cannot be reduced by acquiring additional data or information. Others stem from assumptions or lack of knowledge in representing the physical phenomena (epistemic uncertainty, or uncertainty in general), are dependent on the model selected (e.g. two-dimensional idealizations of structures) (Wen et al., 2003), and are reducible by additional data or improved information. However, many of the factors that determine the

performance of structures under seismic loads, while unpredictable, exhibit statistical regularity and probability and statistics provide rational tools to treat such uncertainties (Ellingwood, 2000). Consequently, probabilistic approaches that incorporate various sources of uncertainty in seismic demand and structural response are increasingly being used in evaluating seismic response and performance evaluation of structures.

Song and Ellingwood (1999a, 1999b, 2001) investigated the role of inherent randomness and modeling uncertainties in ground motion, welded connection behavior, and structural resistance in explaining building performance observed during the Northridge earthquake. In the first part of their study (Song and Ellingwood, 1999a), four WSMFs that suffered damage to welded connections during the Northridge earthquake were evaluated using deterministic approaches, making use of a degrading hysteretic connection model (Gross, 1998) to simulate weld fractures and a single ground acceleration time history. The comparisons of predicted and observed building damage showed unevenness in the ability of deterministic connection models and nonlinear dynamic analysis tools to predict the observed performance. In the second part of their study (Song and Ellingwood, 1999b), the performance of two WSMFs was evaluated with stochastic approaches using an ensemble of ground motions. With this approach, the observed performance fell within the distribution of performance predicted by probabilistic modeling. The contribution of uncertainty in connection hysteresis to building fragility was found to be statistically significant (Song and Ellingwood, 1999b, 1999c) only when a severe limit state (defined by maximum inter-story drift angle of 0.05 rad.) was approached, and its contribution was small in comparison to the contribution of uncertainty due to ground motion.

Wang and Wen (2000a), 2000b) conducted an analytical study to investigate the reliability and redundancy of two-story steel buildings with ductile and brittle connections. The uncertainties in material properties, yield strength of steel and plastic modulus of member cross-sections were modeled as random variables. The damage index that represents the damage capacity of the brittle connection was also modeled as a random variable based on a limited number of test results. The relative performance of two designs, a perimeter frame and a parallel frame, was investigated in terms of maximum drift exceedence probability. The effect of connection fracture on the response was found to be moderate.

Probabilistic evaluation of performance given seismic uncertainties has also been addressed in the SAC Steel Project (FEMA, 2000a; FEMA, 2000e). The resulting probabilistic framework (Cornell et al., 2002) was based on convolving the randomness and uncertainty characteristics of three random elements of the problem: (1) ground motion intensity, (2) structural demand, and (3) structural system capacity, in order to determine the probability of achieving a specific performance level. The performance of a suite of regularly configured model buildings was evaluated using the developed procedures, and the results were tabulated as demand and resistance factors and confidence indices to be used in simplified performance evaluation procedures.

Sakurai et al (2001) investigated the effect of variability in initial connection stiffness on the stochastic response of steel frames with PR connections in the elastic range under wind load. Considering three sources of uncertainty - initial connection stiffness, and bending stiffness of beams and columns - the mean and standard deviation of horizontal frame displacements and inter-story drift ratios were evaluated. The dispersion in both of

the response parameters was found to be less than expected (0.05 to 0.08 for a coefficient of variation of 0.20 in connection stiffness), suggesting that uncertainties in individual connection behavior may be less important than the other aspects of frame behavior.

Barroso and Winterstein (2002) proposed a methodology, referred to as probabilistic seismic control analysis, for the development of probabilistic seismic demand curves for structures with supplemental control devices. The proposed method coupled conventional probabilistic seismic hazard analysis with nonlinear dynamic analyses performed on finite element models of structures with control devices. As a case study, the comparative performance of three different control systems (base isolation, viscous brace dampers and active tendon braces) was investigated. The resulting annual hazard curves provided a basis for comparison between different control strategies considering the variability in seismic demand estimation.

The probabilistic studies on predicted seismic response of SMRFs reviewed in this section considered the uncertainties that arise from the structural modeling process as well as the uncertainties in structural behavior. Combined, these uncertainties make it difficult to predict the performance of a specific structure during a postulated seismic event, leading to the conclusion that the seismic performance evaluation must be probability-based, rather than being deterministic. This aspect of seismic performance evaluation of steel frames with SMA connections is considered further in Chapter 6.

CHAPTER 3

DESCRIPTION OF CASE STUDIES

3.1. Introduction

The objective of the research presented here is to evaluate the role of partially restrained (PR) steel beam-to-column connections with Shape Memory Alloy (SMA) connecting elements (hereafter referred to as SMA connections) as passive control systems for enhancing structural performance under seismic loads. This study focuses on steel moment-resisting frames, and two types of possible SMA connections: one with martensitic connecting elements (hereafter referred to as martensitic SMA connection) and the other with superelastic connecting elements (hereafter referred to as superelastic SMA connection). To provide a realistic test-bed for demonstrating the capabilities of these connections, two structures are selected from the SAC Phase II: the low-rise (three-story) PR system designed for Los Angeles, CA, and the medium-rise (nine-story) PR system designed for Seattle, WA. The response of these frames, with and without SMA connections, is evaluated using the suites of ground motion acceleration records, also from the SAC Phase II project, representing different return periods. The relative performance of these frames is judged based on the maximum and permanent inter-story drift demands, element maximum and permanent deformation demands and dissipated hysteretic energy.

This chapter provides a description of the two structures that are analyzed and the ground motion records that are used to determine the seismic demands. Two different

SMA connection systems are then selected for implementation as passive control systems in these structures.

3.2. Description of Structures

As a part of the SAC steel project, three-story and a nine-story office buildings having PR moment frames as lateral force resisting systems (LFRSs) were designed for Los Angeles, California and Seattle, Washington, respectively. The buildings were redesigns of the SAC model buildings which had special moment frames as LFRSs. The buildings were designed by Stanley D. Lindsey and Associates (Atlanta, GA) for gravity, wind and seismic loads, following the 1994 UBC (ICBO, 1994) requirements. The columns, girders and connections were proportioned so as to keep the building footprints, column spacing, story heights and live loads the same as for the SAC model buildings with pre-Northridge fully restrained (FR) connections.

The PR frames were designed to utilize every beam-to-column connection in the building in resisting the lateral loads, which led to a LFRS consisting of multiple frames rather than just a few heavily loaded FR perimeter frames. By utilizing every connection available, the objective was to lessen the demands on each frame as well as to avoid large energy dissipation demands on connections.

In most cases, force reduction factors (R_w) present in the current design codes are based on past performance and back calibration. There have been relatively limited studies in this area for PR frames, constituting a problem for the proposed procedures to determine appropriate R-factors (Leon, 1998). Consequently, the structural system of the two buildings was assumed to be a special moment resisting frame (SMRF) of steel even

though PR frames were classified as ordinary moment frames (OMF) by the 1994 UBC. The designer's rationale was not to penalize PR design and to have a design base shear similar to that used in the design of the FR buildings, allowing a direct comparison of the two designs. Strict compliance with the UBC would have required a reduction factor of 6 instead 12 and would have doubled the design lateral forces. Additional design details can be found in Maison and Kasai (2000).

The resulting designs were based on state-of-practice techniques for PR construction but, unconventionally, utilized the same design lateral force and drift criteria as that of FR construction. As a result, they provide benchmarks to evaluate how PR buildings might perform in regions of moderate to high seismicity.

3.2.1. Los Angeles Three-Story PR Building

Figure 3.1 shows the plan and the elevation of the 3-story Los Angeles building. A summary of the design parameters is also given in Table 3.1.

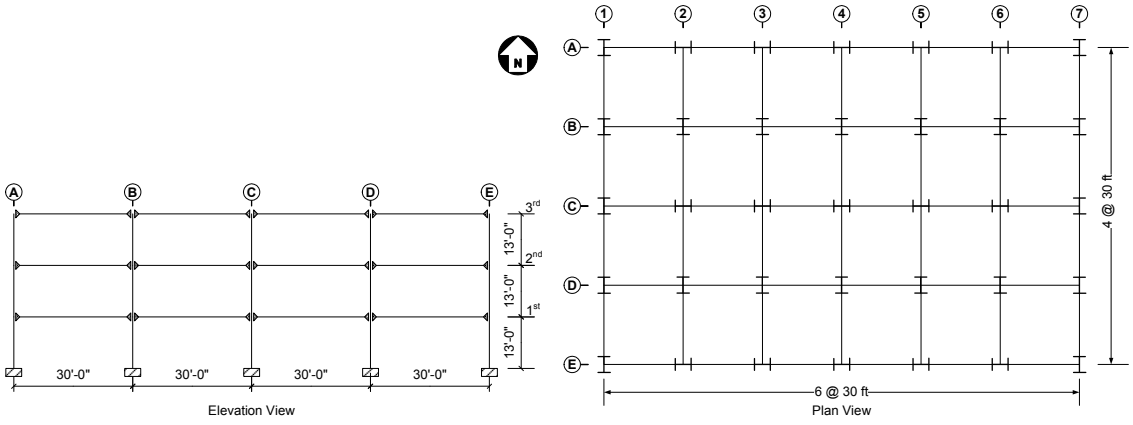

Figure 3.1 LA 3-story PR building plan and elevation views.

Table 3.1 LA 3-story PR building design parameters (Maison and Kasai, 2000).

Parameter	Design Criteria
Building Code	1994 Uniform Building Code
Seismic Zone	4
UBC Equation Period	0.55 sec.
Design Base Shear (Strength)	396 kips
Design Base Shear (Drift)	240 kips
R_w Coefficient	12

The girders and the columns were A572 Gr. 50 steel. The building had seven partially restrained frames in the North-South direction which were symmetric about column row 4. The columns were oriented to provide the structure with similar lateral stiffness in both primary directions. For design purposes, the columns were assumed to be fixed at the base. To take into account the floor slab participating in the frame action, the beams were assumed to have a moment of inertia based on the average of 60% composite beam moment of inertia and 40% bare steel beam moment of inertia, based on the recommendations given by Leon et al. (1996). A concrete-filled deck floor system was used to connect the frames. Column and beam sections were selected following a strong column-weak beam (SCWB) philosophy. The member section sizes for the distinct frames in North-South direction and are given in Table 3.2.

Table 3.2 LA 3-story PR building N-S direction girder and column sizes.

Floor	Frames 1, 7			Frames 2, 6			Frames 3, 4, 5		
	Columns		Girders	Columns		Girders	Columns		Girders
	Exterior	Interior		Exterior	Interior		Exterior	Interior	
3	W14x74	W14x90	W18x35	W14x90	W14x109	W18x35	W14x90	W14x109	W18x35[a] W21x44[b]
2	W14x74	W14x90	W18x35	W14x90	W14x109	W18x35	W14x90	W14x109	W18x35
1	W14x74	W14x90	W18x35	W14x90	W14x109	W18x35	W14x90	W14x109	W18x35

a. Between rows A&B, D&E.
b. Between rows B&C, C&D.

Based on the previous experience of the designer with low-rise PR construction, a combination of composite PR connections and top and bottom seat angle PR connections (Figure 3.2) were used in the design of the three-story building. Composite connections were utilized at all locations where the column was in strong axis bending, and where the slab was continuous across the column. Composite connection details consisted of a bottom seat angle, a double angle connecting the girder web to the column flange, and continuous slab reinforcement across column lines. The design took advantage of the reinforcing steel in the concrete slab to form a tension-compression couple with the seat angles, adding significant moment capacity to the connection over that of a typical top and seat angle connection. At all other locations, top and seat angle connections were utilized.

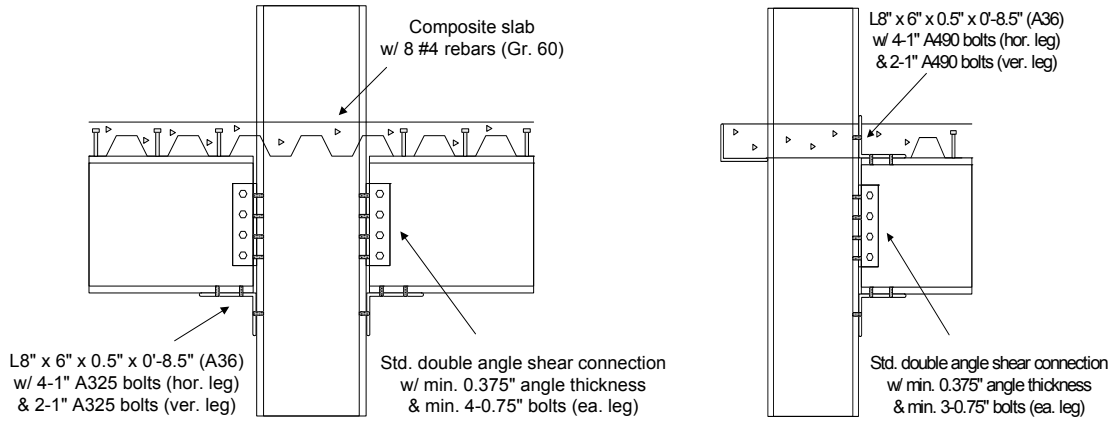

Figure 3.2 Typical composite (left) and top and seat angle (right) connection details (Maison and Kasai, 2000).

The composite PR connections were detailed based on the recommendations given by Leon et al. (1996). The top and seat angle connections were detailed so that the angle would yield prior to bolt failure. The fact that actual PR connections do not show an unbounded increase in the strength with increasing deformation was also considered by placing bounds on the connection ultimate moment capacities during the design process.

Table 3.3 LA 3-story PR building ratios of connection, girder, and column panel zone properties.

Ratio	Composite	Top, Seat and Web Angle
K_{conn} / K_{girder}	5	3
M_{conn} / M_{girder}	0.8	0.5
K_{conn} / K_{panel}	0.3	0.2
M_{conn} / M_{panel}	0.5	0.3

Key connection, girder (W18x35) and column panel zone (W14x109) properties are given in Table 3.3. K_{conn} and M_{conn} are connection initial stiffness and ultimate moment; K_{beam}

and M_{beam} are the composite girder stiffness and plastic moment; K_{panel} and M_{panel} are column panel zone stiffness and ultimate moment calculated using the equations given in Krawinkler (1978) and assuming inflection points at story mid-heights. The final design ended up having PR, partial-strength (PS) connections that had initial stiffness greater and ultimate moments less than those of the girder. The column panel zones were much stiffer and stronger than the connections, making the connections the weakest component of the beam-column joint.

3.2.2. Seattle Nine-Story PR Building

Figure 3.3 shows the plan and the elevation of the 9-story Seattle building. A summary of the design parameters is also given in Table 3.1.

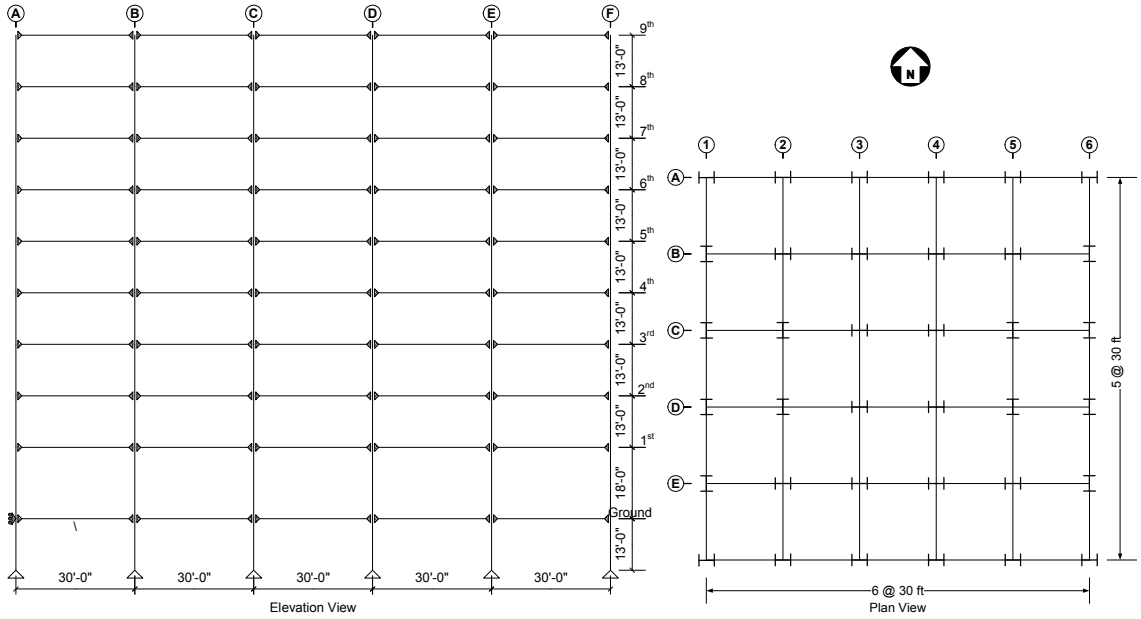

Figure 3.3 SE 9-story PR building plan and elevation views.

Table 3.4 SE 9 -story PR building design parameters (Maison and Kasai, 2000).

Parameter	Design Criteria
Building Code	1994 Uniform Building Code
Seismic Zone	4
UBC Equation Period	1.28 sec.
Design Base Shear (Strength)	586 kips
Design Base Shear (Drift)	335 kips
R_w Coefficient	12

The girders and the columns were A572 Gr. 50 steel. The building had six partially restrained frames in the North-South direction which were symmetric about the center of the building. The columns were oriented to provide the structure with similar lateral stiffness in both primary directions. For design purposes, the columns were assumed to be pinned at the base. The beams were assumed to have the bare steel beam moment of inertia, which is more typical of rigid frame design. The basement level was also assumed to be horizontally restrained at the ground level. A concrete-filled deck floor system was used to connect the frames. Table 3.5 shows the member section sizes for three different frames in North-South direction.

Table 3.5 SE 9 -story PR building N-S direction girder and column sizes.

Floor	Frames 1,6			Frames 2,5			Frame 3,4		
	Columns		Girders	Columns		Girders	Columns		Girders
	Exterior	Interior		Exterior	Interior		Exterior	Interior	
9	W14x74	W14x90	W18x35	W14x90	W14x99	W18x35	W14x90	W14x99	W18x35[a] W21x44
8[c]	W14x74 W14x99	W14x90 W14x132	W24x55[a] W27x84	W14x90 W14x132	W14x99 W14x120	W18x35 W24x55[b]	W14x90 W14x132	W14x99 W14x120	W18x35
7	W14x99	W14x132	W24x55 W27x84	W14x132	W14x120	W18x35 W24x55[b]	W14x132	W14x120	W18x35
6[c]	W14x99 W14x120	W14x132	W30x90	W14x132 W14x145	W14x120 W14x145	W21x44[a] W30x90	W14x132 W14x145	W14x120 W14x145	W18x35
5	W14x120	W14x132	W30x90	W14x145	W14x145	W21x44[a] W30x90	W14x145	W14x145	W18x35
4[c]	W14x120 W14x145	W14x132 W14x159	W30x90	W14x145 W14x159	W14x145 W14x176	W30x90	W14x145 W14x159	W14x145 W14x176	W24x55
3	W14x145	W14x159	W30x90	W14x159	W14x176	W30x90	W14x159	W14x176	W24x55
2[c]	W14x145 W14x211	W14x159 W14x311	W30x90	W14x159 W14x342	W14x176 W14x257	W30x90	W14x159 W14x342	W14x176 W14x257	W30x90
1	W14x211	W14x311	W30x90	W14x342	W14x257	W30x90	W14x342	W14x257	W30x90
G	W14x211	W14x311	W30x90	W14x342	W14x257	W30x90	W14x342	W14x257	W30x90

a. Exterior bays only.
b. Center bay only.
c. Column splice in this story.

PR T-stub connections were utilized at all beam-column joints because a stiffer and stronger connection is usually needed to provide the stiffness, strength and ductility required for a building of this height. The connections consisted of T-stubs from WT sections bolted to the column and girder flanges, and a shear tab welded to the column and bolted to the girder web (Figure 3.4).

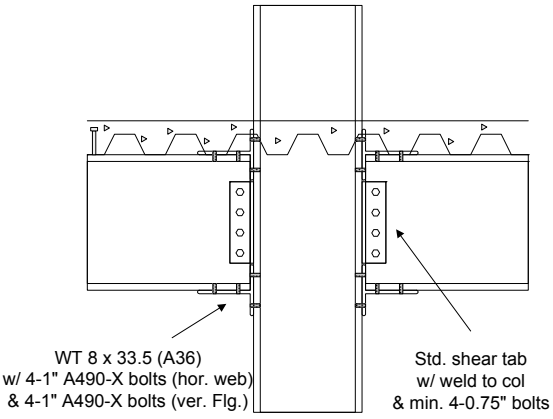

Figure 3.4 Typical T-Stub connection detail (Maison and Kasai, 2000).

The T-stub PR connections used in the design (Maison and Kasai, 2000) were based on an experimental study conducted at Lehigh University (Mayangarum, 1996).

Table 3.6 SE 9 -story PR building ratios of connection, girder, and column panel zone properties.

Ratio	T-Stub Connection
K_{conn} / K_{girder}	3
M_{conn} / M_{girder}	0.2
K_{conn} / K_{panel}	0.2
M_{conn} / M_{panel}	0.2

Key connection, girder (W30x90) and column panel zone (W14x145) properties are given in Table 3.6. The final design ended up having PR, PS connections that had initial stiffness greater and ultimate moments considerably less than those of the girder. The column panel zones were much stiffer and stronger than the connections, making the connections weakest component of the beam-column joint. The selection of a relatively

weak PR connection was based on designer's reluctance to utilize connections outside standard industry practice (Maison and Kasai, 2000).

3.3. Ground Motion Time History Records

The probabilistic seismic hazard maps developed by the USGS (2007) provide non-site specific estimates of the zero-period acceleration and spectral ordinates at periods of 0.2, 0.3 and 1.0 seconds. However, methods used in seismic demand and/or capacity analysis require a more detailed model of input ground motions than is required by conventional design codes. In particular, nonlinear time history analysis and incremental dynamic analysis (IDA) both require ground motion acceleration records. Sets of recorded and simulated ground motions having probabilities of exceedence of 50% in 50 years (50%/50 yr.), 10% in 50 years (10%/50 yr.), and 2% in 50 years (2%/50 yr.) were assembled for Los Angeles, Seattle and Boston as a part of the SAC project (Somerville, 1997). The ground motions assembled for the Los Angeles and Seattle regions are used for the simulations performed in this study.

For the Los Angeles region, the accelerograms in the 50%/50 yr. and 10%/50 yr. sets (with return periods of 72 and 475 years, respectively) were all derived from crustal earthquakes in soft rock to stiff soil; in contrast, the accelerograms in the 2%/50 yr. set (with return period of 2,475 years) were from near-fault recordings or simulations because at a 2,475 year return period, the seismic hazard in Los Angeles is dominated by events close to the site (less than 20 km). These ground motions are characterized by one or more strong pulses that cause large displacement demands in one direction without the reversal observed in regular ground motions. For the Seattle region, the accelerograms in both the 2%/50 yr. and 10%/50 yr. sets (with return periods of 2,475

and 475 years, respectively) were derived from recordings on stiff soil. In contrast to the short duration impulsive ground motions in Los Angeles, Seattle ground motions are longer duration and broader in frequency content.

Each set represented ten earthquakes with records from two horizontal orthogonal directions, for a total of twenty accelerograms per set. The records were scaled in such a way that their average spectral values matched (in a least-square error sense) the USGS (2007) mapped values at 0.3, 1.0, and 2.0 seconds and a predicted value at 4.0 seconds, for the appropriate return period and location. These periods also cover the range of interest for the flexible steel structures that are analyzed in this study. The resulting median spectral accelerations (S_a) for a damping ratio of 5% for Los Angeles and Seattle ground motion sets are shown in Figure 3.5.

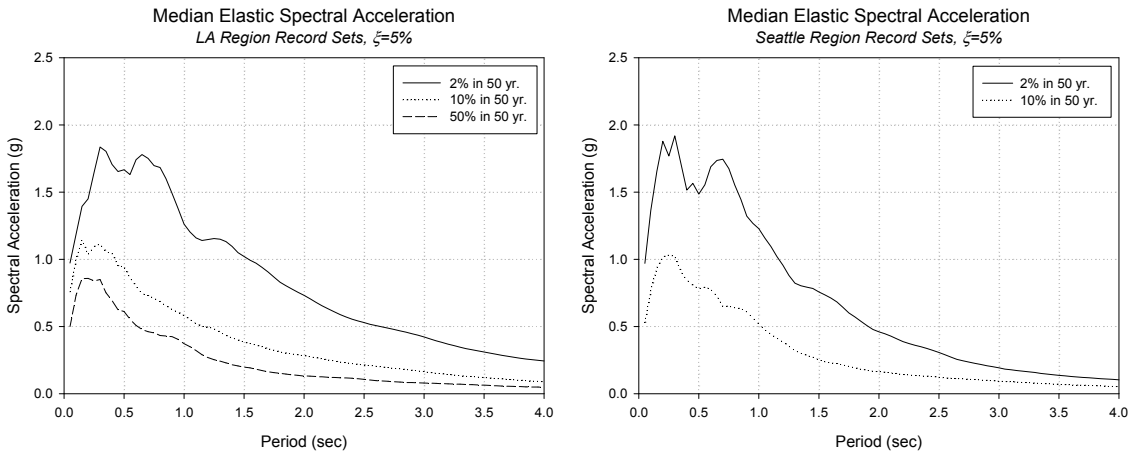

Figure 3.5 Median elastic spectral acceleration for Los Angeles region (left) and Seattle (right) ground motion sets.

An important note regarding these acceleration records is that they can represent the specified hazard level only when used as a set. At any particular period, the median spectral acceleration of the set may match the target values reasonably well; however, any individual record may have a value considerably different than target spectral acceleration. Therefore, performance assessment must be done based on the predicted seismic demands obtained by utilizing the whole set. The dispersions[1] for the spectral accelerations for Los Angeles and Seattle ground motion sets are given in Figure 3.4.

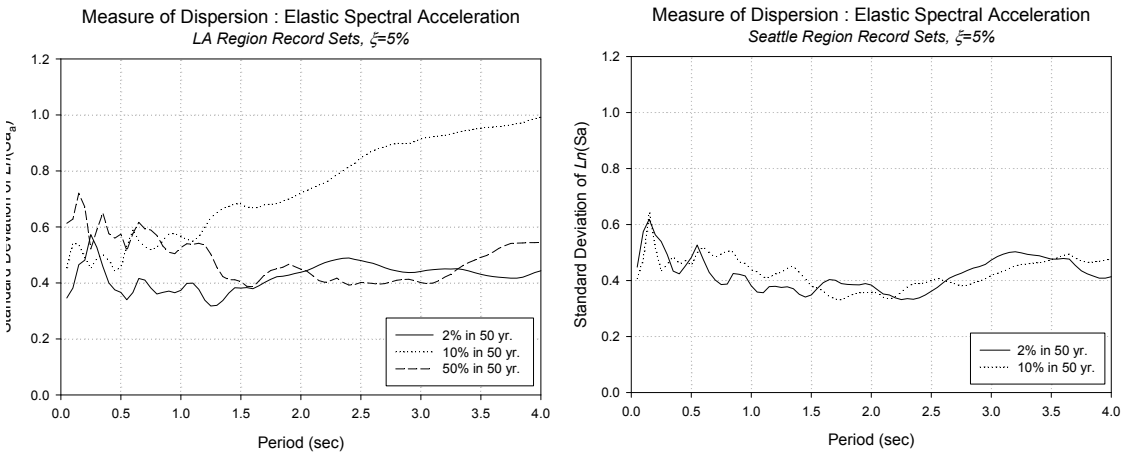

Figure 3.6 Dispersion of the elastic spectral acceleration for Los Angeles region (left) and Seattle (right) ground motion sets.

3.4. Passive Control Systems with SMA Connections Designed and Evaluated

Two passive control systems utilizing SMA-based, partial-strength, partially restrained moment connections are chosen for implementation with the two PR buildings: (1)

1. The dispersion is defined as and the standard deviation of the natural logarithm of the data, σ_{ln}, assuming that the data are log-normally distributed.

martensitic SMA connection system and (2) superelastic SMA connection system. Both systems are based on the connection prototype (Figure 3.7) tested by Ocel et al. (2004).

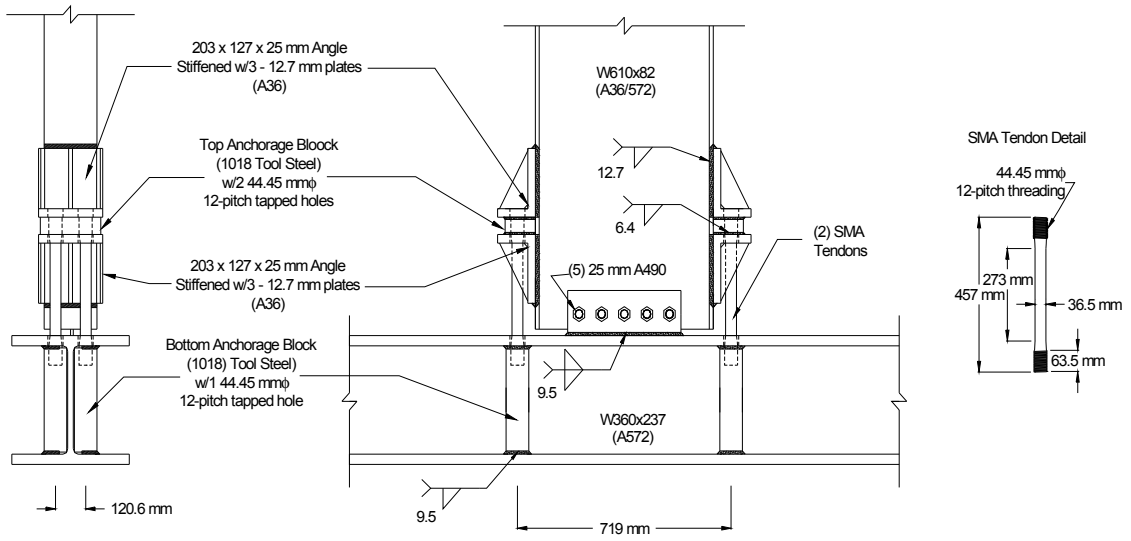

*Figure 3.7 Details of SMA-based connection (*Ocel et al., 2004*).*

The connection consisted of four large-diameter martensitic SMA bars connecting the beam flange to the column flange and serving as the primary moment transfer mechanism. The design was based on exploiting the favorable deformation modes of the material. SMA tendons have been shown to be most efficient when deformed under axial force when compared to the behavior under bending and torsion (MANSIDE, 1998), hence the optimum connection design must maximize the axial deformations of the SMA. This was achieved by placing the SMA bars on the outside of the beam flanges and utilizing a slotted shear tab to force the rotation about the beam's neutral axis, maximizing the axial deformation of the tendons.

The moment-rotation characteristics of the connection in Figure 3.7 depend mainly on the mechanical properties of the alloy, bar diameter and length, and the moment arm (beam depth) of the tension-compression couple formed by the SMA bars. Since SMAs are more flexible and weaker than structural steel (see Table 2.1), particularly in the martensitic form, the prototype is a partial-strength, partially restrained connection. Even though the resulting connection detail in Figure 3.7 may not necessarily reflect a typical connection, it does allow for a proof-of-concept investigation of the feasibility of integrating SMAs into steel moment connections.

The design of a SMA connection first requires the selection of the alloy. (See Section 2.3 for detailed explanation of SMAs and their properties). SMAs are characterized by their transformation temperature, but to specify the transformation temperature alone is not enough to obtain the desired material for a specific application. The chemical composition (impurity levels), the mechanical properties, dimensions and tolerances, and the surface finish are common data on the materials specification sheet (Serneels, 1999). However, structural design decisions are based on the mechanical properties of the alloy rather than its chemical composition, and on the assumption that a manufacturer should be able to provide the alloy with the required composition that has the desired mechanical properties.

A certain composition of the alloy with a given initial modulus of elasticity and loading plateau stress in superelastic and martensitic forms is selected for each PR frame design and is used in all SMA connections. This decision is based on the argument that it would be impractical to specify an alloy with different composition (leading to different initial moduli of elasticity and loading plateau stresses) for each type of connection.

The SMA bar dimensions are selected so that the resulting SMA connection detail has an initial stiffness that is equal to that of the PR connection detail it is replacing. Moreover, the resulting SMA connection should have an ultimate moment equal to or greater than that of the equivalent PR connection (Figure 3.8). This equivalence is achieved by limiting the yield moment of the SMA connection to the ultimate moment capacity of its PR counterpart. Additional moment capacity can be provided by means of non-zero post-yield stiffness. These two design constraints are based on keeping the frames with SMA connections code-compliant by means of satisfying the drift and strength requirements imposed on the original PR designs.

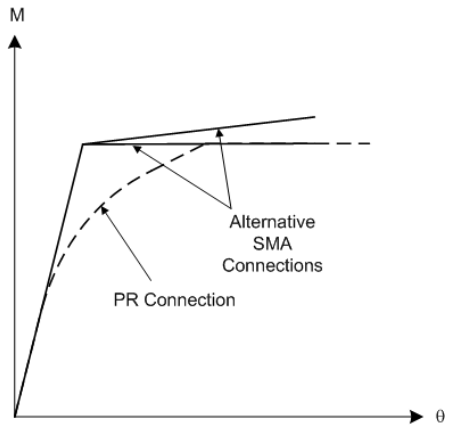

Figure 3.8 PR and SMA connection moment-rotation backbone curves.

After selecting the alloy, the dimensions of the SMA bars must be determined. Again, for practical reasons (such as to prevent high cost and difficulties in machining and treating the material), the bar diameter and the bar length are limited to 1.5 in. and 15 in., respectively. The bar diameter is selected to meet the ultimate moment criteria while the bar length is adjusted to meet the initial stiffness constraint imposed on the design. The

design also optimizes the length of the SMA bars so as to achieve rotation in the connection to reach the limits where the characteristics of the alloy start to degrade. This approach results in a connection detail with high rotational ductility, but also requires the SMA bars to be restrained from buckling.

The design and implementation of the passive control systems with martensitic and superelastic SMA connection for the three- and the nine-story PR frames are described in the following sections.

3.4.1. Martensitic SMA System

The martensitic SMA connection uses martensitic SMA bars as the elements connecting the beam flange to the column web at beam-to-column joints. Utilization of martensitic SMA bars as the main deformable component of the connection is aimed at having high energy dissipation and plastic rotation capacity, and the possibility of recovering the permanent deformations, based on the unique characteristics of the martensitic SMA material. Martensitic SMA connections are designed through the selection of material properties, such as initial modulus of elasticity, loading plateau stress and stiffness, and physical properties, such as bar length and diameter. The properties of martensitic SMA bars satisfying the design constraints explained in the previous section are presented in Table 3.7.

Table 3.7 Dimensions and mechanical properties of martensitic SMA bars for 3- and 9 -story PR building connections.

Corresponding PR Connection Detail	Initial Elastic Modulus (ksi)	Loading Plateau Stress (ksi)	Number of Bars per Beam Flange	Gage Length (in)	Bar Diameter (in)
LA 3-Story PR					
Top and Seat Angle	6000	39	2	8.50	1.19
Composite			2	8.10	1.50
SE 9-Story PR					
T-Stub on W18	5100	20	3	10.80	1.48
T-Stub on W21			3	11.80	1.48
T-Stub on W24			3	12.70	1.48
T-Stub on W27			3	13.80	1.48
T-Stub on W30			3	14.70	1.48

3.4.2. Superelastic SMA System

The superelastic SMA connection uses superelastic SMA bars as the elements connecting the beam flange to the column web at beam-to-column joints. Utilization of superelastic SMA bars as the main deformable component of the connection is aimed at having recentering capability as well as some energy dissipation capacity. Superelastic SMA connections are designed through the selection of material properties, such as initial modulus of elasticity, loading and unloading plateau stresses and loading plateau stiffness, and physical properties, such as bar length and diameter. The properties of superelastic SMA bars satisfying the design constraints explained at the previous section are presented in Table 3.8.

Table 3.8 Dimensions and mechanical properties of superelastic SMA bars for 3- and 9 -story PR building connections.

Corresponding PR Connection Detail	Initial Elastic Modulus (ksi)	Loading Plateau Stress (ksi)	Number of Bars per Beam Flange	Gage Length (in)	Bar Diameter (in)
LA 3-Story PR					
Top and Seat Angle	9200	39	2	12.50	1.19
Composite			2	12.50	1.50
SE 9-Story PR					
T-Stub on W18	8100	31	3	11.10	1.19
T-Stub on W21			3	12.10	1.19
T-Stub on W24			3	13.10	1.19
T-Stub on W27			3	14.10	1.19
T-Stub on W30			3	15.00	1.19

CHAPTER 4

DESCRIPTION OF MODELING AND ANALYSIS

4.1. Introduction

Seismic performance evaluation is accomplished through various analysis methods performed on a mathematical representation of the structure. The process includes the development of a mathematical model for both the structure and the loading conditions, performing the analysis, and interpretation of the results.

Aseismically designed structures are expected to deform in the inelastic range even when subjected to design level earthquake ground motions. The seismic energy input is dissipated in the form of hysteretic energy at the components forming the structure. With the addition of SMA connections as a passive control system, the amount of the energy that must be dissipated within the steel structural elements can be reduced and/or the permanent deformations can be decreased. Development of a mathematical model to represent such a structure requires consideration of the inelastic behavior of both steel structural elements and SMA connections.

This chapter discusses the basic structural modeling approach adopted for representing the PR frames and passive control systems with SMA connections described in Chapter 3. The representation of the element behavior in the finite element platform of choice is discussed, including the implementation of new features to enhance the modeling capabilities. The assumptions in the element level as well as global level are documented.

4.2. Evaluation Platform

The Open System for Earthquake Engineering Simulation (OpenSees) is a software framework for advanced simulation of structural and geotechnical systems using finite element methods (McKenna, 1997; OpenSees, 2007; Mazzoni et al., 2007). OpenSees utilizes an object-oriented architecture to maximize modularity and extensibility for implementing models for behavior, solution methods and data processing.

OpenSees has been chosen as the finite element platform for this work for several reasons. First, it allows selection of various material models and finite element formulations, along with different approximations of kinematics to simulate geometrically nonlinear (P-Δ) effects. Second, the platform provides a wide range of solution procedures and algorithms that can be used to analyze the response of highly nonlinear systems subjected to static and dynamic loads. A third feature is that OpenSees has a fully programmable scripting language in Tcl/Tk (Welch et al., 2003) for defining models and solution procedures and for post-processing, making it ideal for parametric studies of large, complex systems. Finally, as an open-source project, it is possible to add additional capability with new material and element formulations and new solution and data processing algorithms.

The following sections describe built-in modeling and analysis capabilities of OpenSees that have been utilized in modeling the PR buildings reviewed in Chapter 3. The modifications done to the finite element platform to add the capability of modeling PR connections, superelastic SMA material behavior, and calculating energy quantities are explained in detail. The command line reference for the new features implemented to OpenSees is presented in Appendix A.

4.2.1. One-Dimensional Hysteretic Force-Deformation Response Models

OpenSees uses a generic one-dimensional hysteretic force-deformation response model (`UniaxialMaterial`[1]) to represent material nonlinearity at the lowest level. In general, uniaxial force-deformation response models are defined by a backbone enveloping the response, unloading/reloading paths, and rules to control the hysteresis and degradation (if any). `UniaxialMaterial` objects are required to model the hysteretic response at cross-sections of nonlinear beam-column elements, at zero-length elements, and at individual fibers of a discretized cross-section.

As a part of this study, two new uniaxial force-deformation response models are implemented. The first represents the moment-rotation behavior of PR connections in a zero-length element, while the second is needed to model the stress-strain behavior of SMAs in the austenitic state in a discretized fiber SMA connection model. To represent the stress-strain behavior of other materials such as structural steel and SMAs in the martensitic state, built-in uniaxial force-deformation response models available in OpenSees are utilized.

4.2.1.1.PR Connection Uniaxial Force-Deformation Relationship

To be able to evaluate the comparative performance of PR frames with SMA connections, the seismic performance of the original PR frame designs should be known. Previous research conducted on these structures (Maison and Kasai, 2000; Maison et al., 2000) utilized a different finite element platform (PC-ANSR; Maison, 1992) along with frame and connection models that were somewhat different from those utilized herein.

1. OpenSees commands/classes corresponding to a certain feature are presented with a different style, e.g. `UniaxialMaterial`.

Therefore, it is necessary to reinvestigate the seismic demands on the original PR frames using the same finite element platform and modeling assumptions as those used to evaluate the frames with SMA connections. This approach reduces the source of differences in the predicted response to utilization of SMA connections alone, making it easier to assess their effect on the seismic performance.

The inelastic behavior of PR connections is intrinsically complex because of the behavior of their components, such as bolts, angles and plates and their interaction. Thus, a PR connection is susceptible to a variety of failure modes that interact with each other. The lack of test data for the PR connection details specified in the frames motivates the selection of a relatively simple empirical model rather than a complicated mechanical model to represent PR connections analytically in the finite element models. Although OpenSees provides a variety of hysteretic uniaxial force-deformation response models, none is capable of adequately modeling the behavior of PR connection details used in the two PR designs. Consequently, a uniaxial force-deformation response model that can represent the moment-rotation behavior of a variety of PR connections is implemented into OpenSees.

The original PR connection moment-rotation algorithm used in the SAC study (Maison and Kasai, 2000) is capable of modeling key trends observed by Leon (1997) from actual connection tests:

- The backbone curve represents the nonlinear behavior observed under monotonic loading, which has shown to provide an accurate envelope of the experimental cyclic data (Bursi et al., 1996; Swanson and Leon, 2000). The envelopes are defined independently; hence this force-deformation response model can be used to simulate

the behavior of structural components with different properties in each loading direction.

- The slip plateau, which can also be defined independently, represents a pinching phenomena related to the development of a gap between the connection components and the column flange. Pinching is characterized by an increase in rotation without significant increase in moment, thus resulting in a reduction of the stiffness of the connection, and is pronounced especially in bolted connections (Astaneh-Asl et al., 1989; Harper and Radziminski, 1990; Bernuzzi et al., 1996).

- Reduced loading stiffness represents softening with increasing inelastic rotation history.

- Limited strain hardening leading to a finite force capacity represents the bounded moment capacity of PR connections.

The original PR connection algorithm is found to model the moment-rotation behavior of various PR connection details reasonably well for small rotations even though it assumes fully ductile behavior. However, the demands reported by Maison and Kasai (2000) from dynamic analyses for the three-story PR frame for the 2% in 50 yr. accelerograms are found to be quite large (median 0.066 rad., 84^{th} percentile 0.097 rad.), and lie beyond the range which many PR connections have been tested. The ability of all connections to survive these events without hysteretic deterioration is highly unlikely.

It is well documented (FEMA, 2000d) that multiple failure modes dominate the behavior of the connection in the inelastic range, and determine the connection resistance and ductility. The failure results in a dramatic loss of resistance and stiffness and/or significant deterioration in behavior, but the connection retains some stiffness and resistance. Due to the influence of a slab, an access hole, or simply due to the asymmetry of the

connection geometry, the connection may fail at different plastic rotation amplitudes and have different residual capacities in positive and negative bending. The retained capacity is not negligible for many connections. Lacking a practical theoretical model that can accurately predict PR connection failure, the PR connection model developed by Maison and Kasai (2000) is extended to account for the limited ductility of PR connections under high rotation demands. Additional parameters are introduced to the original PR connection algorithm along with new logic to handle loading and unloading after the failure. Figure 4.1 shows the envelope for the `PRConnection` uniaxial force-deformation response model and the response for a sample loading (following the sequence a, b, c, d, e, f, g, b, h, i, j, k, l, i, m, n, o). The key points in the force-deformation response explained given in Table 4.1.

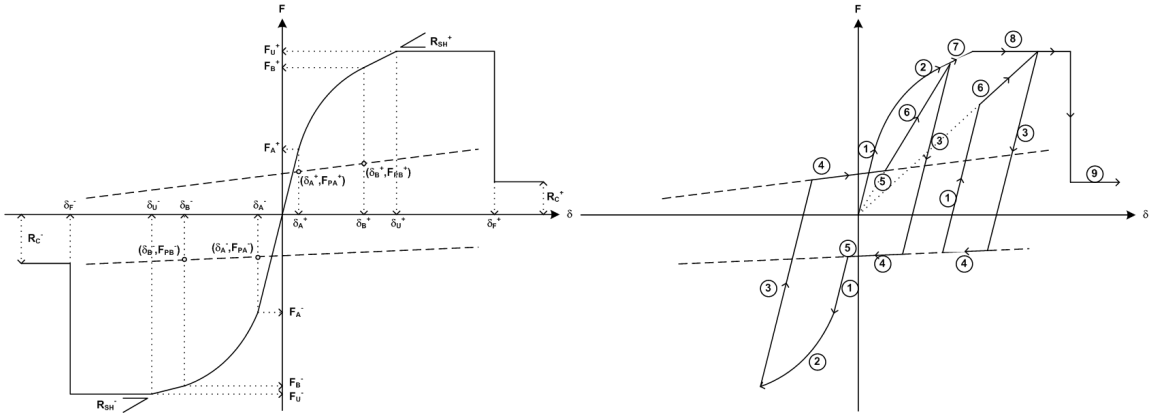

Figure 4.1 Loading envelope for PRConnection force-deformation response model (left, based on Maison and Kasai, 2000) and sample hysteresis (right).

Table 4.1 PRConnection uniaxial force-deformation response model envelope key points.

Segment	Explanation	Deformation (δ)	Force (F)	Stiffness
0-a	Loading with elastic slope	$\delta < \delta_A$	$K_i \cdot \delta$	K_i
a-b	Loading on Richard-Abbot curve	$\delta_A \le \delta < \delta_B$	Equation 4.1	Equation 4.2
b-h	Loading with hardening stiffness	$\delta_B \le \delta < \delta_U$	$F_B + K_p \cdot (\delta - \delta_B)$	K_p
h-i	Force capacity reached	$\delta_U \le \delta < \delta_F$	F_U	Very small
n-o	Deformation capacity reached	$\delta > \delta_F$	$F_U \cdot R_C$	Very small

The terms in Figure 4.1 are defined as follows: δ_A is the control deformation that defines the linear elastic portion of the envelope curve. F_A is the force value corresponding to the control deformation δ_A. The elastic stiffness, K_i, is defined as the ratio of F_A to δ_A. δ_B is the control deformation that defines the end of envelope curve that starts from [δ_A, F_A]. F_B is the force value corresponding to the control deformation δ_B. R_{SH} is the strain hardening constant that defines the plastic stiffness, K_p, after [δ_B, F_B] as a ratio of the initial stiffness K_i. The curve between [δ_A, F_A] and [δ_B, F_B] and its slope are defined by Equation 4.1 and Equation 4.4 that are based on Richard and Abbot (1975) function,

$$F(\delta) = F_A + K_p \cdot \delta + \frac{(K_i - K_p) \cdot \delta}{(1 + \left|C_1 \cdot \delta\right|^n)^{\frac{1}{n}}} \tag{4.1}$$

$$\frac{d}{d\delta}F(\delta) = K_p + \frac{K_i - K_P}{(1 + (\left|C_1 \cdot \delta\right|)^n)^{\frac{n+1}{n}}} \tag{4.2}$$

where K_p is the hardening stiffness obtained by scaling the initial stiffness with the hardening ratio, F_0 is a constant calculated internally, n is the fitting parameter, and the constants C_1 and C_2 are given by Equation 4.3 and Equation 4.4, respectively.

$$C_1 = \frac{1}{\delta_B - \delta_A} \cdot (C_2 - 1)^{1/n} \tag{4.3}$$

$$C_2 = \left| \left(\frac{(K_i - K_p) \cdot (\delta_B - \delta_A)}{(F_B - F_A) - (K_p \cdot (\delta_B - \delta_A))} \right)^n \right| \tag{4.4}$$

F_{PA} and F_{PB} are the control forces corresponding to δ_A and δ_B that lie on the pinching envelope. F_U is the force corresponding to the ultimate strength while δ_U is the deformation where the ultimate strength is reached. Field as well as experimental observations indicate that a failure mode can occur prior to the occurrence significant plastic deformation; typically, however, the initial failure is assumed to occur when the total deformation reaches a particular amplitude, δ_F. R_C is the residual strength left (as a ratio of the ultimate strength) after the deformation capacity δ_F is reached. Once failure has occurred, the moment strength drops for bending at both positive and negative directions, the pre-failure strain hardening is lost and the hysteresis becomes bilinear with the residual strength as the limiting force.

4.2.1.2.Superelastic SMA Uniaxial Force-Deformation Relationship

Modeling of SMA hysteretic behavior is critical to evaluating the performance of PR frames with SMA connections. As was the case for PR connection moment-rotation behavior, it was not possible to simulate the stress-strain behavior of SMAs in the austenitic state that exhibit the superelastic effect with the available uniaxial force-deformation response models in OpenSees, and a new `UniaxialMaterial` was

implemented. A phenomenological force-displacement relationship based on key trends observed from limited material tests on large diameter SMA bars (DesRoches et al., 2004) was chosen for this purpose. The proposed response model is capable of representing the following:

- The envelopes are defined independently; hence this force-deformation response model can be used to model the behavior of SMAs in the austenitic state with different properties in each loading direction.

- Loading and unloading plateaus where transformation from austenite to martensite and vice versa takes place forms a hysteresis loop and represents the superelastic effect. Both plateaus are idealized to occur with the same stiffness at a constant force.

- Transformation from austenite to martensite is completed at the end of the loading plateau. Increased loading stiffness following the loading plateau represents elastic deformation of fully-transformed martensite.

Figure 4.2 shows the envelope for the `SuperelasticSMA` uniaxial force-deformation response model and the response for a sample loading (following the sequence a, b, c, d, e, f, g, b, h, i, j, k, l, i, m, n). The key points in the force-deformation response are given in Table 4.2.

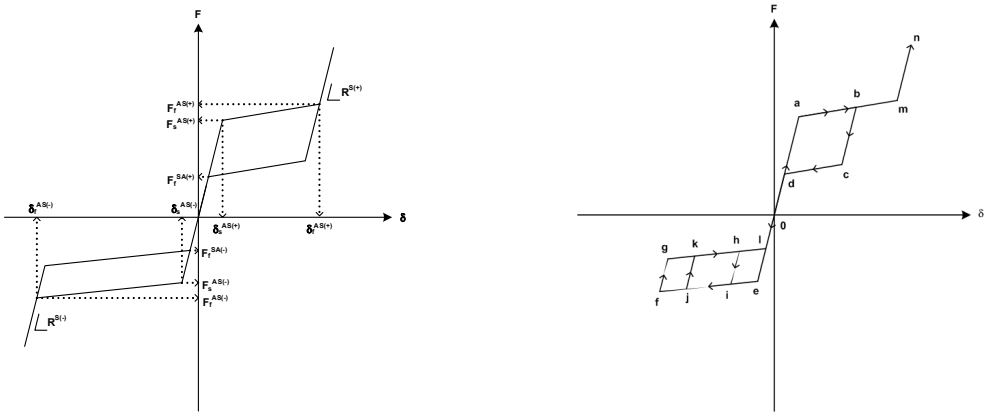

Figure 4.2 Envelope for SuperelasticSMA uniaxial force-deformation response model (left, based on DesRoches et al., 2004) and sample hysteresis (right).

Table 4.2 SuperelasticSMA uniaxial force-deformation response model envelope key points.

Segment	Explanation	Deformation (δ)	Force (F)	Stiffness
0-a	Elastic deformation of Austenite	$\delta < \delta_s^{AS}$	$K_i \cdot \delta$	K_i
a-m	Transformation from Austenite to Martensite	$\delta_s^{AS} \le \delta < \delta_f^{AS}$	$F_s^{AS} + K_i \cdot (\delta - \delta_s^{AS})$	$\frac{F_s^{AS} - F_f^{AS}}{\delta_s^{AS} - \delta_f^{AS}} \cdot K_i$
b-h	Elastic deformation of Martensite	$\delta \le \delta_f^{AS}$	$F_f^{AS} + R^S \cdot K_i \cdot (\delta - \delta_f^{AS})$	$R^S \cdot K_i$

The terms in Figure 4.2 are defined as follows: F_s^{AS} is the control force that defines the start of the loading plateau where transformation from austenite to martensite takes place. δ_s^{AS} is the deformation value corresponding to the control force F_s^{AS}. The initial modulus of elasticity, K_i, is defined as the ratio of F_s^{AS} to δ_s^{AS}. F_f^{AS} is the control force that defines the end loading plateau and the point of transformation from austenite to martensite. δ_f^{AS} is the deformation value corresponding to the control force F_f^{AS}. Similarly, F_f^{SA} is the control force that defines the end of transformation from martensite

to austenite. R^S is the hardening constant that defines the elastic stiffness of fully transformed martensite as a ratio of the initial stiffness K_i.

The ability of the `SuperelasticSMA` force-deformation response model to represent the stress-strain behavior of SMAs in their austenitic state is verified using the experimental data for a 280 mm. long, 25.4 mm. diameter Ni-Ti superelastic SMA bar that was tested dynamically by DesRoches and Delemont (2002). A single degree-of-freedom model consisting of one `SuperelasticSMA` spring is developed using OpenSees and its stress-strain response is obtained by imposing the experimental strain history of the superelastic SMA rod as loading. Good agreement between the experimental and simulated stress-strain responses is achieved (Figure 4.3).

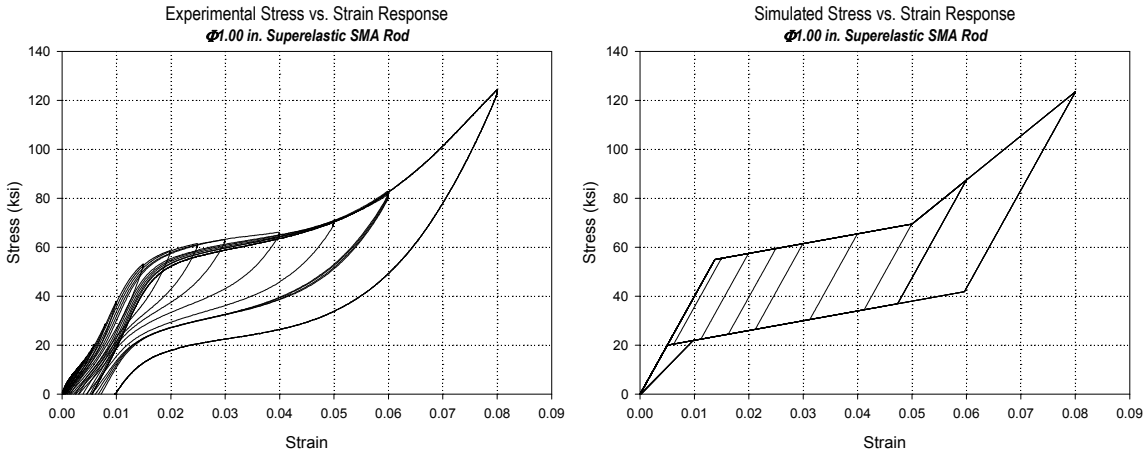

Figure 4.3 Experimental (right, DesRoches and Delemont, 2002) and simulated (left) stress-strain response of 6.00in long superelastic SMA rod (ϕ1.00in).

Even though the phenomenological superelastic SMA model presented in this section captures the hysteretic behavior and the superelastic effect, it still has several limitations. This model neither has the ability to capture degradation of the loading and unloading

plateaus nor the accumulation of residual strain with continued cyclic loading. Furthermore, incomplete cycling is accounted for by unloading at the initial stiffness until the unloading plateau is reached, which has been shown to be inconsistent with experimental data. Previous studies have shown that mechanically training (McCormic et al., 2005) or prestressing superelastic SMAs could result in stable properties which are consistent with the proposed model. Furthermore, sensitivity studies to determine the most appropriate method of modeling the superelastic effect in terms of both accuracy and ease of implementation have led to the recommendation to use simplified phenomenological models instead of more detailed micro mechanical models (Andrawes et al., 2004).

4.2.1.3.Martensitic SMA Uniaxial Force-Deformation Relationship

Unlike the case for the PR moment-rotation and superelastic SMA stress-strain behavior, it was possible to model the stress-strain behavior of SMAs in the martensitic state with `Hysteretic` uniaxial force-deformation model available in the OpenSees material library with reasonable accuracy. The model has a trilinear backbone that can be defined independently for each loading direction, and can represent degraded unloading stiffness based on ductility[1].

1. Ductility is defined as the ratio of the maximum deformation to the deformation at yield.

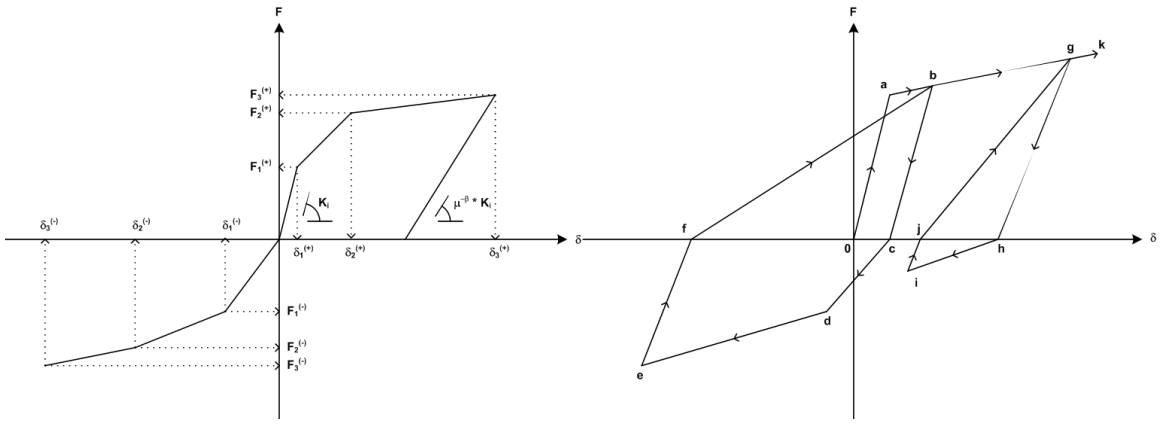

Figure 4.4 Envelope for hysteretic uniaxial force-deformation response model (OpenSees, 2007) and sample hysteresis (right).

Figure 4.4 shows the envelope for the uniaxial force-deformation response model to be used in modeling the stress-strain behavior of martensitic SMAs. The parameters are defined as follows: F_1 and F_2 are the forces at the first and second change of stiffness. δ_1 and δ_2 are the deformations corresponding to the forces F_1 and F_2 respectively. F_3 is a force at the third stiffness branch (any point). δ_3 is the deformation corresponding to the force F_3. The initial modulus of elasticity, K_i, is defined as the ratio of F_1 to δ_1. β is the power used to determine the degraded unloading stiffness based on ductility, μ.

The ability of the `Hysteretic` uniaxial force-deformation response model to represent the stress-strain behavior of SMAs in the martensitic state is verified using the experimental data for an 18 in. long, 1.4375 in. diameter Ni-Ti bar tested by Ocel (2002). A single degree-of-freedom model consisting of one `Hysteretic` spring is developed using OpenSees and its stress-strain response is obtained by imposing the experimental strain history of the martensitic SMA rod as loading. Good agreement between the experimental and simulated stress-strain responses is achieved (Figure 4.5).

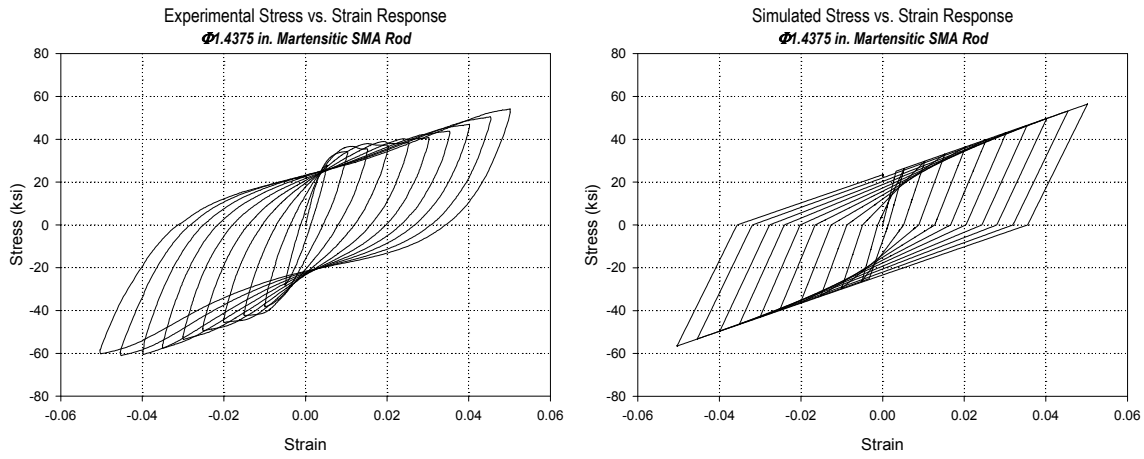

Figure 4.5 Experimental (right) and simulated (left) stress-strain response of 10.75in long martensitic SMA rod (ϕ1.4375in).

Even though the phenomenological martensitic SMA model presented in this section captures the hysteretic behavior and the high energy dissipation capacity of the material, it also has several limitations. The model slightly underestimates the reloading stiffness during cycling of the material in small strains. Plastic deformation of twinned martensite that takes place at high strain levels (> 6-8%) is not modeled, either. However, the latter is less of a concern since a good design of the SMA connection should not result in demands pushing the material into the range of undesirable behavior. Finally, the "yield plateau" observed in the experimental response under small strains is not fully captured. The model uses a lower yield stress and a constant strain hardening slope, resulting in a more accurate representation of strength and stiffness at larger strains at the expense of underestimated strength and stiffness at smaller strains.

4.2.2. Section Force-Deformation Response Models

OpenSees uses `Section` objects to represent the stress resultant relationship at a cross-section of a beam-column element or in a zero-length element. Each `Section`

object uses one or more `UniaxialMaterial` object(s) to define the nonlinear description of the force-deformation response. Two basic approaches are available to find the response of a cross-section: resultant models and fiber section models.

Resultant models explicitly define section response in terms of moment-curvature, axial load-axial strain, etc. and represented with `UniaxialSection` objects in OpenSees. A `UniaxialSection` object represents the response of a cross-section in one degree-of-freedom, following linear or nonlinear relationships defined by a `UniaxialMaterial` object. Several `UniaxialSection` objects can be combined in an uncoupled way to model the complete response of the cross-section (e.g. combining a moment-curvature with a shear force-shear deformation relationship).

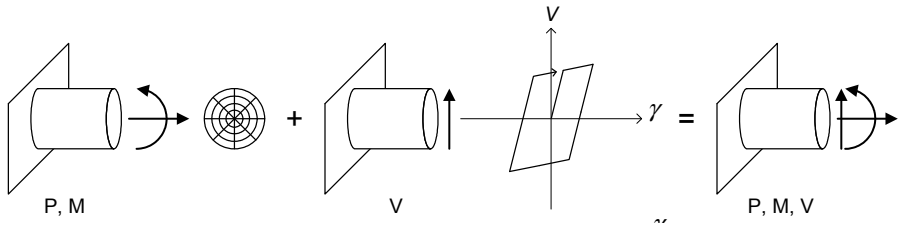

Figure 4.6 Complete representation of a cross-section by aggregation of fiber and uniaxial section responses.

Fiber section models are based on discretization of the cross-section into smaller regions (fibers) for which the material stress-strain response is integrated over the cross-sectional area to obtain stress resultants such as axial force and bending moment, and is represented with `FiberSection` objects in OpenSees. A `FiberSection` object represents the response in two degrees-of-freedom, axial translation and rotation. The stress-strain response of each fiber is defined by a `UniaxialMaterial` object. The

fiber formulation is based on the assumption that plane sections remain plane, which is reasonably accurate even well into the inelastic range. Even though the shear stresses are neglected when calculating the section response, a `FiberSection` object can still be combined (again, without coupling) with a `UniaxialSection` object that represents shear force-shear strain relationship to have a complete representation of the cross-section (Figure 4.6). The axial force-moment interaction is inherent in such models.

In this study, two connection section models were developed in OpenSees to be used in zero-length connection elements. The connection section models make use of the previously implemented (`PRConnection`, `SuperelasticSMA`) and already available (`Hysteretic`) uniaxial material models to represent the force-deformation behavior. The first is a resultant section model for modeling the original PR connections. The second is a fiber section model for modeling SMA connections.

4.2.2.1.PR Connection Section

A resultant section model is developed to model the moment-rotation behavior of the PR connections in the original PR frame designs. A `UniaxialSection` is defined with a `PRConnection` uniaxial force-deformation response model and the section behavior is set to represent the moment-rotation response. The resulting connection section has a single degree-of-freedom that is rotation.

4.2.2.2.SMA Connection Section

The SMA connection tested by Ocel et al. (2004) was designed with the philosophy of simplifying the analysis of internal forces within the connection. The slotted holes in the shear tab allowed for free rotation of the beam, and the moment is transferred through a

force couple due to tension-compression of the SMA bars. This makes it possible to simplify SMA connections subject to cyclic bending moments to SMA bars under tension and compression and facilitates utilization of a fiber modeling approach. The fiber modeling approach is based on the observation that cyclic behavior of beam-to-column connections can be predicted by properly combining the cyclic response of its basic components. The connection is idealized as two rigid bars connected by an assembly of nonlinear springs representing the axial response of connection components contributing to the stiffness and moment resisting capacity.

In fiber modeling of a SMA connection, each structural component, such as a shear tab or a SMA bar, is a fiber. A `FiberSection` object is constructed with three fibers, two of which are for the SMA bars sitting at the top and the bottom flanges of the beam, and the last one is for the shear tab. Fibers corresponding to SMA bars are offset away from beam's neutral axis such that the they are separated by a distance equal to the beam depth, and the shear tab fiber is placed at the neutral axis of the beam. The rotation of the beam transforms into pure axial displacement at the SMA bars. Each SMA fiber is assigned an appropriate `UniaxialMaterial` corresponding to the type of SMA used in the connection detail (`SuperelasticSMA` for superelastic or `Hysteretic` for martensitic SMA connection). The shear tab fiber is assigned a very stiff elastic material to eliminate pure axial deformation mode of the resulting fiber connection model. This is based on the assumption that the axial force would be transferred to the beam by the shear tab, without causing axial deformations on the SMA bars. Making use of the "plane sections remain plane" assumption, fiber stresses are calculated from fiber strains. Fiber stresses are, then, integrated over the cross-sectional area to obtain the stress resultants

such as axial force and moment. The resulting fiber section (Figure 4.7) has two degrees of freedom: axial deformation and rotation.

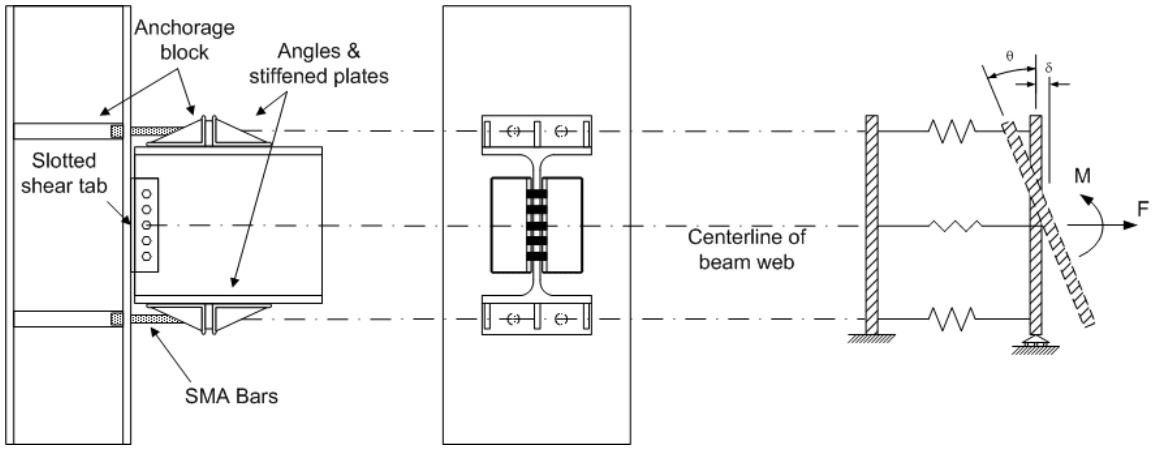

Figure 4.7 Fiber SMA connection section.

4.2.3. Zero-Length Elements

OpenSees uses `ZeroLengthSection` objects to represent elements defined by two nodes at the same geometric location, hence they have zero length. Each `ZeroLengthSection` object uses a `Section` object which represents the force-deformation relationship for the element to connect its nodes. The degrees-of-freedom of the `Section` object determines the degrees-of-freedom of the resulting zero-length element. In this study, two zero-length connection elements were developed in OpenSees to be used in modeling the PR and SMA connections in the finite element models of the frames. The connection elements make use of the previously developed connection section models PR and SMA connections to represent the section behavior of the connection. The first is a connection element for modeling the original PR connections and the second is for modeling SMA connections.

4.2.3.1.PR Connection Zero-Length Element

A connection element that can represent the moment-rotation relationship of a PR connection can be obtained by assigning a PR connection section to a `ZeroLengthSection` element. Rotational degree-of-freedom of the two nodes of the element is connected by the PR connection section object. The remaining translational degrees-of-freedom are constrained to move together with two multi-point constraints.

The ability of the original PR connection algorithm to represent the moment-rotation behavior of PR connections was demonstrated by Maison and Kasai (2000) against experimental data for top and seat angle (Bernuzzi et al., 1996) and T-stub connections (Leon et al., 1994). The empirical approach for modeling the moment-rotation response of PR connections adopted for this study, as well as in the SAC project, is suitable for curve-fitting the actual experimental cyclic response. It should be noted that the actual PR connection details for the three- and nine-story frames were not tested, and the parameters for the connection model had to be obtained from design guidelines and/or experimental studies on comparable connection details by Maison and Kasai (2000).

4.2.3.2.SMA Connection Zero-Length Element

A connection element to model the moment-rotation relationship of a SMA connection can be obtained by assigning an SMA connection section to a zero-length element (`ZeroLengthSection`). Axial and rotational degrees-of-freedom of the two nodes of the element are connected by the SMA connection section object. To take into account the effect of the shear tab, the remaining translational degree-of-freedom is constrained by a multi-point constraint. This could have also been achieved by assigning a rigid elastic uniaxial material to represent the section behavior under shear, and combining it

with the fiber section to obtain a zero-length element with three degrees-of-freedom. However, the aforementioned approach has found to be computationally more efficient since it uses one less degree-of-freedom per connection element and created less convergence problems in preliminary studies.

The ability of the fiber connection model to predict the moment-rotation behavior of a martensitic SMA connection was verified using the experimental data for the SMA connection tested by Ocel (2002). The verification is two-fold. First, the parameters for the `Hysteretic` uniaxial force-deformation response model that is used to model the SMA in the martensitic state are obtained by curve fitting the experimental stress-strain data for one of the SMA tendons obtained during the testing of the SMA connection (Figure 4.8).

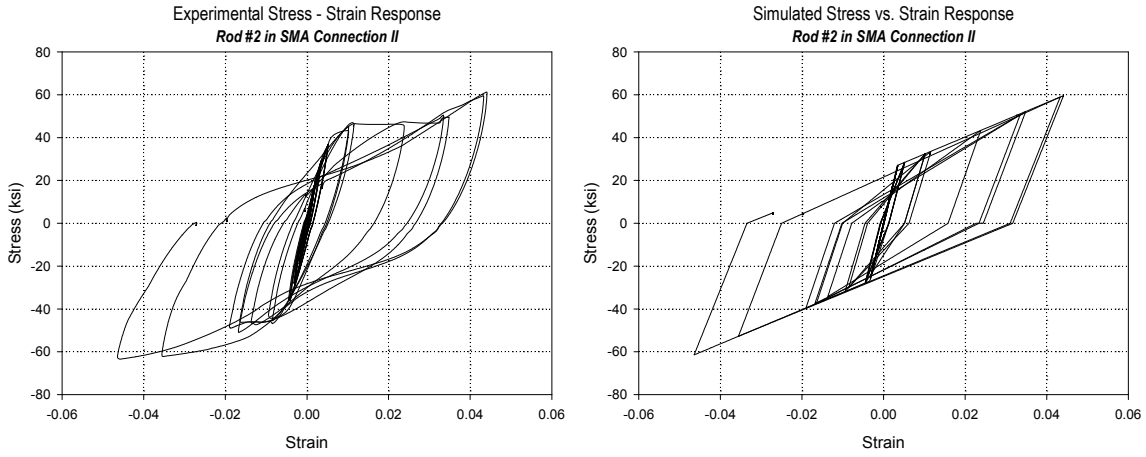

Figure 4.8 Experimental (right, Ocel, 2002) and simulated (left) stress-strain response of martensitic SMA bar #2 during experimental testing of SMA connection.

Second, the fiber connection model is constructed using the physical dimensions of the tested connection and by assigning the `Hysteretic` uniaxial force-deformation

response model calibrated previously to the fibers representing the SMA bars in the connection. A rigid fiber is assigned to shear tab.

A three degree-of-freedom model consisting of one SMA Connection zero-length element connecting two nodes at the same coordinates is built in OpenSees and its moment-rotation response is obtained by imposing the experimental concentrated rotation history of the SMA connection as loading. A good agreement between the experimental and predicted moment-rotation responses is achieved (Figure 4.9), proving the capability of the proposed fiber connection model to predict the moment-rotation response of different SMA connection details. It is always possible to improve the accuracy of the fiber model by employing refined uniaxial models for fibers and by using a finer discretization for the connection cross-section.

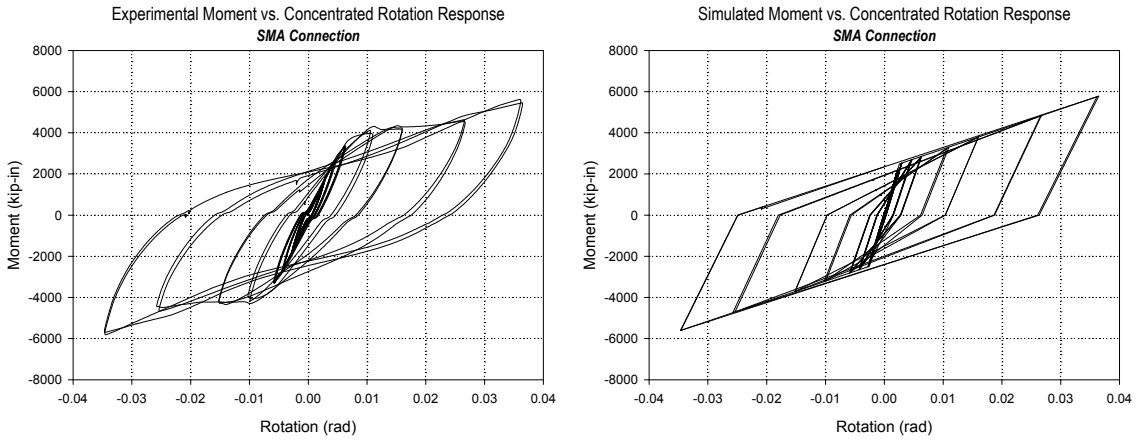

Figure 4.9 Experimental (right, Ocel, 2002) and simulated (left) moment-concentrated rotation response of SMA connection II.

Ideally, the same verification procedure should be followed to test the ability of the proposed fiber connection model to predict the moment-rotation response of a superelastic SMA connection. Due to the lack of test data for the connection detail with superelastic SMA components, it is assumed that the same fiber connection model is applicable to both types of SMA connections investigated in this study.

4.2.4. Monitoring of Energy Quantities

OpenSees uses `Recorder` objects to monitor the state of the model during an analysis, and to store this state to a file or database at selected intervals. The monitored parameter could be the drift history between two nodes in a transient analysis, or the entire state of the model at the end of each converged analysis step. Usually several recorder objects are created by the analyst to monitor various response quantities during the analysis. Recorders provide the flexibility of selecting the response quantities that are to be stored, saving valuable storage space and speeding up the analysis by not accessing the storage unit as frequently as it is the case for storing every possible response quantity.

Energy quantities such as the damping and hysteretic energy are of importance for performance evaluation since they provide insight to the distribution of dissipated earthquake energy and the development of the structural damage. OpenSees does not provide any means of recording energy quantities during a transient analysis; hence a new `Recorder` that can monitor kinetic, damping and strain energy quantities is implemented. The energy stored in a structure at any instant of a transient analysis can be decomposed into the strain (recoverable elastic strain and dissipated hysteretic) energy, damping energy and kinetic energy. Starting from the equations of motion of a multi degree-of-freedom (MDOF) structure subjected to ground motion (Equation 4.5),

$$[M]\cdot\left\{\frac{d^2}{dt^2}U(t)\right\}+[C]\cdot\left\{\frac{d}{dt}U(t)\right\}+[K(t)]\cdot\{U(t)\}=-[M]\cdot\{1\}\cdot\left\{\frac{d^2}{dt^2}Y(t)\right\} \tag{4.5}$$

where *[M]* is the mass matrix, *[C]* is the damping matrix, *[K(t)]* is the tangent stiffness matrix at time *t*, *{U(t)}* is the displacement vector at time *t*, and $\left\{\frac{d^2}{dt^2}Y(t)\right\}$ is the ground acceleration vector at time *t*; the energy quantities can be calculated as follows (Zahrah and Hall, 1982):

- The total energy input to the structure due to the ground acceleration is given by

$$E_I=-\int_0^t\left(\left\{\frac{d}{dt}U(t)\right\}^T\cdot[M]\cdot\{1\}\cdot\left\{\frac{d^2}{dt^2}Y(t)\right\}\right)dt \tag{4.6}$$

- The total kinetic energy is given by

$$E_K=\int_0^t\left(\left\{\frac{d}{dt}U(t)\right\}^T\cdot[M]\cdot\left\{\frac{d^2}{dt^2}U(t)\right\}\right)dt \tag{4.7}$$

- The total energy dissipated by viscous damping is given by

$$E_D=\int_0^t\left(\left\{\frac{d}{dt}U(t)\right\}^T\cdot[C]\cdot\left\{\frac{d}{dt}U(t)\right\}\right)dt \tag{4.8}$$

- Finally, the total energy dissipated by hysteresis including the recoverable strain energy stored at any instant can be found by

$$E_H+E_D=\int_0^t\left(\left\{\frac{d}{dt}U(t)\right\}^T\cdot[K(t)]\cdot\{U(t)\}\right)dt \tag{4.9}$$

For energy equilibrium, the input energy from ground motion must be equal to the energy stored and dissipated in the structure (Equation 4.10).

$$E_I=E_S+E_D+E_K \tag{4.10}$$

4.3. Structural Modeling Approach

The focus of this study is on developing a better understanding of the seismic demands on partially restrained steel moment frames with and without SMA connections when subjected to a multitude of ground motions. A compromise between accuracy and efficiency is usually necessary given the scope of the problem being addressed. The critical requirement of the desired model is that it represents all major characteristics of the structure such that the behavior is estimated accurately and, at the same time, is simple enough to be used in deterministic and probabilistic evaluation of seismic demands.

4.3.1. Finite Element Models

As a part of this study, two-dimensional centerline models of the structures are developed using OpenSees. The basic argument in favor of this modeling approach is that the additional flexibility introduced to the system due to using centerline dimensions compensates for the omission of panel zones and the contribution of non-structural elements. The validity of representing three-dimensional structures with two-dimensional frames can be supported by the minimal torsional effects due to the regular floor plan of the structures chosen for investigation.

Deformations in panel zones of beam-to-column joints may contribute significantly to the lateral drift in a SMRF, and even may lead to prediction of an incorrect failure mechanism. However, the effect of modeling panel zones on the predicted response depends on the relative strengths and stiffness of the panel zones and the girders framing into them. More accurate modeling considering panel zones has been reported to have negligible effect on structures with relatively strong panel zones on which the beams are capable of

developing their plastic moment capacity (Krawinkler and Gupta, 1998). Since the panel zones of both PR frames are much stiffer and stronger than the PR connections on the framing girders (Table 3.3, Table 3.6), they are not included in the finite element models based on the recommendations of Gupta and Krawinkler (2000a). This assumption may still lead to overestimated element demands since the moments in the beams and columns are computed at the intersection of the centerlines as opposed to the faces of the columns and the beams. Using Krawinkler's nomenclature (FEMA, 2000f), this corresponds to M1 model utilized in most of the analytical studies of the SAC project.

The contribution of each PR frame to the LFRS is accounted for by including each distinct frame in the finite element model and constraining them to have the same lateral displacements at common floor levels to model the stiff horizontal diaphragm action provided by the concrete filled deck floor system. The beams and the columns are assumed to be made of compact sections with adequate lateral restraint to prevent local buckling. Both structures also have their columns oriented in such a way to provide the structure with similar lateral stiffness in both primary directions, therefore only the frames in the North-South direction are analyzed.

The three-story building has seven PR frames in the North-South direction which are symmetric about column row four (Figure 3.1). Three planar frames are used in the analysis model, making use of the symmetry. The first two frames have properties to model the actual frame members on rows one and two, respectively. The third frame has its stiffness and yield force quantities scaled by one-half so that the stiffness and hysteretic properties of the three frames can capture the behavior of one-half of the building. The columns are assumed to be fixed at the base. The finite element model

(Figure 4.10) has 396 degrees-of-freedom and a total of 81 beam-column and 72 connection elements.

The nine-story building has six PR frames in the North-South direction which are symmetric about the center of the building (Figure 3.3). Three planar frames are used in the analysis model, making use of the symmetry. All frames have properties to model the actual frame members. The columns are assumed to be pinned at the base. The basement level is also restrained horizontally at the ground level. The finite element model (Figure 4.11) has 1989 degrees-of-freedom and a total of 510 beam-column and 300 connection elements.

The following sections describe the modeling approach and assumptions adopted for loads and behavior of structural components.

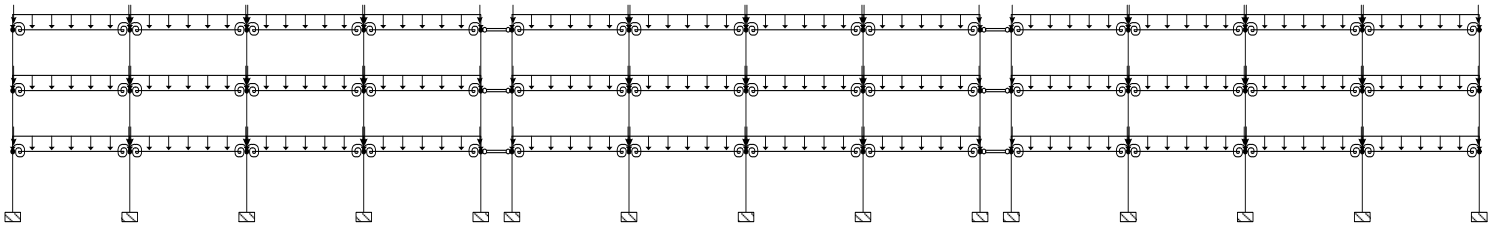

Figure 4.10 LA 3 -story model structure.

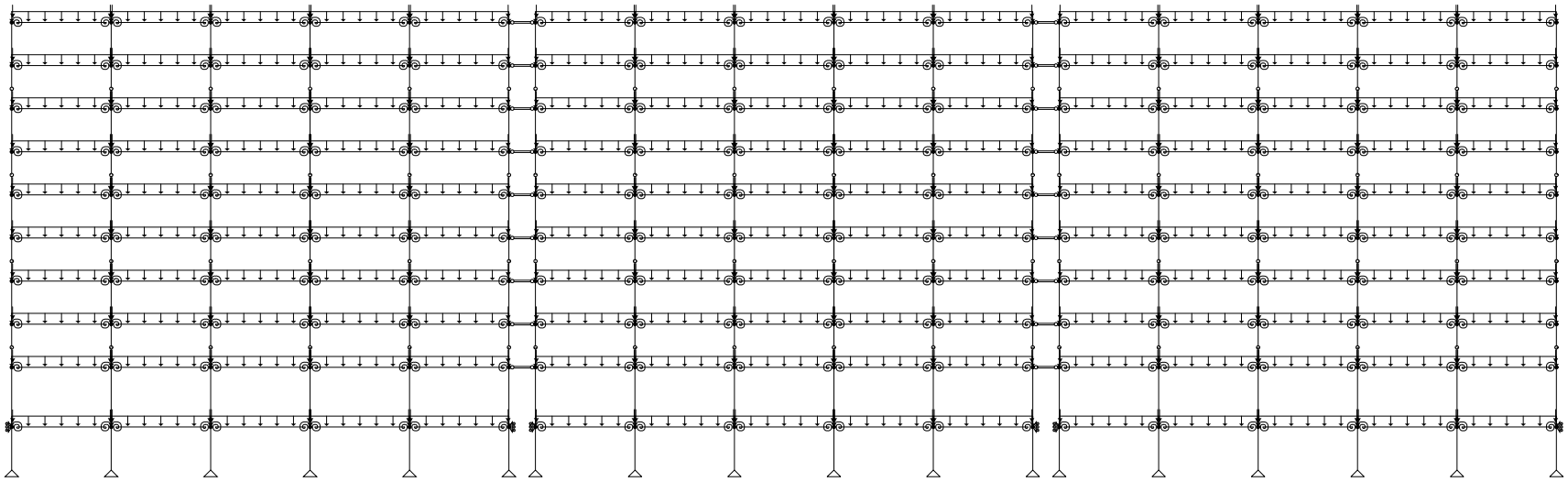

Figure 4.11 SE 9 -story model structure.

4.3.2. Modeling of Beams

Depending on the stage of the analysis, beams consist of elastic portions and partially or completely plastified regions (if any), the location, length and strain distribution of which depend on the geometric properties, boundary conditions, and the loading. In general, the effect of the gravity loads is significantly less than that of the lateral loads, and the regions of plasticity are more likely to occur near the faces of the columns at the beam-to-column connections. Consequently, most engineering analyses adopt a beam model in which the plastified region is represented as a point at beam ends (Chen and Powell, 1982; Prakash et al., 1993; among others). Such a lumped plasticity approach deals with inelastic material behavior in an approximate yet computationally efficient manner. Based on this approach, the beams are modeled with one linear elastic beam-column element (`ElasticBeamColumn`) connected to nonlinear rotational spring elements (`ZeroLengthSection`) at the ends. Each rotational spring element represents the PR beam-to-column connection where the nonlinearity is concentrated. Shear deformations are also are neglected.

The composite floor slab is an integral part of the structural system of the three-story building. For beams typically used in floor systems, the increase in the bending stiffness under positive moment due to the presence of a composite floor slab is in the range of 1.6-1.9 times that of the steel beam alone (Leon, 1998). The effect of the floor slab on the lateral stiffness of the frame is significant, since a considerable portion of floor beams is under positive bending even under large lateral loads. Therefore, to take into account the floor slab participating in the frame action, the beams in three-story frame are assumed to have a moment of inertia based on the average of 60% composite beam moment of inertia and 40% bare steel beam moment of inertia, as suggested by Leon et al. (1996).

The beams in the nine-story building are assumed to have the bare steel beam moment of inertia which is more typical to rigid frame design.

4.3.3. Modeling of Columns

The presence of significant axial force in columns leads to inelastic strain distributions and moment-curvature relationships that are greatly affected by the loading history. As the axial force increases, the plastified regions extend from the ends of the column to a significant portion of the column, diminishing the accuracy of the concentrated plasticity approximation adopted to model beams. This behavior can be modeled more accurately by a distributed plasticity approach that accounts for axial force-moment interaction, where the spread of plasticity along the element length as well as the cross-section is considered.

The flexibility-based distributed plasticity models have been found to be more advantageous for the finite element analysis of framed structures with nonlinear material behavior than the traditional stiffness-based models (Neuenhofer and Filippou, 1997). Flexibility-based elements determine the curvature from equilibrium of forces at each section (integration point), allowing the nonlinear curvature to be captured even with a single element; in contrast, multiple stiffness-based elements with linear curvature are required to approximate the nonlinear curvature distribution along the length of the structural member. The accuracy of the flexibility-based modeling approach can be improved by increasing the number of sections. In contrast, finer discretization and consequently higher computational effort are required to achieve comparable accuracy for stiffness-based models.

Based on the above discussion, one flexibility-based distributed plasticity beam-column element (`ForceBeamColumn`) with four integration points is used when modeling the columns of the three-story building. The nine-story building has column-splices at every other story and requires two elements per column. The moment-curvature relationship of the column cross-sections is represented with a fiber section model. A bilinear steel material model with 3% kinematic hardening is assigned to each of the fibers of the discretized cross-section. The designs are usually based on nominal strength of steel which is very different from the expected strength of the material. However, for performance evaluation, the actual strength of the structural system is better modeled using the mean value of the yield strength rather than the nominal strength (Ellingwood, 2001). Therefore, a mean yield strength of 57.6 ksi (instead of a nominal yield strength of 50 ksi) is used for columns made of A572 Gr. 50 steel.

4.3.4. Modeling of PR Connections

Beam-to-column connections experience several types of deformations when subjected to forces and moments. In general, most connections can transfer axial forces, shears and moments. However, only bending deformation is considered when modeling since it is the predominant deformation for the PR beam-to-column connections investigated in this study.

To be able to make a realistic comparison of the seismic demands for model structures with PR versus SMA connections, values for the parameters defining the empirical connection model described in this chapter (Section 4.2.1.1) can be best estimated form experimental data. However, in this study it was decided to adopt the same parameters as those used to define the PR connection moment-rotation relationship in the SAC study

(Maison and Kasai, 2000). Additional difficulties arise in defining the ultimate rotation capacity of PR connections. Even though a significant number of experimental studies have been carried out on full-scale PR beam-to-column joints under cyclic loads, a general criterion for predicting the plastic rotation capacity is difficult to establish due to the multiplicity of connection details and the high sensitivity of the response to the geometric properties of the connection.

No experimental data on either the connection details or the components utilized in the original PR designs were available to define their ductility and the residual capacity. One possible way is to make use of the fact that the ultimate rotation capacity of the connection is strictly related to the plastic deformation capacity of the weakest component (Faella et al., 1997a; Faella et al., 1997b). This approach makes it possible to predict the ductility of the connection by the ratio of the ultimate deformation capacity of its main moment-resisting component (such as the angle in top, bottom and web angle connections and the T-stub in T-stub connections) to the moment arm (beam depth), but cannot provide information on the remaining residual capacity. Furthermore, experimental tests on connection components and analytical work done on modeling of such components reviewed in Section 2.1.2 recommended caution when using the component models outside the limits of the test cases. Another possible option is to use values from general guidelines (FEMA, 1997; FEMA, 2000g) that provide values for ductility and residual capacity of a variety of PR connections. However, those parameters define monotonic force-deformation relationships, and are highly conservative since they are intended to be used for design rather than for performance evaluation.

As a result, the ductility and the residual capacity of the PR connections of concern are estimated by engineering judgment using the field and laboratory data on the performance of comparable connection details reviewed in Chapter 2. Despite testing and analysis, there remains major uncertainty associated with when and why a PR connection will fracture and how the strength and stiffness of the connection is affected by the failure. Even though the selected values that define the ductility and residual capacity of the PR connection model represent a probable estimate, the actual values that define the mode of failure are random (i.e. vary among similar connection details) and uncertain (due to limited empirical data). However, sensitivity studies done on a similar brittle connection model by Luco and Cornell (2000) showed little sensitivity of the story drift demands to variations in rotation capacity and residual strength. Similar insensitivity was also reported by Song and Ellingwood (1999a, 1999b). Even though the values the PR connection model related to failure are uncertain, the insensitivity of story drift demands to variations in these parameters observed in previous studies suggests that it is not necessary to consider them as random variables for dynamic analysis. Consequently, this effect is ignored in the subsequent analyses.

The following subsections explain the parameters used in the connection models developed for this study and how they are obtained.

4.3.4.1.Top, Seat and Web Angle and Composite Connections

The parameters for the PR connection model for top and seat angle and composite connections (Table 4.3) are the same as the parameters used in the SAC study (Maison and Kasai, 2000):

- The backbone curve and the ultimate moment capacities are based on Leon et al. (1996) and they are different for positive (slab in compression) and negative (slab in tension) bending.

- Initial connection stiffness is derived from the backbone curves as the secant stiffness at +/- 0.0025 rad. rotation. This is intended to represent the stiffness when the connections have undergone several cycles of service level loadings upon which the connections have "shaken down" (Leon, 1997).

- The slip plateaus are based on judgment form connection tests.

Table 4.3 Modeling parameters for composite and top & seat angle connections.

Connection Parameters	Composite Connection		Top & Seat Angle Connection
	(+)	(-)	(+)/(-)
δ_A (rad)	0.00161	0.00161	0.0025
F_A (kip-in)	810	1700	750
δ_B (rad)	0.024	0.020	0.030
F_B (kip-in)	2700	2700	1600
R_{SH}	0.137	0.075	0.036
n	0.5	0.5	0.5
F_{PA} (kip-in)	800	1200	500
F_{PB} (kip-in)	900	1270	600
F_U (kip-in)	2700	2700	1700
δ_U (rad)	0.05	0.05	0.1
R_C	0.333	0.333	0.333
K_i (kip-in)	503106		30000
M_U (kip-in)	2700.0		1700.0
M_{pbeam}(kip-in)	3271.8		3271.8

Although SMRFs with composite connections are a common type of structural system used in low- and mid-rise construction, very little is known about their ultimate strength and ductility. The additional parameters of the modified PR connection algorithm, the

failure rotation and the residual strength, are based on engineering judgment and limited experimental tests on clip angles (Bernuzzi et al., 1996) and composite connections.

4.3.4.2.T-Stub Connections

Similarly, the parameters for the PR connection model for T-Stub connections (Table 4.4) are the same as the parameters used in the SAC study (Maison and Kasai, 2000):

- The backbone curve is that used by the designer.
- Initial connection stiffness is derived from the backbone curves as the secant stiffness at +/- 0.0025 rad. rotation.
- The slip plateaus are based on judgment form connection tests.

Table 4.4 Modeling parameters for T-Stub connections.

T-Stub Connection Parameters	Section				
	W18x35	W21x44	W24x55	W27x84	W30x90
	(+)/(-)	(+)/(-)	(+)/(-)	(+)/(-)	(+)/(-)
δ_A (rad)	0.0025	0.0025	0.0025	0.0025	0.0025
F_A (kip-in)	1180.0	1430.0	1690.0	1970.0	2230.0
δ_B (rad)	0.0200	0.0200	0.0200	0.0200	0.0200
F_B (kip-in)	1870.0	2180.0	2500.0	2820.	3120.0
R_{SH}	0.0045	0.0037	0.0029	0.0029	0.0025
n	0.5	0.5	0.5	0.5	0.5
F_{PA} (kip-in)	590.0	715.0	845.0	985.0	1115.0
F_{PB} (kip-in)	690.0	815.0	945.0	1085.0	1215.0
F_U (kip-in)	1964.0	2290.0	2630.0	2960.0	3280.0
δ_U (rad)	0.065	0.072	0.087	0.092	0.092
R_C	0.2	0.2	0.2	0.2	0.2
K_i (kip-in)	472000	572000	676000	788000	892000
M_U (kip-in)	1964	2290	2630	2960	3280
M_{pbeam}(kip-in)	3271.8	4693.68	6592.8	12004.8	13923.6

The additional parameters of the modified PR connection algorithm, the failure rotation and the residual strength, are based on engineering judgment and experimental tests on T-stub components (Faella et al., 2000; Swanson and Leon, 2000).

4.3.5. Modeling of SMA Connections

The SMA connections are designed to have an initial stiffness that is equal to that of the PR connection detail it is replacing. Their ultimate moment is also required to be equal to or greater than the ultimate moment of the corresponding PR connection. The SMA material model parameters are selected to satisfy the above criteria. Their behavior is modeled to be the same in tension and compression. Tables 4.5 and 4.6 show the parameters used in the uniaxial material models for the martensitic and superelastic SMA bars, respectively.

Table 4.5 Modeling parameters for martensitic SMA material (10% hardening).

Hysteretic Uniaxial Material Parameters	LA 3-Story Building Connections	SE 9-Story Building Connections
	(+)/(-)	(+)/(-)
F_1 (ksi)	39.0	20.0
δ_1	0.00650	0.00392
F_2 (ksi)	78.0	40.0
δ_2	0.07150	0.04314
β	0.25	0.25

Table 4.6 Modeling parameters for superelastic SMA material (10% hardening).

Superelastic SMA Uniaxial Material Parameters	LA 3-Story Building Connections	SE 9-Story Building Connections
	(+)/(-)	(+)/(-)
K_i (ksi)	9200.0	8100.0
F_s^{AS} (ksi)	39.0	31.0
F_f^{SA} (ksi)	73.0	71.0
δ_f^{AS}	0.04120	0.05321
R^S	0.45	0.45

4.3.6. Geometric Nonlinearities

The low strength of PR connections (when compared to their FR counterparts) leads to weak connection-strong column mechanisms under lateral loads, which may increase second order (P-Δ) effects. P-Δ effect is the dominant geometric nonlinearity for frames subjected to lateral loads, and can lead to instability by overcoming the story shear resistance. Consequently, it must be modeled accurately when assessing the seismic performance of flexible structures such as the PR frames investigated in this study. A second order "leaning truss" transformation is utilized to account for the global P-Δ effect. It should be noted that this approach does not account for the influence of axial force on the flexural stiffness of an individual member, i.e. the P-δ effect. Local geometric nonlinearities, such as local buckling of steel components are not considered based on compact sections and laterally braced members assumptions.

4.3.7. Modeling of Viscous Damping

Rayleigh type damping is utilized to model the viscous damping in the structures. It can be represented as

$$[C] = \alpha \cdot [M] + \gamma \cdot [K_i] \tag{4.11}$$

where $[K_i]$ is the initial stiffness matrix, $[M]$ is the mass matrix, and $[C]$ is the damping matrix. Proportional constants α and γ are determined by assigning 2% viscous damping to the first mode and at T = 0.2 sec. This is based on selecting a mode that cumulatively gives a mass participation exceeding 95% and ensuring that none of the relevant modes is getting damped out (Gupta and Krawinkler, 1999).

4.3.8. Modeling of Gravity Loads

The uniformly distributed floor dead and live loads result in uniformly distributed gravity loads on the beams of the SMRF and concentrated loads on the columns due to the orthogonal beams. The uniformly distributed loads are applied to the model as element loads. The concentrated loads that are transferred from orthogonal beams to the columns are modeled as joint loads. An equivalent uniform floor weight of 126 psf representing total dead and live loads is assumed to be present during the earthquake.

4.3.9. Modeling of Seismic Mass

The seismic mass of the structure is lumped at the nodes at each floor level. Only the mass contributing to inertial forces in the horizontal direction is considered. An equivalent uniform floor mass of 100 psf is assumed when determining the corresponding joint masses.

4.3.10. Modeling of Seismic Loads

The seismic base excitation is applied at all column supports simultaneously. When performing nonlinear time history analyses, only the horizontal component of the strong

ground motion is considered. Even though it may be enough to use the portion of the time history reflecting the strong motion duration to obtain response maxima, the entire length of the ground motion record is used for the analysis to facilitate determination of residual response quantities.

CHAPTER 5

EVALUATION OF SEISMIC DEMANDS

5.1. Introduction

In a subsequent chapter (Chapter 6), a probabilistic seismic demand analysis is carried out to evaluate the utility of Shape Memory Alloy (SMA) connections as a passive control system with respect to the drift demand hazard for PR SMRF buildings. As a first step, the effects of SMA connections on the seismic demands are quantified in this chapter. This is achieved by comparing the results of static pushover and nonlinear dynamic analyses for a three- and a nine-story building with PR and SMA connections. Building designs and ground acceleration records summarized in Chapter 3 are considered. As one might expect, the effect of SMA connections depends on the building model, the ground acceleration record, and the structural demand measure of interest. Rather than comparing demand measures for buildings with PR versus SMA connections on a record-to-record basis, several different demand statistics across earthquake records are investigated.

This chapter presents a summary of statistics of several common seismic demand measures to permit the comparison of the performance of SMRFs with SMA connections to their PR counterparts. The determination of structure and component specific limit states for a complete performance evaluation are outside the scope of this study; instead, the relative performance of the controlled and uncontrolled model structures are assessed by the changes (reduction/increase) in the predicted seismic demands.

5.2. Analysis Procedures

In the following sections, the analyses performed using the finite element models representing the structural system are explained.

5.2.1. Modal Analysis

A detailed seismic performance evaluation of a structure requires an understanding of its natural vibration modes, as the large amount of energy acting on a system during seismic activity varies with frequency. An eigen-analysis of the finite element model of the structure is used to extract the periods and mode shapes. The calculated modal properties are based on the elastic stiffness of all elements included in the analytical model.

5.2.2. Static Nonlinear Pushover Analysis (SNPA)

A static nonlinear pushover analysis (SNPA) is a tool used to evaluate the expected performance of a structural system in terms of its strength and deformation demands. Such demands are obtained from a static nonlinear analysis in which the lateral loads are applied to the structure using force patterns that approximately represent the relative inertial forces and are scaled up incrementally until the desired deformation levels are reached either at the structure or the component level. The SNPA is based on the assumption that the response of the system is dominated by a single mode shape which remains constant thorough the time history response. Extensive research (e.g. Krawinkler and Seneviratna, 1998) has been carried out to evaluate the efficacy of this analysis technique under different conditions. It has also been implemented in recent seismic guidelines as a tool to estimate the strength and deformation demands on structural systems (e.g. FEMA, 1997; FEMA, 2000g). This procedure provides an insight into the

load-deformation behavior of the structure over a complete range, from elastic response through yielding and finally to collapse. Nevertheless, it can only identify one possible collapse mechanism; other weaknesses may not be exposed due to the selection of a specified load pattern.

Pushover analyses of the finite element models of the three- and nine-story structures are performed using the design load pattern in the FEMA (1997) guidelines. The relationship between the load pattern and floor heights and seismic weights is given as:

$$C_x = \frac{w_x \cdot h_h^k}{\sum_{i=1}^{n} w_i \cdot h_i^k} \tag{5.1}$$

where C_x is the normalized load at floor level x, w_i and w_x are the seismic weights at floors i and x, respectively; h_i and h_x are heights from the ground level to floors i and x, and k is a factor related to the shape of the fundamental mode that has been taken as 2 for a parabolic load pattern.

Static pushover analysis, when carried out using displacement rather than force control, is particularly useful for estimating sensitivity to P-Δ effects, as the analysis is able to identify the drift range in which a negative post-yield story stiffness develops. This is particularly important since the predicted response becomes very sensitive to modeling assumptions as well as structure and ground motion characteristics if the inertial forces drive the structure into a negative post-yield stiffness range (Gupta and Krawinkler, 1999). It should also be noted that the frame capacity obtained from a static pushover analysis is very conservative (Foutch and Yun, 2002). The elongation of natural period of the structure along with the cyclic nature of the lateral forces induced by the ground

motions help the structure sustain larger drifts in dynamic response than would be predicted by a static pushover analysis.

5.2.3. Nonlinear Time History Analysis (NTHA)

Structures designed to conform to current earthquake specifications are expected to deform well into the inelastic region. A nonlinear time history analysis (NTHA) captures the response of the structure under seismic loads more accurately than is possible with a static analysis. NTHAs performed for this study use a time step of 0.02 seconds or the digitization frequency of the ground acceleration record, whichever is smaller. For the stages of the analysis where difficulties in convergence are encountered, the time step is reduced to a fraction of its original value and the analysis is carried out with the reduced time step until the difficulty in reaching a converged solution is overcome. Residual (permanent) values of the response quantities are obtained by analyzing the free vibration response of the structure after the ground acceleration is finished. The relative displacement, velocity and acceleration of a control node are monitored during the free vibration analysis to determine the point at which the structure reaches to a steady state.

5.3. Seismic Demand Measures

Given the finite element models of the two structures (hereafter referred to as “model structures”) and suites of ground motions representing different levels of seismic hazard, simple measures of performance of the structural systems are necessary to be able to assess the impact of the SMA connections. To represent the structural response, story drift angles, connection rotations, base shear, and the normalized hysteretic energy are chosen as the primary demand measures (DM).

5.3.1. Deformation Based Demand Measures

Among deformation based DMs, roof drift angle (RDA) and inter-story drift angle (ISDA) are the most common measures used to represent the structural response on the global level. The RDA is defined as

$$RDA = \frac{\delta}{H} \tag{5.2}$$

where δ is the peak (over time) roof displacement and H is the structure height. The ISDA is more widely accepted for moment resisting frames since its peak value (over time) has been found to correlate reasonably well with structural damage (Ellingwood, 2001) and structural stability (FEMA, 1997). Furthermore, as a global DM, maximum (over all stories) peak story drift angle ($ISDA_{max}$) is more appropriate than the RDA since in individual stories it may exceed the latter and be indicative of incipient formation of a story mechanism. The $ISDA_{max}$ is defined as

$$ISDA_{max} = max\left(\frac{\delta_i}{h_i}\right), i = 1 \ldots n \tag{5.3}$$

where δ_i is the peak (over time) story drift for story i, h_i is the story height, and n is the number of stories. In an effort to understand better how the SMA connections alter the deformation demands over the height of the structure, the spatial variation of peak story drift angles ($ISDA_i$) will also be investigated.

The low strength of PR connections when compared to the other components of the beam-column joint (panel zone, framing columns and beams) leads to weak connection-strong column mechanisms under lateral loads on the two PR frames considered (Section 3.2). Since most of the local deformation is expected to be concentrated at the

PR connections, the maximum (over all connections) connection rotation (CR_{max}) is also investigated as a deformation based DM.

Limit states of structural performance during earthquakes are measured most frequently in terms of maximum deformations (Song and Ellingwood, 1999b). However, residual deformations are also of importance since they represent the state of the structure after the earthquake. Therefore, the maximum (over all stories) residual story drift angle ($rISDA_{max}$) and its spatial variation ($rISDA_i$), as well as the maximum (over all connections) residual connection rotation (rCR_{max}) are also investigated as residual deformation based DMs.

5.3.2. Force and Energy Based Demand Measures

One of the benefits of using PR frames as LFRSs is the period elongation and the reduced inertial forces due to the additional flexibility introduced to the structure. Peak (over time) base shear (BS) experienced during a seismic event is representative of the magnitude of the inertial forces attracted by the structure, and hence is investigated as a force-based DM.

While $ISDA_{max}$ provides an indication of the structural damage, it does not take into account the cumulative nature of the damage caused by repeated cycles of inelastic deformation. Structural damage is a function of both peak as well as cumulative values of deformation (Williams and Sexmith, 1995), and the hysteretic energy dissipated at various parts of the structure provides additional insight to the development of structural damage. Therefore, the spatial variation of the normalized hysteretic energy (NHE_i) is investigated as a non-dimensional, energy-based DM for different components of the

LRFS. Only the flexural component of the elastic energy capacity is considered in the following formulation of the NHE. This is based on the assumption that the shear and axial force-deformation behaviors are practically linear and the energy dissipation is negligible compared to that due to flexural deformation of the members. The total energy dissipated by hysteresis (including the recoverable strain energy stored) for any component at any instant can be found by

$$E_h = \int_0^t \left(\left\{ \frac{d}{dt} U(t) \right\}^T \cdot [K(t)] \cdot \{U(t)\} \right) dt \tag{5.4}$$

where *[K(t)]* is the tangent stiffness matrix and *{U(t)}* is the nodal displacement vector, both at time *t*. To obtain a non-dimensional DM, the flexural hysteretic energy is normalized by the element's elastic energy capacity, E_e, given by

$$E_e = M_p \cdot \theta_p \tag{5.5}$$

where M_p is the plastic moment capacity and θ_p is the plastic rotation. For beams and columns, with the assumption that the inflection point is at the mid-point, the plastic rotation can be obtained from

$$\theta_p = \frac{M_p}{k} = \frac{M_p \cdot L}{6 \cdot EI} \tag{5.6}$$

where *L* is member length, *E* is the modulus of elasticity, and *I* is the moment of inertia. Finally, normalized hysteretic energy (NHE) can be calculated as

$$NHE = \frac{E_h}{E_e} \tag{5.7}$$

where E_h is obtained from the finite element model as an output of a NTHA using the energy recorders (see Section 4.2.4) implemented into OpenSees as a part this study.

5.3.3. Statistical Analysis of Predicted Demands

The DMs presented in the previous section are each defined with respect to a single seismic event. A statistical analysis is necessary to combine these results across the ground motions in a specific suite representing a specific seismic hazard. As a representative value of a set of values of a specific DM, the primary statistics of interest are the “median” and “one-sigma level” statistics. Along with the dispersion of the data set, this information as a whole provides an estimator for the expected demands on the structural system as well as the scatter in the results.

The median is estimated in two different ways. The log-normal based median (also known as the geometric mean) is a common statistic used in earthquake engineering practice and is the maximum likelihood estimator of the median provided that the data is sampled from a log-normal distribution. The response statistics obtained by log-normal based calculations provide statistical measures that are not highly impacted by the changes in any single data, hence suitable for data sets that may contain outliers. Peak (over time) deformation-based DMs ($ISDA_{max}$, $ISDA_i$, CR_{max}) are found to be characterized by skew-positive distributions and can be suitably modeled by log-normal distributions. The median of lognormally-distributed response quantities of a sample with n ground motions is defined as

$$\hat{x} = \exp\left(\frac{1}{n} \cdot \sum_{i=1}^{n} \ln x_i\right) \tag{5.8}$$

The median given by Equation 5.8 is not finite when any of the samples in the sample set is “infinite”, that is, when the predicted DM is so large that it is physically not possible for the structure to withstand or the numerical algorithm fails to converge to a solution. These

cases are referred to as “collapses” in the subsequent sections. The second estimate is the standard “counted” estimate of the median. The counted median represents the value of which half of the response values in the sample set are above and half are below, and is estimated as the average of 10^{th} and 11^{th} values in a set of 20 simulations. This estimate has the advantage of being defined even if one (or more - up to half of the number of ground motions in the suite) of the observations of the DM is “infinite”. It should be noted that log-normal based statistical analysis is not applicable if the underlying data set is not distributed log-normally. This is found to be case for the force (BS) and energy (NHE_i) based DMs as well as the residuals of the deformation based DMs ($rISDA_{max}$, $rISDA_i$, and rCR_{max}).

“One-sigma level” of DMs can also be calculated in two different ways. Under the log-normal distribution assumption, it is estimated as the median times the exponential of the standard deviation of the natural logarithm of the DM (Equation 5.9).

$$\hat{x}_{84} = \hat{x} \cdot \exp(\sigma_{\ln x}) \tag{5.9}$$

$$\sigma_{\ln x} = \sqrt{\frac{1}{n-1} \cdot \sum_{i=1}^{n} (\ln x_i - \ln \hat{x})} \tag{5.10}$$

The standard deviation of the natural logarithm of the DM (Equation 5.10), referred to as the logarithmic standard deviation, is approximately equal to the coefficient of variation (i.e. the standard deviation divided by the mean) for values less than 0.3. The “counted” one-sigma level value is estimated as the average of 16^{th} and 17^{th} values, and has the advantage of being finite even up to three of the observations of the DM are “infinite” in a set of 20 simulations. When working with counted estimates of the median and the one-sigma level statistics, the corresponding dispersion of the data is estimated by the natural

logarithm of the ratio of counted one-sigma level value divided by counted median. The counted statistics defined above do not require any theoretical distribution, but the obtained estimates are still associated with the underlying distribution of the data.

The counted statistics are found to be very useful when dealing with data sets with missing or undefined data points. Throughout the presentation of the simulation results, median, one-sigma level, and dispersion values of the DMs use log-normal based calculations whenever the complete data set is available (i.e. no “infinite” values or “collapses”) and the data show the characteristics of a skew-positive distribution. For the cases where log-normal based statistical analysis is not applicable, the “counted” median, one-sigma level and dispersion values are utilized. The differences in the counted and log-normal statistics are reported to be sufficiently small that they are of minor consequence for seismic demands of deteriorating (Luco, 2002) and non-deteriorating regular SMRFs (Medina and Krawinkler, 2005).

When interpreting the results presented in this chapter, care must be taken not to assume that SMA systems which reduce/increase statistical values for the ground motion sets will reduce/increase demands for an individual acceleration record. In a record-by-record comparison, SMA connections may affect predicted demands in a way that is opposite to that suggested by the statistical values.

5.4. Model Structures and Passive Control Systems

Based on the finite element models of the three- and nine-story PR buildings (Section 4.3.1), a number of model structures are developed to assess the role of SMA connections as passive control systems for enhancing structural performance under

seismic loads. The model structures based on the Los Angeles three-story PR building are denoted with the prefix LA3 while the ones based on the Seattle nine-story PR building are denoted with the prefix SE9.

5.4.1. Uncontrolled PR System

In order to understand the impact of SMA connections as a passive control system, the seismic demands for the uncontrolled PR system should be first understood. This study builds on the previous research conducted on the seismic performance of the two PR buildings (Maison and Kasai, 2000; Maison et al., 2000) by taking into account the limited ductility of PR connections under high rotation demands. Figure 5.1 compares the sample moment rotation responses of a ductile and a degrading PR connection subjected to a uniformly increasing deformation history.

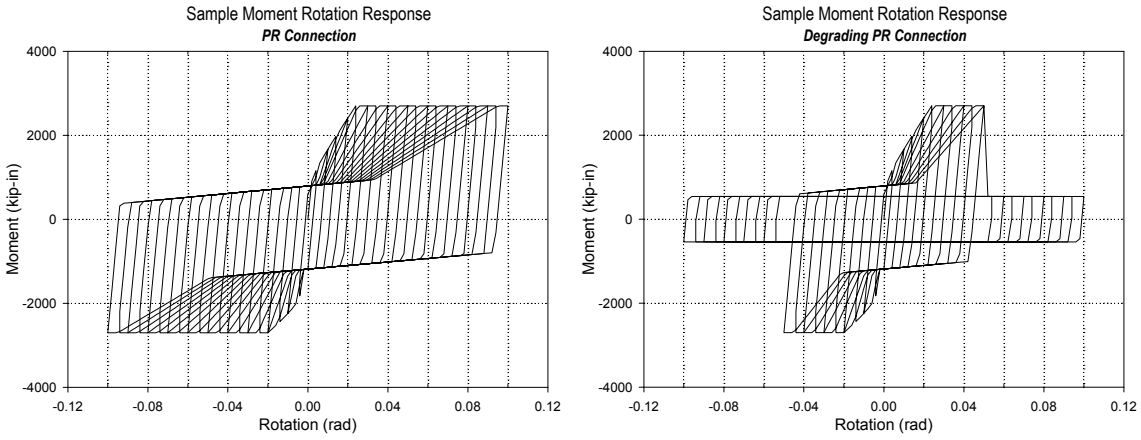

Figure 5.1 Sample moment rotation response of a ductile (left) and a degrading PR connection (right).

In the following sections, the model structures with ductile PR connections are denoted with the suffix PR (LA3PR and SE9PR) while the model structures with degrading PR connections are denoted with the suffix DPR (LA3DPR and SE9DPR).

5.4.2. Passive Control Systems with SMA Connections

The transformation temperatures and mechanical characteristics of SMAs are influenced by the material composition, amount of cold-work and heat treatment. Mechanically training SMAs shows promise to stabilize and adjust the characteristics of the material for seismic applications (McCormic et al., 2005), making it possible to design different SMA connections tailored for specific structures. However, as with most passive control systems, the design of SMA connections is an iterative process. In order to identify the key parameters, the impact of the variations in SMA connection design on the predicted seismic demands for the two PR frames needs to be investigated.

As explained in Section 3.4, the initial stiffness and the ultimate moment capacity of the SMA connections are designed to satisfy the drift and strength requirements imposed on the original PR designs. The loading plateau stress and the initial stiffness of the SMA material are constrained by this design requirement and are kept constant. Among the remaining parameters that define the superelastic and martensitic SMA material models, the loading plateau stiffness (hereafter referred to loosely as the “hardening” stiffness), which is common to both, is chosen to be varied among different SMA connection designs. This decision is based on the high values of residual drift and connection rotation demands observed for the uncontrolled three-story PR model structure (Section 5.5.1), and the possibility that the zero post-yield stiffness of the PR connections is the reason behind the undesirable seismic response.

Two passive control systems, one utilizing martensitic and the other superelastic SMA-based PR connections (see Section 3.4) are implemented in the three- and nine-story PR buildings. As a passive control system, martensitic SMA connections are intended to control peak deformation demands by means of providing the two structures with high energy dissipation capacity, while superelastic SMA connections are intended to ensure small permanent drifts and connection rotations through self-recentering capabilities even after severe seismic events that lead to significant inelastic transient deformation demands. Consequently, among all the DMs considered, $ISDA_{max}$ is the DM of most importance when selecting a martensitic SMA system while $rISDA_{max}$ and rCR_{max} are given the most weight when selecting a superelastic SMA system to be implemented in the two PR structures.

5.4.2.1.Martensitic SMA Systems

Martensitic SMA bars with three different hardening ratios that are representative of low, typical and high end of observed levels are investigated to determine the impact of hardening stiffness on selected demand measures. Based on the limited experimental data on large diameter martensitic SMA bars (Ocel, 2002), the hardening ratio is chosen to be 0%, 10%, and 25%, respectively, of the initial stiffness. The corresponding model structures are denoted as LA3M00, LA3M10, and LA3M25 for the three-story building, and SE9M00, SE9M10, and SE9M25 for the nine-story building. Figure 5.2 shows sample moment rotation response for all three martensitic SMA connection designs and the PR connection moment rotation response that they are intended to replace.

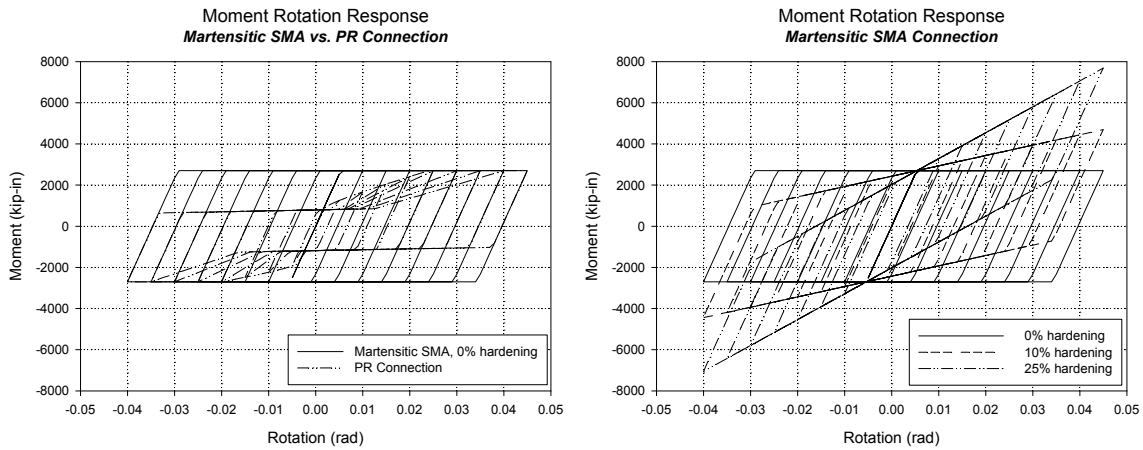

Figure 5.2 Sample moment rotation response of ductile PR vs. martensitic SMA connection (left) and three martensitic SMA connection designs with different hardening ratios (right).

The martensitic SMA connection with no hardening represents the base design to which the alternative designs are compared, even though the typical hardening ratio is observed to be about 10% for the SMA material in its martensitic form. This decision is based on the observation that the martensitic SMA connection with no hardening is the closest to the PR connection it is replacing in terms of hysteretic properties. Even though both connection designs have the same ultimate moment and the same initial stiffness, the base martensitic SMA connection has a higher energy dissipation capacity due mainly to the lack of pinching behavior that is evident with the PR connection. Furthermore, the PR connection yields earlier, strain hardens, and reaches to its ultimate moment at a larger rotation than its martensitic SMA counterpart. The two alternative SMA connection designs with non-zero hardening ratios differ even more due to the fact that they develop larger moments with increasing deformation.

5.4.2.2.Superelastic SMA Systems

Superelastic SMA bars with three different hardening ratios that are representative of low, typical and high end of observed levels are investigated to determine the impact of hardening stiffness on selected demand measures. Based on the limited experimental data on superelastic SMAs (DesRoches et al., 2004; McCormic et al., 2005; McCormick, 2006), the hardening ratio is chosen to be 0%, 5%, and 10%, respectively, of the initial stiffness. The corresponding model structures are denoted as LA3S00, LA3S05, and LA3S10 for the three-story building; SE9S00, SE9S05, and SE9S10 for the nine-story building. Figure 5.3 shows sample moment rotation response for all three superelastic SMA connection designs and the PR connection moment rotation response that they are intended to replace.

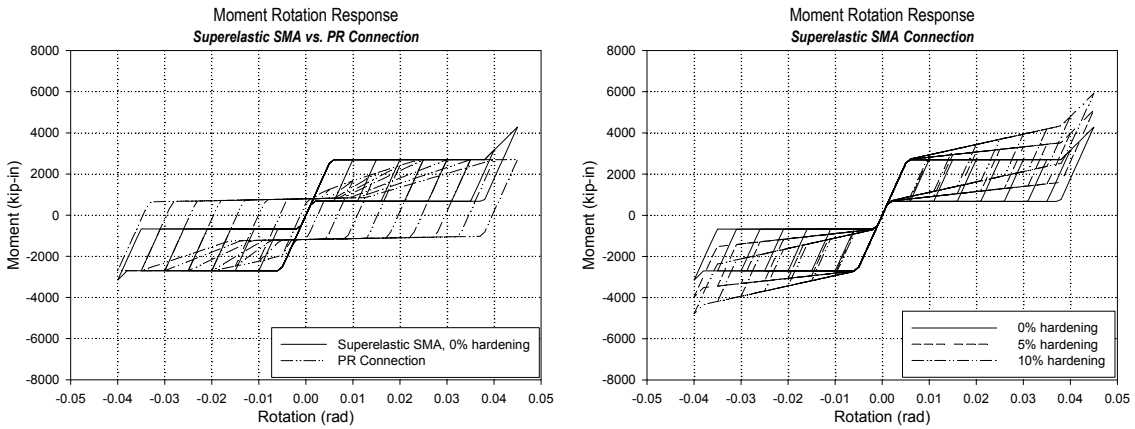

Figure 5.3 Sample moment rotation response of ductile PR vs. superelastic SMA connection (left) and three superelastic SMA connection designs with different hardening ratios (right).

Similar to the case for the martensitic SMA connection, the superelastic SMA connection with no hardening is selected to be the base design to which the alternative designs are compared even though the typical hardening ratio is about 5% for the SMA material in its

superelastic form. Both connection designs have the same ultimate moment and the same initial stiffness, but the base superelastic SMA connection has a smaller energy dissipation capacity mainly due to the flag-shaped hysteresis loop which is the source of its self-recentering capability. The PR connection yields earlier, strain hardens, and reaches to its ultimate moment at a larger rotation than its superelastic SMA counterpart. However, the superelastic SMA connection exhibits a region of increased stiffness following its loading plateau that is not present in the PR connection. This is due to the elastic deformation of fully-transformed martensite and provides the superelastic SMA connection with additional stiffness under high rotation demands.

5.4.3. Summary

Table 5.1 summarizes the 16 model structures investigated in the following sections.

Table 5.1 Summary of model structures.

Model Structure	Connection Type	Connection Design		
		Low	Typical	High
Los Angeles Three-Story	Ductile PR	LA3PR		
	Degrading PR	LA3DPR		
	Martensitic SMA	LA3M00	LA3M10	LA3M25
	Superelastic SMA	LA3S00	LA3S05	LA3S10
Seattle Nine-Story	Ductile PR	SE9PR		
	Degrading PR	SE9DPR		
	Martensitic SMA	SE9M00	SE9M10	SE9M25
	Superelastic SMA	SE9S00	SE9S05	SE9S10

First, the model structures with ductile PR connections are taken as the base case and the effect of connection failures on the predicted demands is investigated. Then, martensitic and superelastic SMA systems are selected to be implemented in the two PR

buildings based on the relative seismic performance of each alternative, and the effect of these systems in comparison to the performance of the uncontrolled structures is evaluated.

5.5. Seismic Demands for the Los Angeles Three-Story Model Structures

The three-story model structure has a fundamental period of 1.27 sec., while the second and third periods are 0.36 and 0.19 sec., respectively. The corresponding modal participating mass ratios are 83%, 13% and 4%, indicating that the three-story model structure is mainly dominated by its first mode.

5.5.1. Seismic Demands for the Uncontrolled PR System

Figure 5.4 shows the relationship between the normalized (by the structure seismic weight) base shear and the RDA for the three-story model structure with ductile (LA3PR) and degrading (LA3DPR) PR connections. The resulting pushover curves can be characterized by an elastic component, a transition zone and a yield plateau of variable length that is followed by a branch of negative stiffness.

The three-story model structure starts to deviate from elastic behavior at as early as an RDA of 0.003 rad. The sharp transition from the elastic component to the yield plateau generally observed in FR buildings is replaced with a gradual yielding zone, explained by the fact that the individual PR connection moment rotation response is modeled with a short linear elastic region followed by a longer nonlinear portion where the connection yields gradually until the ultimate strength is reached. Furthermore, a PR LFRS has more connections that provide stiffness to the structure; hence, yielding of a single PR

connection has a smaller effect on the global response than yielding of a FR connection and results in a much smoother pushover curve.

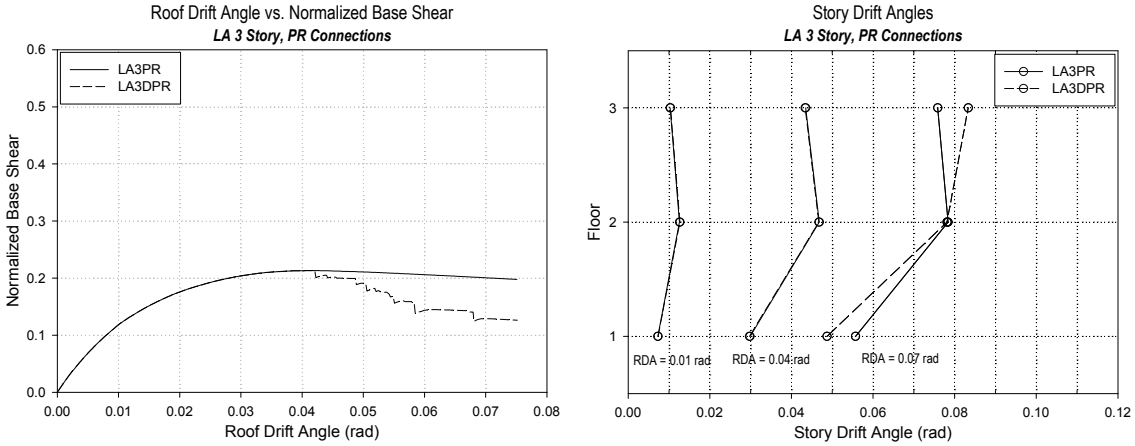

Figure 5.4 Pushover curves (left) and the spatial variation of story drift demands corresponding to different levels of roof drift (right) for LA 3 -story model structure with ductile and degrading PR connections.

At an RDA of 0.040 rad., the three-story model structure reaches to a state of zero lateral resistance. As it is pushed further into the inelastic range, the post-yield story stiffness becomes negative due to the P-Δ/h "shear" counteracting the remaining lateral stiffness. The PR connections start to fail at an RDA of 0.042 rad., leading to small drops in the pushover curve as connections continue to fail. The lateral deformation under increasing RDA is concentrated at the second floor. When the connections are allowed to fail under high rotation demands, the story drift demands are found to pivot about the second floor, decreasing for the first floor while increasing for the roof.

The statistics of peak and residual story drift and connection rotation demands for the two model structures (LA3PR[1] and LA3DPR) under the three sets of Los Angeles region

ground motions (2%, 10%, and 50% in 50 yr.) are given in Table 5.2. The LA3DPR model structure is found to collapse under one out of twenty ground motions belonging to the 2% in 50 yr. set. Consequently, counted statistics are used to assess the predicted seismic demands.

Table 5.2 Statistics of max. peak and residual story drift and connection rotation demands for LA 3-story model structure with ductile and degrading PR connections. Percentage increases from the base case (LA3PR) are given in brackets.

Model Structure	Ground Motion Set	Inter-story Drift Angle						Connection Rotation					
		Peak[a]			Residual[a]			Peak[a]			Residual[a]		
		Median (rad)	1-σ (rad)	σ_{lnx}	Median (rad)	1-σ (rad)	σ_{lnx}	Median (rad)	1-σ (rad)	σ_{lnx}	Median (rad)	1-σ (rad)	σ_{lnx}
LA3PR	2% in 50 yr	0.073	0.098	0.29	0.015	0.044	1.06	0.078	0.105	0.30	0.024	0.052	0.78
	10% in 50 yr	0.031	0.043	0.33	0.002	0.007	1.11	0.036	0.048	0.29	0.011	0.016	0.37
	50% in 50 yr	0.014	0.017	0.23	~0	~0	~0	0.018	0.022	0.21	0.008	0.009	0.08
LA3DPR[b]	2% in 50 yr	0.081 [10%]	0.126 [28%]	0.44	0.025 [61%]	0.103 [134%]	1.43	0.093 [19%]	0.134 [28%]	0.37	0.034 [43%]	0.114 [120%]	1.21

a. Counted statistics.
b. The statistics for the two model structures are found to be almost identical for the 10% in 50 yr. and the 50% in 50 yr. set of ground motions, hence only the results for LA3PR are presented.

The 2% in 50 yr. set results in significant $ISDA_{max}$ demands for the three-story model structure even with the favorable assumption of fully ductile PR connections. The predicted median $ISDA_{max}$ of 0.073 rad. for LA3PR exceeds the recommended limit of 0.050 rad in FEMA-273/356 (FEMA, 1997; FEMA, 2000g) that defines the post-earthquake damage state in which the building is on the verge of partial or total collapse. Even though similar FR SMRFs designed for Los Angeles are reported to remain stable

1. The predicted median story drift demands for the three-story structure with ductile PR connections are found to be within 4% of the median drift demands reported by Maison et al. (2000) for the same structure. The difference can be attributed to typical prediction uncertainty associated with nonlinear finite element analysis platforms.

at even higher story drifts (up to 0.08 - 0.10 rad., FEMA, 2000b), the predicted median $ISDA_{max}$ lies within the region of negative lateral stiffness observed in the pushover curve (Figure 5.4). The ability of the uncontrolled PR system to withstand strong ground accelerations in this region is questionable. Explicit modeling of the limited ductility of the PR connections results in an increase on both peak (median:10%, one-sigma level:28%) and residual (median:61%, one-sigma level:134%) story drift demands and even leads to collapse under one record belonging to the 2% in 50 yr. set. However, the effect of degrading PR connections is statistically insignificant for the lower levels of seismic hazard, leading to almost identical predicted demands for LA3PR and LA3DPR. This is in agreement with previous research conducted on the effect of connection fractures on FR SMRFs (Luco and Cornell, 1998; Song and Ellingwood, 1999b; Luco and Cornell, 2000).

A similar trend is observed for the CR_{max} demands for LA3PR under the 2% in 50 yr. set of ground motions. The predicted median CR_{max} of 0.078 rad. lies beyond the range in which many PR connections have been tested. The consideration of failure of the PR connections is found to increase the residual (median:43%, one-sigma level:120%) more than the peak (median:19%, one-sigma level:28%) connection rotation demands as it is found to be the case for the story drifts. A similar correlation between the peak story drifts and connection rotations has also been reported by Maison and Kasai (2000).

5.5.2. The Effect of Martensitic SMA System Design

5.5.2.1.Deformation Demands

The pushover curves (Figure 5.5) for the three-story model structure indicate that all three martensitic SMA systems start to deviate from elastic behavior as the RDA exceeds 0.006 rad. The effect of the hardening stiffness of the SMAs becomes more apparent as

the structure is pushed further into the inelastic range. At an RDA of 0.032 rad., the story stiffness of the base martensitic SMA system (LA3M00) becomes negative. The additional stiffness provided by the hardening translates into a higher post-yield story stiffness, preventing the two alternative designs (LA3M10 and LA3M25) from experiencing similar behavior. The variation of story drifts with height corresponding to different levels of RDA also indicates that increasing hardening stiffness concentrates deformations at the lower levels, somewhat isolating the roof of the structure.

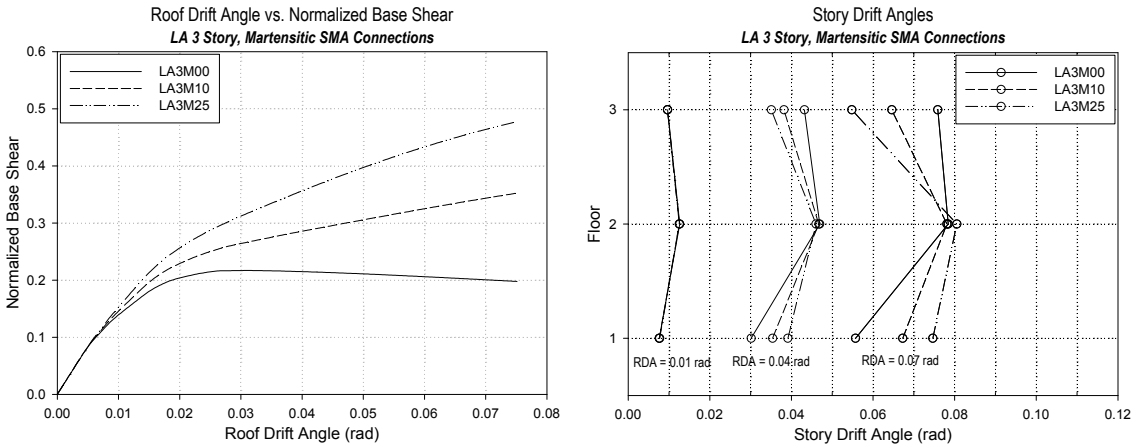

Figure 5.5 Pushover curves (left) and the spatial variation of story drift demands corresponding to different levels of roof drift angle (right) for LA 3 story model structure with three different martensitic SMA connections.

The statistics of peak and residual story drift and connection rotation demands are shown in Table 5.3 for the three different martensitic SMA system designs (LA3M00, LA3M10, and LA3M25) under the three sets of Los Angeles region ground motions (2%, 10% and 50% in 50 yr.). None of the martensitic SMA systems collapse under the three ground motion sets, making it possible to use log-normal based statistics for peak deformation based demand measures.

Table 5.3 Statistics of max. peak and residual story drift and connection rotation demands for LA 3 story model structure with different martensitic SMA connections. Percentage increases from the base case (LA3M00) are given in brackets.

Model Structure	Ground Motion Set	Inter-story Drift						Connection Rotation					
		Peak			Residual[a]			Peak			Residual[a]		
		Median (rad)	1-σ (rad)	σ_{lnx}	Median (rad)	1-σ (rad)	σ_{lnx}	Median (rad)	1-σ (rad)	σ_{lnx}	Median (rad)	1-σ (rad)	σ_{lnx}
LA3M00	2% in 50 yr	0.071	0.112	0.46	0.019	0.061	1.15	0.077	0.119	0.43	0.029	0.071	0.91
	10% in 50 yr	0.030	0.043	0.37	0.005	0.012	0.98	0.035	0.049	0.33	0.013	0.021	0.48
	50% in 50 yr	0.016	0.023	0.38	~0	~0	~0	0.019	0.027	0.36	0.009	0.011	0.21
LA3M10	2% in 50 yr	0.064 [-10%]	0.098 [-13%]	0.42	0.014 [-30%]	0.019 [-70%]	0.30	0.066 [-14%]	0.098 [-17%]	0.40	0.022 [-24%]	0.026 [-63%]	0.18
	10% in 50 yr	0.030 [-1%	0.044 [1%	0.37	0.003 [-39%]	0.007 [-39%]	0.98	0.032 [-9%]	0.046 [-6%]	0.36	0.011 [-15%]	0.016 [-25%]	0.34
	50% in 50 yr	0.016 [2%]	0.023 [3%]	0.38	~0	~0	~0	0.018 [-6%]	0.026 [-7%]	0.35	0.008 [-10%]	0.010 [-7%]	0.24
LA3M25	2% in 50 yr	0.065 [-9%]	0.102 [-10%]	0.45	0.007 [-66%]	0.016 [-75%]	0.86	0.059 [-24%]	0.088 [-26%]	0.40	0.014 [-51%]	0.020 [-72%]	0.34
	10% in 50 yr	0.029	0.044	0.40	0.002 [-57%]	0.004 [-67%]	0.73	0.029 [-18%]	0.042 [-15%]	0.37	0.009 [-31%]	0.010 [-51%]	0.14
	50% in 50 yr	0.016 [5%]	0.024 [6%]	0.38	~0	~0	~0	0.017 [-14%]	0.023 [-15%]	0.34	0.006 [-27%]	0.008 [-28%]	0.20

a. Counted statistics.

The predicted demands under the 2% in 50 yr. set indicate that the hardening stiffness of the SMAs has less than 10% effect on the median $ISDA_{max}$ for the three-story model structure. On the other hand, for LA3M25 the increase in the hardening stiffness is found to reduce the $rISDA_{max}$ considerably (median:66%, one-sigma level:75%) with respect to the base martensitic SMA system design. Certainly, the additional post-yield stiffness observed in the pushover curve (Figure 5.5) helps to control permanent deformations on LA3M10 and LA3M25 designs. Even though both of the alternative martensitic SMA system designs reduce the $ISDA_{max}$ demand with respect to the base case, LA3M10 experiences the smallest $ISDA_{max}$ indicating that relationship between the $ISDA_{max}$ demand and the hardening stiffness of the martensitic SMAs is nonlinear.

The hardening stiffness of the SMAs has a moderate effect on the CR_{max} statistics under the 2% in 50 yr. set, reducing median and one-sigma level demands by 24% and 26%, respectively. The same trend is observed in the rCR_{max}, albeit more pronounced, leading to a reduction of 51% in the median and 72% in the one-sigma level rCR_{max} demands. Note that the CR_{max} demands for LA3M00 model structure are quite large (median:0.077 rad., one-sigma level:0.119 rad.), even for highly ductile martensitic SMA connections. The corresponding strain demands on the martensitic SMA bars lie beyond the limit where the SMA material properties start to degrade and the ability of all SMA connections on the LA3M00 model structure to survive these earthquakes without any deterioration is questionable. Recall that the SMA material model used in these analyses assumes no degradation (Section 4.2.1.3).

5.5.2.2.Force and Energy Demands

The additional hardening stiffness of the two alternative martensitic SMA system designs not only increases the peak lateral force in the structure but also changes the mechanism by which the structure dissipates the input earthquake energy (Figure 5.6). The spatial variation of median NHE dissipated at each floor indicates that the energy dissipation is concentrated more at the lower levels as the hardening stiffness of the SMAs increases, leading to amplified inelasticity at the base of the columns. Even though the SMA connections in the alternate designs with higher hardening stiffness lead to smaller rotation demands, the corresponding moments developed in the connections are also higher, which may help to explain the increased amount of NHE dissipated by the first floor columns.

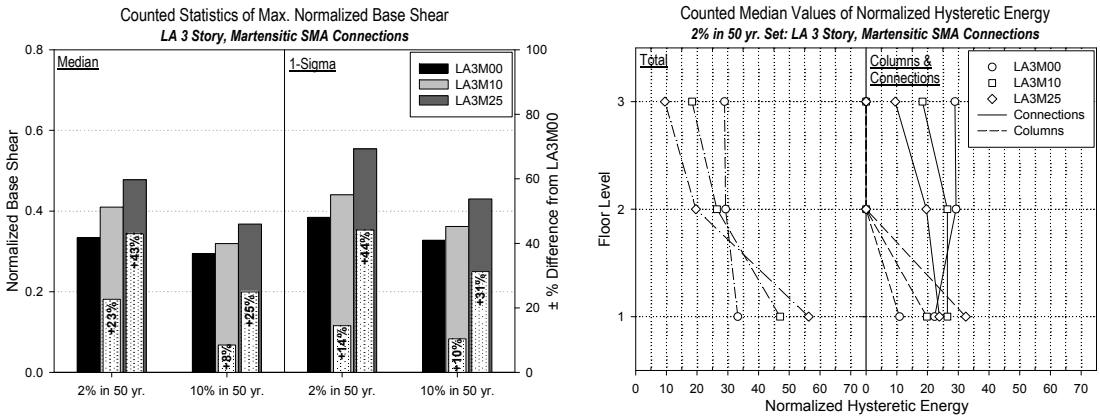

Figure 5.6 Statistics of peak base shear demands (left) and the spatial variation of median normalized hysteretic energy demands (right) for the LA 3 story model structure with different martensitic SMA connections.

5.5.2.3.Summary

At first look, the LA3M00 martensitic SMA connection design seems to be the ideal passive control system. It acts like a deformation fuse, reduces the stiffness of the structure and the peak inertial force it attracts after yielding, dissipates most of the input earthquake energy at the connections, and limits the inelasticity experienced by the other components of the LFRS. However, for this particular system, there are several problems. First, it has the largest peak and residual story drift demands when compared to the alternative LA3M10 and LA3M25 designs. This is particularly important since the structure is susceptible to dynamic instability even at moderate roof drift demands, as is apparent from the negative story stiffness region observed in the pushover curve (Figure 5.5). Second, it sustains the highest connection rotation demands, leading to high strains in the SMA bars and possible deterioration of the material properties.

The LA3M10 system introduces a finite but small hardening stiffness to the connections. Globally, this translates into reduced peak and residual story drift demands at the

expense of increased nonlinearity at the base of the first floor columns. The LA3M25 system adds even more post-yield stiffness to the structure. However, its benefits are counterbalanced by additional nonlinearity in the columns, leading to an increase (albeit small) in the story drift demands. Considering the relative predicted seismic demands for all three martensitic SMA system designs, the LA3M10 design is found to be the most suitable for the Los Angeles three-story building.

5.5.3. The Effect of Superelastic SMA System Design

5.5.3.1. Deformation Demands

Figure 5.7 shows the pushover curves for the Los Angeles three-story structure with three different superelastic SMA systems. Up to an RDA of 0.005 rad., all three superelastic SMA systems deform elastically. As the structure is pushed into the inelastic range, the effect of the hardening stiffness starts to become apparent. The base superelastic SMA system (LA3S00) exhibits an almost zero lateral stiffness range between RDAs of 0.031 to 0.052 rad, and starts stiffening again as the superelastic SMAs fully transform to martensite and start deforming elastically. On the other hand, the increasing hardening stiffness of the superelastic SMAs ensures a positive story stiffness for the two alternative designs (LA3S05 and LA3S10). The spatial variation of story drifts at different levels of RDA also indicate that increasing hardening stiffness concentrates deformations more at the lower levels. Yielding of a lower level acts as a fuse and relieves the higher levels.

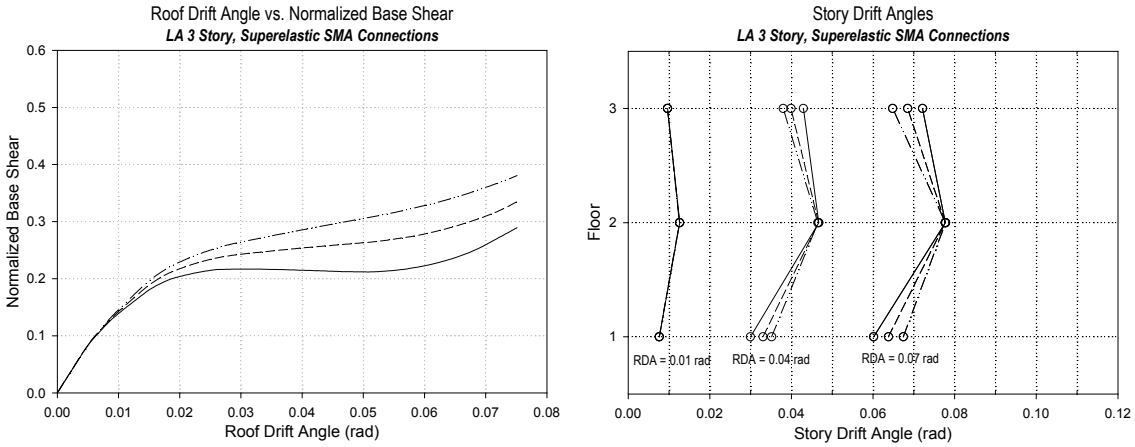

Figure 5.7 Pushover curves (left) and the spatial variation of story drift demands corresponding to different levels of roof drift angle (right) for LA 3 story model structure with three different superelastic SMA connections.

Table 5.4 Statistics of max. peak and residual story drift and connection rotation demands for LA 3 story model structure with different superelastic SMA connections. Percentage increases from the base case (LA3S00) are given in brackets.

Model Structure	Ground Motion Set	Inter-story Drift						Connection Rotation					
		Peak			Residual[a]			Peak			Residual[a]		
		Median (rad)	1-σ (rad)	σ_{lnx}	Median (rad)	1-σ (rad)	σ_{lnx}	Median (rad)	1-σ (rad)	σ_{lnx}	Median (rad)	1-σ (rad)	σ_{lnx}
LA3S00	2% in 50 yr	0.071	0.099	0.33	0.003	0.006	0.56	0.070	0.095	0.31	0.005	0.008	0.34
	10% in 50 yr	0.030	0.048	0.47	0.001	0.004	1.41	0.036	0.053	0.38	0.004	0.006	0.38
	50% in 50 yr	0.014	0.021	0.35	~0	~0	~0	0.019	0.027	0.38	0.003	0.003	0.07
LA3S05	2% in 50 yr	0.065 [-8%]	0.102 [4%]	0.45	0.003]	0.011	1.33	0.068 [-2%]	0.094 [-1%]	0.32	0.005	0.009	0.66
	10% in 50 yr	0.030 [-1%]	0.047 [-2%]	0.46	0.001	0.004	1.54	0.034 [-5%]	0.051 [-4%]	0.38	0.004	0.006	0.38
	50% in 50 yr	0.014 [-1%]	0.021 [3%]	0.40	~0	~0	~0	0.018 [-3%]	0.026 [-4%]	0.38	0.003	0.004	0.10
LA3S10	2% in 50 yr	0.062 [-12%]	0.105 [6%]	0.53	0.005	0.014	1.09	0.066 [-5%]	0.093 [-2%]	0.34	0.005	0.008	0.41
	10% in 50 yr	0.030 [-1%]	0.046 [-4%]	0.44	0.001	0.004	1.40	0.033 [-9%]	0.049 [-8%]	0.39	0.004	0.005	0.28
	50% in 50 yr	0.014 [-1%]	0.022 [6%]	0.42	~0	~0	~0	0.018 [-6%]	0.026 [-7%]	0.38	0.003	0.004	0.12

a. Counted statistics.

The statistics of peak and residual story drift and connection rotation demands are given in Table 5.4 for the three model structures subjected to all three sets of Los Angeles ground motions (2%, 10%, and 50% in 50 yr.). None of the model structures with superelastic SMA connections is found to collapse under any of the ground motions, hence the log-normal statistics are used to assess the seismic demands.

The predicted demands indicate that all three superelastic SMA systems experience negligible $rISDA_{max}$ and rCR_{max} demands. Furthermore, the effect of the hardening stiffness of the superelastic SMAs on both peak and residual deformation statistics is found to be less than 10%. Recall that the same three-story model structure with martensitic SMA systems experienced higher CR_{max} demands where the effect of the hardening stiffness was significant (Table 5.3). This difference in the behavior of martensitic and superelastic SMA systems can be attributed to the stiffening region of the superelastic SMA bars following their loading plateau. The superelastic SMA connections in the three-story structure start to regain stiffness at a rotation of approximately 0.05 rad. The predicted connection rotation demands for the 2% in 50 yr. set indicate that the behavior is governed by the elastic stiffness of the fully transformed martensite in the superelastic SMA systems and the deformation demands are less sensitive to the hardening stiffness than they are for the martensitic SMA systems.

5.5.3.2.Force and Energy Demands

As expected, the two alternative designs with higher post-yield stiffness are found to attract larger inertial forces when compared to the base superelastic SMA system (Figure 5.8). The spatial variation of NHE for columns and connections also indicates that the additional stiffness introduced by the superelastic SMA connections results in increased

inelasticity at the first story columns. A similar effect was observed in the three-story model structure with martensitic SMA connections, but the effect was more pronounced.

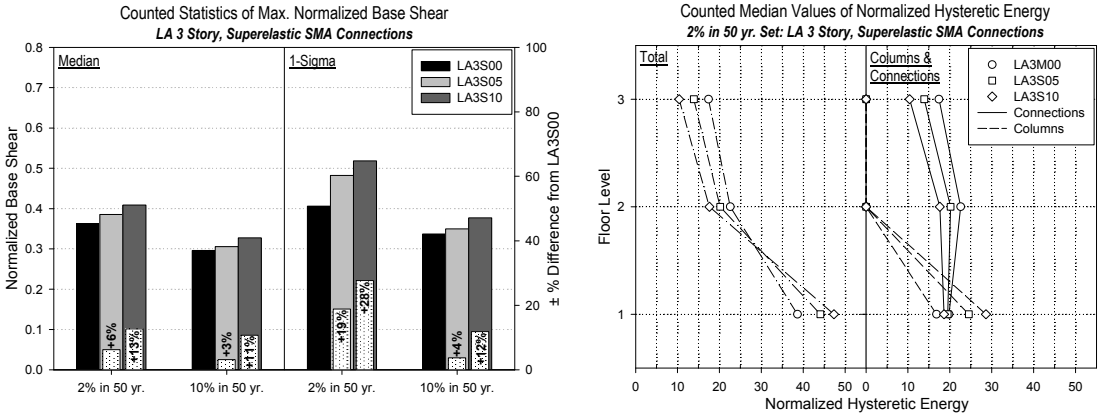

Figure 5.8 Statistics of peak base shear demands (left) and the spatial variation of median normalized hysteretic energy demands (right) for the LA 3 story model structure with different superelastic SMA connections.

5.5.3.3.Summary

Comparison of the predicted peak deformation demands for the three superelastic SMA connection designs does not provide the analyst with enough information to identify the best passive control system. Further more, all three superelastic SMA systems result in negligible residual deformation demands as intended. However, comparison of NHE demands provides valuable information when the differences within different systems are not significant. The LA3S00 system induces the minimum amount of inelastic action to the other members of the LFRS, hence is found to be more suitable of the three superelastic SMA systems for the three-story building.

5.5.4. Comparison of Seismic Demands across SMA Systems

Several possible SMA connection system alternatives were investigated in the previous sections to identify the better performing designs for the martensitic and superelastic SMA systems for the Los Angeles three-story PR building. In this section, the predicted seismic demands of the selected SMA systems (LA3M10 and LA3S00) are compared to the demands of the uncontrolled PR system (LA3DPR). As before, the comparison is based on statistics of story drift, connection rotation, and hysteretic energy demands.

5.5.4.1. Deformation Demands

The statistics of peak and residual story drift and connection rotation demands are given in Table 5.5 for the three systems (LA3DPR, LA3M10, and LA3S00) under the three sets of Los Angeles region ground motions (2% in 50 yr. and 10% in 50 yr.). The percentage changes in the peak and residual story drift demands from the uncontrolled system (LA3DPR) are also shown graphically in Figure 5.9. The LA3DPR model structure collapses under one out of twenty ground motions belonging to the 2% in 50 yr. set, hence the counted statistics are used to assess the seismic demands.

Table 5.5 Statistics of max. peak and residual story drift and connection rotation demands for LA 3 story model structure with PR and SMA connections. Percentage increases from the uncontrolled PR system (LA3DPR) are given in brackets.

Model Structure	Ground Motion Set	Inter-story Drift						Connection Rotation					
		Peak[a]			Residual[a]			Peak[a]			Residual[a]		
		Median (rad)	1-σ (rad)	σ_{lnx}	Median (rad)	1-σ (rad)	σ_{lnx}	Median (rad)	1-σ (rad)	σ_{lnx}	Median (rad)	1-σ (rad)	σ_{lnx}
LA3DPR	2% in 50 yr	0.081	0.126	0.44	0.024	0.103	1.43	0.093	0.134	0.37	0.034	0.114	1.21
	10% in 50 yr	0.031	0.043	0.33	0.002	0.007	1.11	0.036	0.048	0.29	0.011	0.016	0.37
	50% in 50 yr	0.014	0.017	0.23	~0	~0	~0	0.018	0.022	0.21	0.008	0.009	0.09
LA3M10	2% in 50 yr	0.062 [-23%]	0.096 [-24%]	0.43	0.014 [-44%]	0.018 [-82%]	0.30	0.063 [-32%]	0.095 [-29%]	0.41	0.022 [-36%]	0.026 [-77%]	0.18
	10% in 50 yr	0.029 [-5%]	0.044 [2%]	0.40	0.003 [16%]	0.007 [2%]	0.98	0.033 [-10%]	0.047 [-2%]	0.37	0.011 [4%]	0.016 [1%]	0.34
	50% in 50 yr	0.015 [8%]	0.022 [28%]	0.40	~0	~0	~0	0.017 [-3%]	0.024 [11%]	0.35	0.008 [-2%]	0.010 [15%]	0.24
LA3S00	2% in 50 yr	0.071 [-12%]	0.099 [-22%]	0.33	0.003 [-86%]	0.006 [-94%]	0.56	0.069 [-26%]	0.090 [-33%]	0.27	0.005 [-84%]	0.008 [-93%]	0.34
	10% in 50 yr	0.030 [-2%]	0.048 [12%]	0.47	0.001 [-62%]	0.004 [-49%]	1.41	0.036 [-0%]	0.053 [12%]	0.39	0.004 [-65%]	0.006 [-64%]	0.38
	50% in 50 yr	0.014 [2%]	0.021 [19%]	0.35	~0	~0	~0	0.018 [-0%]	0.025 [16%]	0.36	0.003 [-60%]	0.003 [-61%]	0.07

a. Counted statistics.

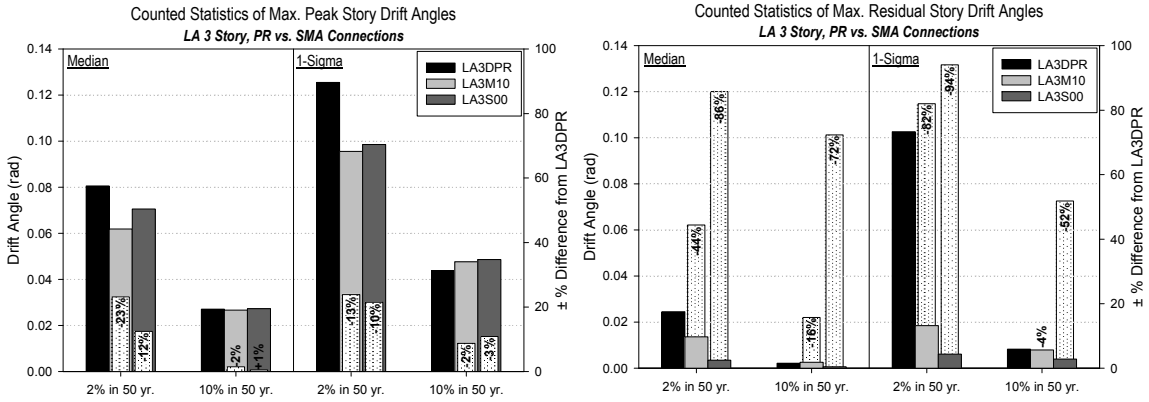

Figure 5.9 Statistics of max. peak (left) and residual (right) story drift demands for LA 3 story model structure with PR and SMA connections. Percentage increases from the base case (LA3DPR) are shown as white bars.

Among the two passive control systems, the martensitic SMA system is the most effective in reducing the $ISDA_{max}$ demands under the 2% in 50 yr. set. A 23% and a 24% reduction in the median and one-sigma level $ISDA_{max}$ demands are observed for the martensitic SMA system while the superelastic SMA system leads to a reduction of 12% and 22%, respectively. On the other hand, the superelastic SMA system is the most effective solution for controlling $rISDA_{max}$ demands, leading to an 86% and a 94% reduction on the median and one-sigma level $rISDA_{max}$ demands. The martensitic SMA system is also effective in controlling $rISDA_{max}$ by reducing the median and one-sigma level demands by 44% and 82%, respectively. Both SMA systems prevent the collapse case observed for the uncontrolled system by reducing the $ISDA_{max}$ demands mainly at the higher seismic hazard levels. The predicted demands for 10% and 50% in 50 yr. sets indicate that both SMA systems lead to a small increase in the $ISDA_{max}$ demands (no larger than 12%) while the superelastic SMA system is still effective controlling the $rISDA_{max}$ demands regardless of the level of the seismic hazard.

The spatial variations of the $ISDA_i$ demands over the height of the three-story model structure (Figure 5.10) indicate that both of the SMA systems increase the story drift demand in the first story, while decreasing it moderately in the second story and considerably in the third story under the 2% in 50 yr. set. While the martensitic SMA system is more effective in controlling peak story drifts, both SMA systems are capable of reducing the large permanent deformations that the uncontrolled system experiences under the 2% in 50 yr. set.

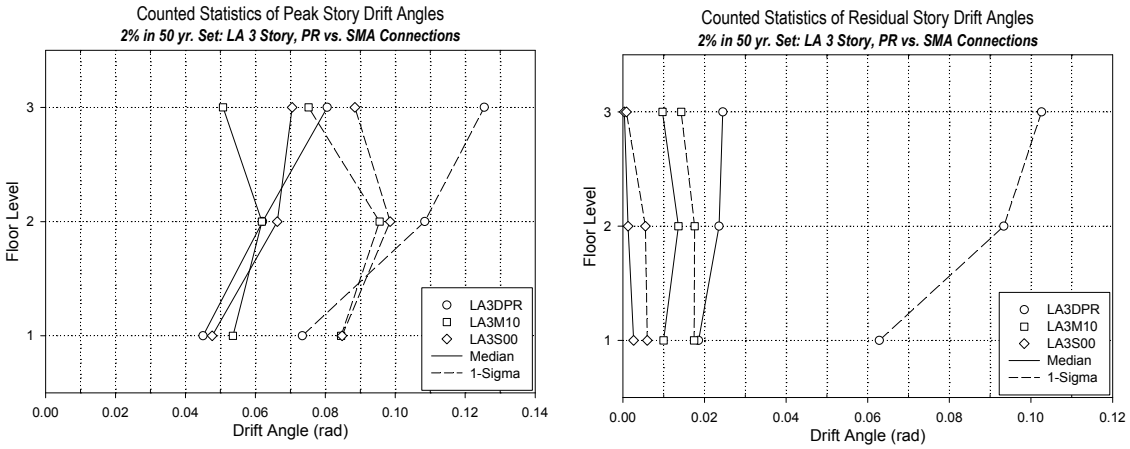

Figure 5.10 Spatial variation of peak (left) and residual (right) of story drift demand statistics under 2% in 50 yr. set for the LA 3 story model structure with PR and SMA connections.

Both passive control systems are effective in reducing the CR_{max} demands under the 2% in 50 yr. set (Figure 5.11). A 32% and a 27% reduction in the median and one-sigma level CR_{max} demands are observed for the martensitic SMA system while the superelastic SMA system leads to a reduction of 26% and 34%, respectively. On the other hand, the superelastic SMA system is the most effective solution for reducing the rCR_{max} demands, leading up to an 84% and a 93% reduction on the median and one-sigma level values. The martensitic SMA system is also effective in limiting the rCR_{max} demands by reducing the median and one-sigma level demands by 36% and 77%.

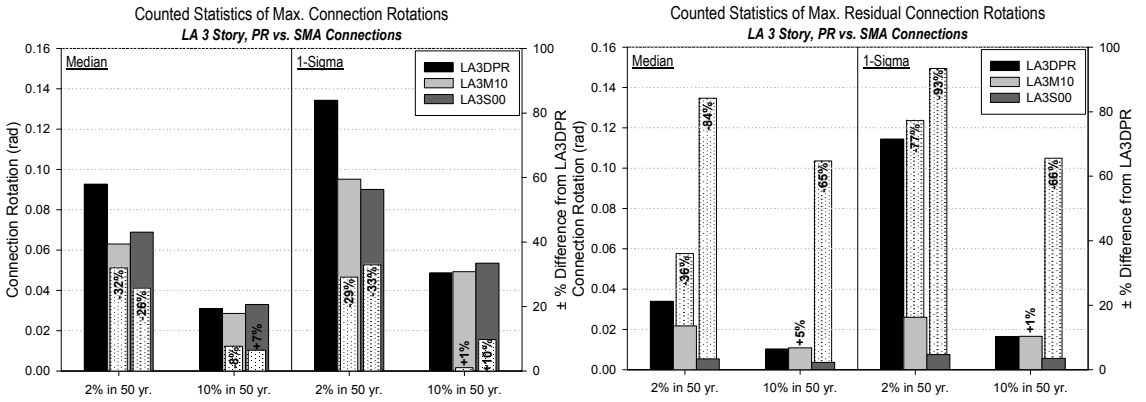

Figure 5.11 Statistics of max. peak (left) and residual (right) story connection rotation demands for LA 3 story model structure with PR and SMA connections. Percentage increases from the base case (LA3DPR) are shown as white bars.

5.5.4.2.Force and Energy Demands

Both of the SMA systems lead to an increase in the peak lateral force that is attracted by the structure and the spatial variation of total NHE dissipated at each floor indicates that the SMA systems alter the way the structure dissipates input earthquake energy (Figure 5.12). Again, both SMA systems concentrate the inelastic action at the first floor mainly by concentrating inelastic action at the base of the columns. Even though it is not ideal for passive control systems to induce inelastic action in the other members of the LFRS, the yielding of the first floor columns isolates the upper stories in the three-story model structure, leading to reduced energy, story drift and connection rotation demands when compared to the uncontrolled PR system.

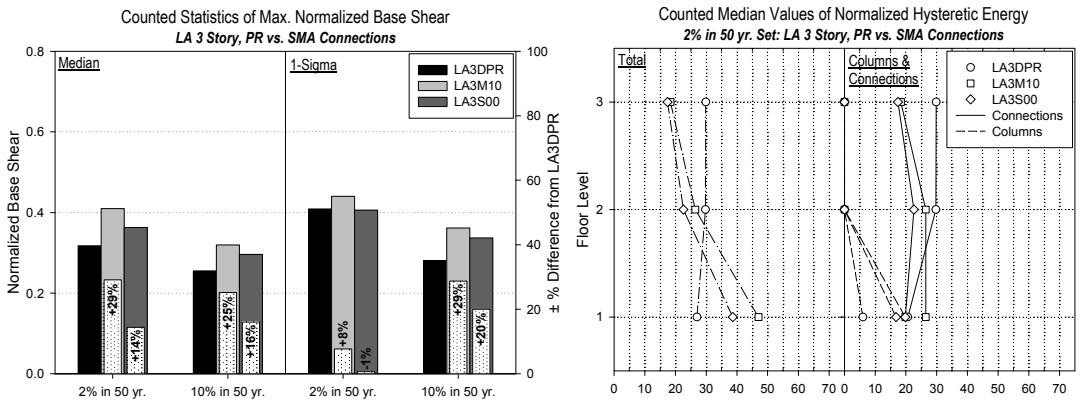

Figure 5.12 Statistics of peak base shear demands (left) and the spatial variation of median normalized hysteretic energy demands (right) for the LA 3 story model structure with PR and SMA connections.

5.5.4.3.Summary

The most important drawback of the uncontrolled three-story model building is its relatively weak and flexible PR connections. Due to the fact that it is the weakest component of the beam-column joint and has no stiffness after reaching its ultimate moment capacity, most of the inelastic action in the frame is concentrated at the PR connections. This leads to high story drifts, dynamic instabilities, and connection rotation demands high enough to cause failure. On the other hand, the same PR connections attract most of the plastic deformations are concentrated at the PR connections, other members of the LFRS experience minimum amount of inelasticity.

Due to their high rotational ductility, where the PR connections fail the SMA connections can survive. Increased post-yield stiffness and energy dissipation capacity provided by the martensitic SMA system reduces the peak deformation demands while the self-recentering capability of superelastic SMA system virtually eliminates permanent story drifts and connection rotations. The peak connection rotation demands, even for the

highest level of seismic hazard considered, are within the limits where the SMAs are expected to deform without significant degradation of their properties. Most of the benefits of using martensitic and/or superelastic SMA systems are observed under high seismic hazard, and are less apparent at lower levels of seismicity. The only exception to this observation is the self-recentering capability of the superelastic SMA system.

5.6. Seismic Demands for the Seattle Nine-Story Model Structures

The nine-story model structure has a fundamental period of 3.07 sec., while the second and third periods are 1.12 and 0.64 sec., respectively. The corresponding modal participating mass ratios are 76%, 11% and 4%.

5.6.1. Seismic Demands for the Uncontrolled PR System

The pushover curves for the nine-story model structure (Figure 5.13) indicate that the structure remains elastic up to an RDA of 0.003 rad. Scaling up the lateral loads further leads to a state of zero lateral resistance at an RDA of 0.014 rad, a value considerably smaller than what was observed for the three-story model structure (Section 5.4.1). The shorter elastic region may be attributed to the amplified P-Δ effects due to the height (nine vs. three stories) and the additional flexibility at the column bases (flexible vs. fixed) of the nine-story structure. The loss of lateral resistance under such a small RDA makes the uncontrolled nine-story structure susceptible to dynamic instability even under moderate levels of story drift demands. The PR connections begin failing as early as at an RDA of 0.034 rad., even though the effect of these failures on the pushover response does not become apparent until an RDA of 0.046 rad. is reached. Since the effects of the degrading PR connections become apparent only in the negative story stiffness range, it is unlikely that the nine-story model structure will experience failed connections before

becoming dynamically unstable. The spatial variation of story drifts also indicates that largest deformation demands are experienced between the third and the fifth floors with increasing RDA.

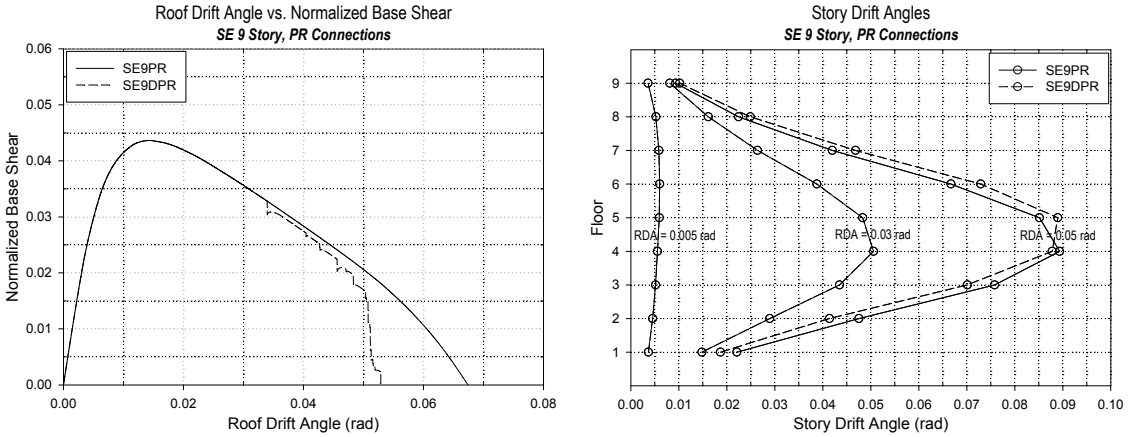

Figure 5.13 Pushover curves (left) and the spatial variation of story drift demands corresponding to different levels of roof drift (right) for SE 9 story model structure with ductile and degrading PR connections.

The statistics of peak and residual story drift and connection rotation demands for SE9PR[1] under the two sets of Seattle ground motions (2% and 10% in 50 yr.) are given in Table 5.6. The SE9PR model structure is found to collapse under two out of twenty ground motions belonging to the 2% in 50 yr. set; hence the counted statistics are used to assess the seismic demands. As expected, the deformation demands that do not lead to dynamic instability are not high enough for the PR connections to fail; hence the SE9DPR model structure is omitted in the subsequent discussions.

1. The predicted median story drift demands for the nine-story structure with ductile PR connections are found to be within 4% of the median drift demands reported by Maison et al. (2000) for the same structure. The difference can be attributed to typical prediction uncertainty associated with nonlinear finite element analysis platforms.

.

Table 5.6 Statistics of max. peak and residual story drift and connection rotation demands for SE 9 story model structure with ductile PR connections.

Model Structure	Ground Motion Set	Inter-story Drift						Connection Rotation					
		Peak[a]			Residual[a]			Peak[a]			Residual[a]		
		Median (rad)	1-σ (rad)	σ_{lnx}	Median (rad)	1-σ (rad)	σ_{lnx}	Median (rad)	1-σ (rad)	σ_{lnx}	Median (rad)	1-σ (rad)	σ_{lnx}
SE9PR[b]	2% in 50 yr	0.025	0.038	0.43	0.006	0.016	0.98	0.034	0.045	0.28	0.023	0.023	0.31
	10% in 50 yr	0.014	0.018	0.20	0.002	0.004	0.83	0.024	0.026	0.10	0.018	0.018	0.16

a. Counted statistics.
b. The statistics for the two model structures are found to be identical for all the two sets of ground motions, hence only the results for SE9PR are presented.

The 2% in 50 yr. ground motion set results in a median $ISDA_{max}$ demand of 0.025 rad. for SE9PR, which is less than the FEMA-273/356 (FEMA, 1997; FEMA, 2000g) recommended limit of 0.050 rad. that is representative of the state of partial or total collapse. Similarly, the predicted median CR_{max} demand of 0.034 rad. for the 2% in 50 yr. set falls within the FEMA-273/356 recommended acceptance range of 0.010 to 0.035 rad. of inelastic connection rotation. Overall, the predicted peak and residual deformation demands for the uncontrolled nine-story model structure are considerably less than those predicted for the three-story model structure (Table 5.2). However, it is apparent from the two observed collapse cases that the SE9PR model structure is susceptible to dynamic instability.

5.6.2. The Effect of Martensitic SMA System Design

5.6.2.1. Deformation Demands

The pushover curves for the nine-story model structure (Figure 5.14) indicate that the structure remains elastic for all three martensitic SMA systems (SE9M00, SE9M10, and SE9M25) up to an RDA of 0.005 rad. The effect of the hardening stiffness of the

martensitic SMAs becomes more apparent as the structure is pushed further into the inelastic range. At an RDA of 0.015 rad., the base martensitic SMA system (SE9M00) reaches a state of zero lateral resistance while the two alternative martensitic SMA systems (SE9M10 and SE9M25) maintain positive stiffness. Furthermore, the spatial variation of story drifts indicates that increasing hardening stiffness decreases the story drifts considerably at the middle, while increasing it at the top and the bottom levels.

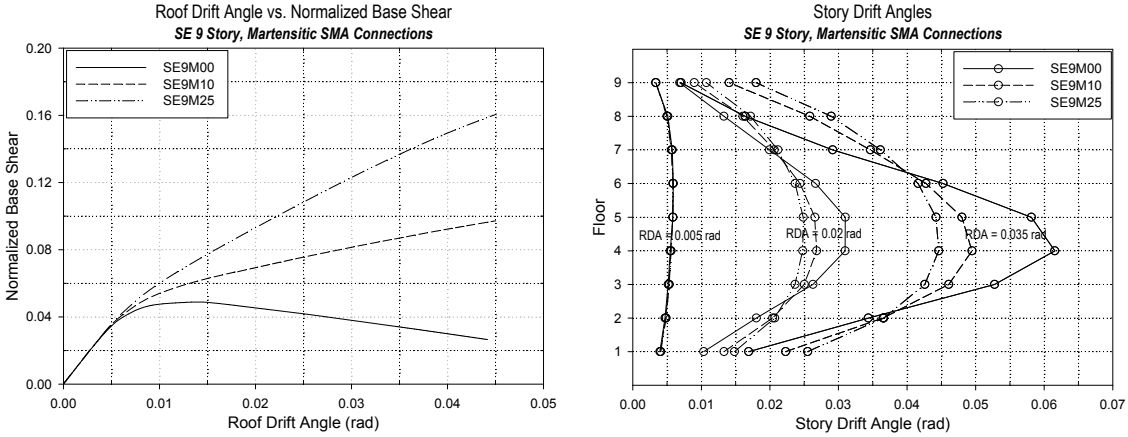

Figure 5.14 Pushover curves (left) and the spatial variation of story drift demands corresponding to different levels of roof drift angle (right) for SE 9 story model structure with three different martensitic SMA connections.

The statistics of peak and residual story drift and connection rotation demands are shown in Table 5.7 for the three different martensitic SMA system designs (SE9M00, SE9M10, and SE9M25) under the two sets of Seattle ground motions (2% in 50 yr. and 10% in 50 yr.). The SE9M00 model structure collapses under two out of twenty ground motions belonging to the 2% in 50 yr. set. Consequently, counted statistics are used to assess the predicted seismic demands.

Table 5.7 Statistics of max. peak and residual story drift and connection rotation demands for SE 9 story model structure with different martensitic SMA connections. Percentage increases from the base case (SE9M00) are given in brackets.

Model Structure	Ground Motion Set	Inter-story Drift						Connection Rotation					
		Peak[a]			Residual[a]			Peak[a]			Residual[a]		
		Median (rad)	1-σ (rad)	σ_{lnx}	Median (rad)	1-σ (rad)	σ_{lnx}	Median (rad)	1-σ (rad)	σ_{lnx}	Median (rad)	1-σ (rad)	σ_{lnx}
SE9M00	2% in 50 yr	0.030	0.043	0.35	0.010	0.018	0.62	0.041	0.052	0.23	0.030	0.043	0.35
	10% in 50 yr	0.018	0.023	0.23	0.003	0.007	0.78	0.026	0.033	0.24	0.020	0.025	0.24
SE9M10	2% in 50 yr	0.030 [-2%]	0.040 [-6%]	0.30	0.004 [-61%]	0.009 [-52%]	0.82	0.031 [-24%]	0.038 [-27%]	0.20	0.020 [-35%]	0.024 [-44%]	0.20
	10% in 50 yr	0.018 [1%]	0.021 [-6%]	0.16	0.001 [-53%]	0.003 [-58%]	0.65	0.020 [-24%]	0.024 [-29%]	0.17	0.014 [-32%]	0.016 [-36%]	0.17
SE9M25	2% in 50 yr	0.033 [9%]	0.042 [-1%]	0.25	0.001 [-87%]	0.004 [-81%]	1.05	0.027 [-33%]	0.034 [-34%]	0.23	0.012 [-60%]	0.015 [-64%]	0.22
	10% in 50 yr	0.018 [2%]	0.022 [-1%]	0.20	0.001 [-78%]	0.001 [-84%]	0.47	0.016 [-39%]	0.019 [-43%]	0.17	0.009 [-54%]	0.010 [-60%]	0.11

a. Counted statistics.

The effect of the hardening stiffness of the SMAs on $ISDA_{max}$ statistics is not significant, leading to a maximum of 9% increase in the predicted demands. On the other hand, $rISDA_{max}$ statistics are reduced considerably under the 2% in 50 yr. set (median:81%, one-sigma level:87%) as the hardening stiffness of the martensitic SMAs increases, consistent with what was observed in the three-story model structure. A similar reduction is observed for CR_{max} (median:33%, one-sigma level:34%) and rCR_{max} (median:60%, one-sigma level:64%) demands. Overall, even though the increasing hardening stiffness has only a modest effect on $ISDA_{max}$ statistics, the reduction observed in predicted $rISDA_{max}$, CR_{max} and rCR_{max} demands for the 2% in 50 yr. set of ground motions and the elimination of two collapse cases is substantial and indicates the beneficial effect of the non-zero post yield stiffness present in the two alternative martensitic SMA systems.

5.6.2.2.Force and Energy Demands

The increasing hardening stiffness of the martensitic SMAs increases the amount of energy dissipated at the connections and the peak inertial force the structure attracts under the 2% in 50 yr. set (Figure 5.15). Contrary to the three-story model structure, little or no inelasticity is observed in the columns of the nine-story model structure and almost all inelastic deformations are concentrated at the connections in all three martensitic SMA systems.

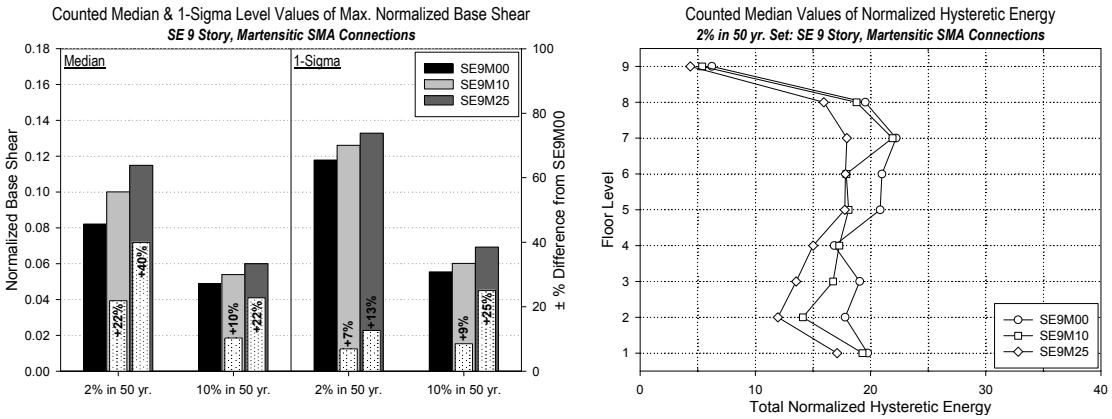

Figure 5.15 Statistics of peak base shear demands (left) and the spatial variation of median normalized hysteretic energy demands (right) for the SE 9 story model structure with different martensitic SMA connections.

5.6.2.3.Summary

When assessing seismic performance, the most common seismic demand measure is the $ISDA_{max}$. Among the three martensitic SMA system designs, none is found to lead to significantly less $ISDA_{max}$ demand than the others. This can easily lead to a conclusion that the hardening stiffness of the SMAs is less important for the nine-story structure than was observed in the three-story structure. However, investigation of other demand

measures proved to be valuable to determine the more suitable passive control system. The base martensitic SMA system (SE9M00) is the only passive control system that experienced collapse. The SE9M10 design introduces finite but small post-yield stiffness to the connections that prevents the collapses and leads to the smallest predicted peak story drift demand. The most apparent benefit of the SE9M10 design is the reduction in residual story drifts and peak and the residual connection rotation demands. The SE9M25 system reduces the deformation demands on connections even further, but leads to a small increase in the peak story drift demands. Considering the relative seismic demands for all martensitic SMA system designs, SE9M10 is found to be most suitable of the three alternatives for the nine-story building.

5.6.3. The Effect of Superelastic SMA System Design

5.6.3.1.Deformation Demands

The pushover curves for the nine-story model structure (Figure 5.16) indicate that all three superelastic SMA systems deviate from elastic behavior at an RDA of approximately 0.0045 rad. The effect of the hardening stiffness becomes more apparent with increasing levels of deformation. The base superelastic SMA system (SE9S00) experiences a negative story stiffness between RDAs of 0.014 to 0.036 rad., and starts stiffening again as the superelastic SMA bars complete their transformation to martensite and start deforming elastically. The additional hardening stiffness is found to help the two alternative designs (SE9M05 and SE9M10) to maintain a positive story stiffness. The spatial variation of story drifts corresponding to different levels of RDA also indicates that increasing the hardening stiffness reduces the story drift considerably between floors four to six, while increasing it at the top and the bottom floors. A similar trend was observed for the three-story structure with martensitic SMA connections (Figure 5.14).

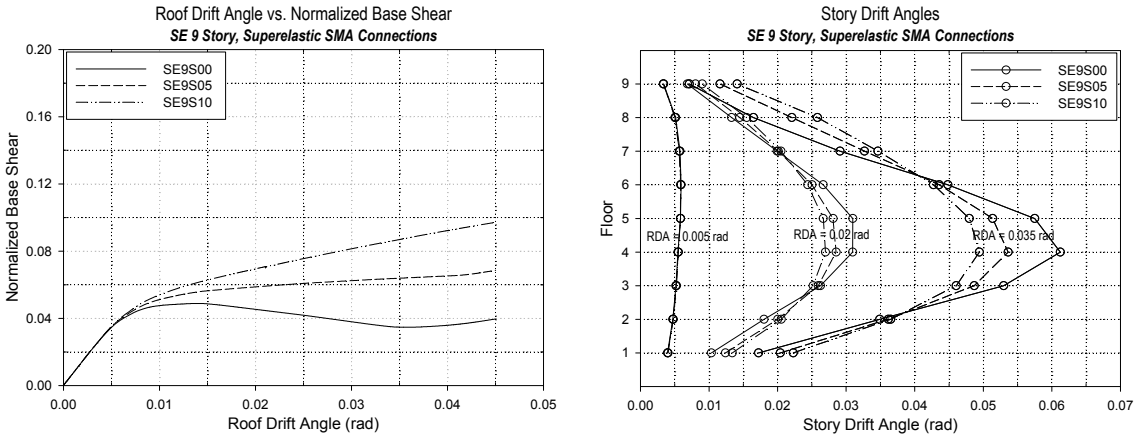

Figure 5.16 Pushover curves (left) and the spatial variation of story drift demands corresponding to different levels of roof drift angle (right) for SE 9 story model structure with three different superelastic SMA connections.

The statistics of peak and residual story drift and connection rotation demands are given in Table 5.8 for the three different martensitic SMA system designs (SE9S00, SE9S05 and SE9S10) under the two sets of Seattle region ground motions (2% and 10% in 50 yr.). None of the model structures with superelastic SMA connections is found to collapse under any of the ground motions, hence the log-normal statistics are utilized.

As was the case for the three-story model structure, all three superelastic SMA systems result in negligible $rISDA_{max}$ and rCR_{max} demands. The $ISDA_{max}$ demand is insensitive to the hardening stiffness of the superelastic SMAs while the CR_{max} statistics are reduced to some extent under the 2% in 50 yr. set (median:20%, one-sigma level:17%) with increasing hardening stiffness of the superelastic SMAs. The corresponding strain demands on the superelastic SMA bars lie within the loading plateau and the response is governed by the hardening stiffness rather than the elastic stiffness of the fully transformed martensite.

Table 5.8 Statistics of max. peak and residual story drift and connection rotation demands for SE 9 story model structure with different superelastic SMA connections. Percentage increases from the base case (SE9S00) are given in brackets.

Model Structure	Ground Motion Set	Inter-story Drift						Connection Rotation					
		Peak			Residual[a]			Peak			Residual[a]		
		Median (rad)	1-σ (rad)	σ_{lnx}	Median (rad)	1-σ (rad)	σ_{lnx}	Median (rad)	1-σ (rad)	σ_{lnx}	Median (rad)	1-σ (rad)	σ_{lnx}
SE9S00	2% in 50 yr	0.036	0.049	0.31	0.001	0.001	0.31	0.046	0.058	0.23	0.009	0.010	0.07
	10% in 50 yr	0.018	0.023	0.29	~0	~0	~0	0.024	0.031	0.26	0.009	0.0010	0.05
SE9S05	2% in 50 yr	0.037 [1%]	0.050 [1%]	0.31	~0	~0	~0	0.041 [-11%]	0.053 [-9%]	0.25	0.008 [-17%]	0.009 [-16%]	0.08
	10% in 50 yr	0.018 [0%]	0.023 [-2%]	0.27	~0	~0	~0	0.021 [-12%]	0.027 [-13%]	0.24	0.008 [-15%]	0.008 [-16%]	0.03
SE9S10	2% in 50 yr	0.037 [2%]	0.050 [2%]	0.31	~0	~0	~0	0.037 [-20%]	0.048 [-17%]	0.27	0.007 [-28%]	0.008 [-26%]	0.10
	10% in 50 yr	0.018 [1%]	0.023 [-2%]	0.26	~0	~0	~0	0.019 [-21%]	0.024 [-23%]	0.23	0.007 [-26%]	0.007 [-26%]	0.04

a. Counted statistics.

5.6.3.2.Force and Energy Demands

The increase in the hardening stiffness of the two alternative SMA connection designs attracts larger inertial forces in nine-story structure (Figure 5.17). The spatial variation of NHE for connections also indicates that the SE9S00 system dissipates more energy at almost all floors of the nine-story structure. This is intuitive since the same system is found to have larger connection rotation demands when compared to the two alternative systems. Little or no inelasticity in the columns is observed for all the three superelastic SMA systems for the two levels of seismic hazard considered.

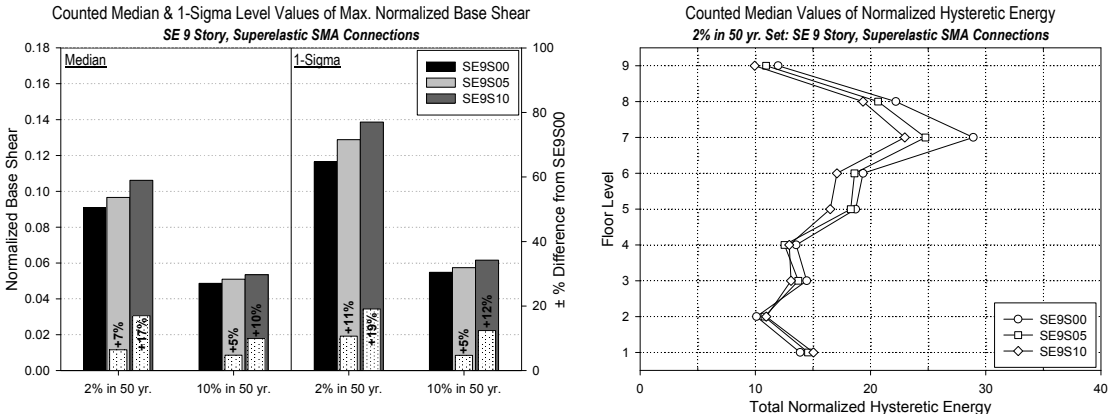

Figure 5.17 Statistics of peak base shear demands (left) and the spatial variation of median normalized hysteretic energy demands (right) for the SE 9 story model structure with different superelastic SMA connections.

5.6.3.3.Summary

Among the three superelastic SMA systems investigated, none leads to significantly less peak story drift demands than the others. Even though all three superelastic SMA systems result in negligible permanent deformation demands, the SE9S10 system has the smallest peak connection rotation demands, making it more suitable as a passive control system than the other two alternatives.

5.6.4. Comparison of Seismic Demands across SMA Systems

Several possible SMA connection system alternatives have been investigated in the previous sections to identify the better performing designs for the martensitic and superelastic SMA systems for the Seattle nine-story PR building. In this section, the predicted seismic demands of the selected SMA systems (SE9M10 and SE9S10) are compared to the demands of the uncontrolled PR system (SE9PR). This comparison is based on the statistics of story drift, connection rotation, and hysteretic energy demands.

5.6.4.1.Deformation Demands

The statistics on peak and residual story drift and connection rotation demands are summarized in Table 5.9 for the uncontrolled PR (SE9PR), martensitic SMA (SE9M10), and superelastic SMA (SE9S10) systems under the two sets of Seattle region ground motions (2% and 10% in 50 yr.). The percentage changes in the peak and residual story drift demands from the uncontrolled PR system are also shown graphically in Figure 5.18. The SE9PR model structure collapses under two out of twenty ground motions in the 2% in 50 yr. set; hence the counted statistics are used to assess the seismic demands.

Table 5.9 Statistics of max. peak and residual story drift and connection rotation demands for SE 9 story model structure with PR and SMA connections. Percentage increases from the uncontrolled PR system (SE9PR) are given in brackets.

Model Structure	Ground Motion Set	Inter-story Drift						Connection Rotation					
		Peak[a]			Residual[a]			Peak[a]			Residual[a]		
		Median (rad)	1-σ (rad)	σ_{lnx}	Median (rad)	1-σ (rad)	σ_{lnx}	Median (rad)	1-σ (rad)	σ_{lnx}	Median (rad)	1-σ (rad)	σ_{lnx}
SE9PR	2% in 50 yr	0.025	0.038	0.43	0.006	0.016	0.98	0.034	0.045	0.28	0.023	0.031	0.31
	10% in 50 yr	0.015	0.018	0.20	0.002	0.004	0.83	0.024	0.026	0.10	0.018	0.022	0.16
SE9M10	2% in 50 yr	0.030 [19%]	0.040 [4%]	0.30	0.004 [-34%]	0.009 [-44%]	0.82	0.031 [-9%]	0.038 [-16%]	0.20	0.020 [-13%]	0.024 [-22%]	0.20
	10% in 50 yr	0.018 [26%]	0.021 [21%]	0.16	0.001 [-23%]	0.003 [-35%]	0.65	0.020 [-16%]	0.024 [-10%]	0.17	0.014 [-26%]	0.016 [-25%]	0.17
SE9S10	2% in 50 yr	0.035 [40%]	0.048 [24%]	0.31	~0	~0	~0	0.035 [3%]	0.046 [2%]	0.26	0.007 [-70%]	0.007 [-76%]	0.10
	10% in 50 yr	0.018 [23%]	0.021 [21%]	0.18	~0	~0	~0	0.019 [-21%]	0.023 [-14%]	0.19	0.007 [-63%]	0.007 [-67%]	0.04

a. Counted statistics.

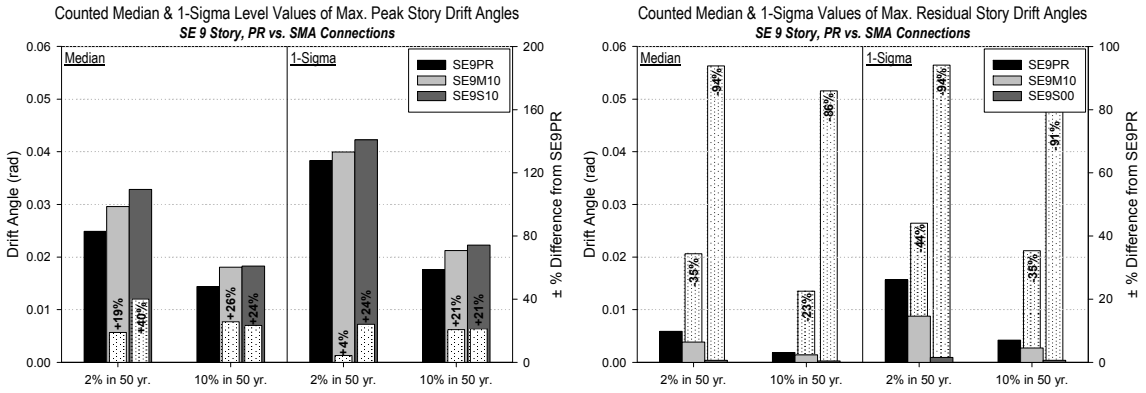

Figure 5.18 Statistics of max. peak (left) and residual (right) story drift demands for SE 9 story model structure with PR and SMA connections. Percentage increases from the base case (SE9PR) are shown as white bars.

The results presented in Table 5.9 indicate that neither martensitic nor superelastic SMA system is effective in reducing $ISDA_{max}$ demands for the nine-story model structure. A 19% increase in the median $ISDA_{max}$ demand is observed for the martensitic SMA system while the superelastic SMA system leads to a increase of 40% under the 2% in 50 yr. set. On the other hand, the martensitic SMA system is effective in controlling the $rISDA_{max}$ (reducing the median level demands by 34%) while the superelastic SMA system practically eliminates permanent story drifts. Even though they lead to increased $ISDA_{max}$ demands, both SMA systems prevent the collapses observed on the uncontrolled PR system under the 2% in 50 yr. events. Recall that the SMA systems were found to be effective mostly under high deformation demands for the three-story building. Even the 2% in 50 yr. level seismic hazard for Seattle region does not lead to as high deformation demands, rendering both SMA systems ineffective in controlling peak story drifts. However, two of the Seattle ground acceleration records cause deformation demands that lead to dynamic instability on the uncontrolled PR system; in these two cases, both SMA systems function as expected and prevent the collapse cases.

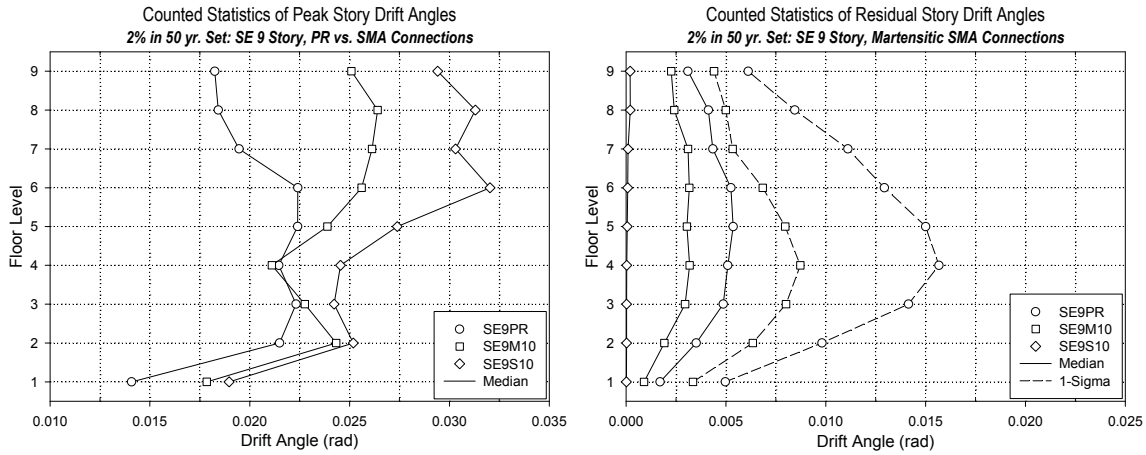

Figure 5.19 Spatial variation of peak (left) and residual (right) story drift demand statistics under the 2% in 50 yr. set for the SE 9 story model structure with PR and SMA connections.

The spatial variations of the $ISDA_i$ statistics (Figure 5.19) indicate that the $ISDA_{max}$ is observed at the third floor for the uncontrolled PR system, and seems to isolate the rest of the structure from excessive deformations. Implementation of either of the SMA systems prevents such isolation and lead to an amplified $ISDA_{max}$ demand at one story below the roof.

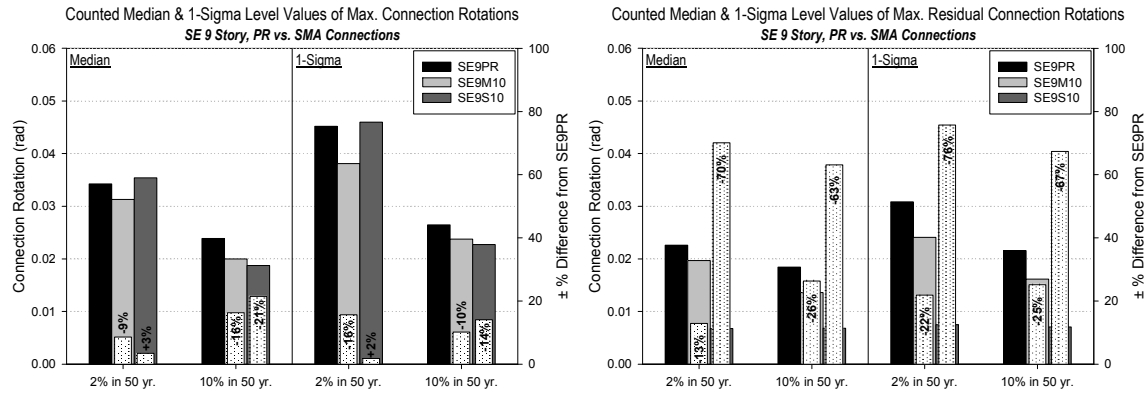

Figure 5.20 Statistics of max. peak (left) and residual (right) story connection rotation demands for SE 9 story model structure with PR and SMA connections. Percentage increases from the base case (SE9PR) are shown as white bars.

None of the SMA systems is particularly effective in reducing the CR_{max} (Figure 5.20). A 9% and a 16% reduction on the median and one-sigma level CR_{max} demands are observed for the martensitic SMA system while the superelastic SMA system leads to a small increase. On the other hand, the superelastic SMA system is the most effective solution for reducing the rCR_{max}, leading to a 70% and a 76% reduction on the median and one-sigma level rCR_{max} demands. The martensitic SMA system is less effective controlling rCR_{max}, leading to a reduction in the median and one-sigma level demands by 13% and 22%.

5.6.4.2.Force and Energy Demands

Both of the SMA systems lead to an increase in the peak lateral force attracted by the structure and the spatial variation of total NHE dissipated at each floor indicates that both SMA systems decrease the amount of dissipated energy at the sixth floor and below while increasing it for the upper floors (Figure 5.21). Apparently, the concentration of the inelastic action at the lower levels isolates the upper levels in the uncontrolled PR system while the additional post-yield stiffness of the SMA connections prevent this effect, leading to the higher peak story drift demands on the upper levels of the nine-story model structure.

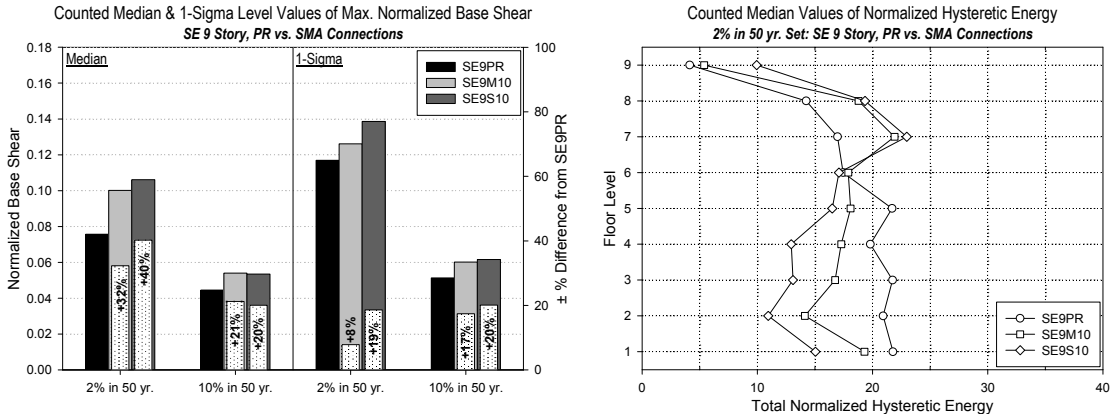

Figure 5.21 Statistics of peak base shear demands (left) and the spatial variation of median normalized hysteretic energy demands (right) for the SE 9 story model structure with PR and SMA connections.

5.6.4.3.Summary

For most of the acceleration records, even for the ones that represent the high seismic hazard, the PR connections in the nine-story model structure stay within the ductile range. However, the zero post yield stiffness of the connections make the nine-story frame susceptible to dynamic instability under large story drift demands. Both the martensitic and the superelastic SMA systems provide additional post-yield stiffness to the structure in the form of a non-zero hardening stiffness to control excessive deformations and prevent dynamic instabilities observed in the uncontrolled structure, albeit at the expense of amplified peak story drift demands.

An analyst looking only at the peak story drifts may easily come to the conclusion that neither of the SMA connection designs is effective as a passive control system. However, the modest increases from the uncontrolled system to the martensitic and superelastic SMA systems in an average sense do not reflect their benefits under those particular ground motions that cause the largest story drifts. Furthermore, the superelastic SMA

system is very effective in controlling permanent deformation demands at both the global and the local levels.

5.7. Conclusions

The results presented in this chapter provide insight into the controlled and uncontrolled behavior of the three and the nine-story buildings under different levels of seismic hazard. The fundamental difference between the behavior of the two buildings is that the columns dissipate a portion of the input earthquake energy in the three-story structure while all the inelastic deformations are concentrated at the PR connections in the nine-story structure. The deformation demands on the nine-story structure are also considerably small when compared to the three-story structure. Even though the three-story structure is designed for a base shear (as a percentage of its seismic weight) that is larger than the nine-story structure, it experiences considerably higher inertial forces (as a percentage of its seismic weight), possibly leading to the differences in the observed deformation demands. The martensitic and superelastic SMA systems alter the response of the three and nine-story buildings, not only by introducing additional energy dissipation and self-recentering capability but also by changing the mechanism through which the LFRS dissipates the input earthquake energy.

The martensitic SMA system is most effective in controlling peak story drift and connection rotation demands on structures under ground motions that induce large deformation demands, such as those in the 2% in 50 yr. set for Los Angeles. On the other hand, the superelastic SMA system is effective in controlling permanent story drift and connection rotation demands on both model structures under all levels of seismic hazard considered in this study. Conflicting demands of peak and residual deformations are also

observed, in which implementation of a specific SMA system is found to reduce one DM while increasing another. There seems to be no single SMA passive control system that can improve all aspects of seismic performance; hence, the selection of a particular system must be based on a specific performance objective.

CHAPTER 6

PROBABILISTIC SEISMIC DEMAND ASSESSMENT

6.1. Introduction

Just as the response of a structure can vary significantly from one acceleration record to another, so can the implementation of SMA connections lead to uncertainties in the system performance. Thus, in addition to quantifying the effects of SMA connections on structural demands for the SAC earthquake record sets (Chapter 5), a concise way to summarize the uncertainties in performance across a range of ground motion characteristics and intensity levels is also needed. This issue can be addressed through the development of probabilistic seismic demand curves.

Probabilistic Seismic Demand Analysis (PSDA) is a method for evaluating the annual probability of exceeding a specified seismic demand for a given structure at a designated site (Cornell, 1996). PSDA involves a convolution of a ground motion hazard curve based on an specific intensity measure (IM, e.g. spectral acceleration) with a demand measure (DM, e.g. inter-story drift) from nonlinear time history analysis (NTHA) of the structure under a suite of ground motions. By conditioning on an IM, the resulting DM statistics can be used to assess the effect of SMA connections in a manner that is less dependent on the earthquake records in a specific set, and the way in which they are scaled. The final product of PSDA is the mean annual frequency (MAF)[1] of exceeding a specific demand, which is a single value that can be compared for structures with PR versus SMA

1. The MAF and the annual probability are approximately equal for the small values of interest, and are used interchangeably hereafter.

connections. The performance of SMA connections over a range of demand levels, thus, can be evaluated by comparing the demand hazard curves.

6.2. Probabilistic Seismic Demand Assessment

PSDA is already at the core of recent performance-based seismic design guidelines such as FEMA 350 and 353 for SMRFs (FEMA, 2000a; FEMA, 2000c), and is used to assess the comparative performance of steel frames with SMA connections within this dissertation. A brief review of the approach proposed by Cornell et al. (2002) is provided in the following sections.

6.2.1. Review of Probabilistic Seismic Demand Analysis (PSDA)

In continuous integral form, the MAF of the DM exceeding any specified demand value y (i.e. the DM hazard, $\lambda_{DM}(y)$) is given by

$$\lambda_{DM}(y) = \int G_{DM|IM}(y|x)\left|d\lambda_{IM}(x)\right| \tag{6.1}$$

in which $\lambda_{IM}(x)$ is the MAF of the IM exceeding the value x (i.e. the ground motion hazard), $G_{DM|IM}(y|x)$ is the probability of the DM exceeding any specified demand value y conditioned on IM = x. The term $G_{DM|IM}(y|x)$ is usually estimated from NTHA results for a suite of ground acceleration records and accounts for the variability of the demand for a given intensity that stems from the differences among ground motions. When combined with structural capacity information (e.g. for “immediate occupancy”, Song and Ellingwood, 1999b; for incipient collapse, Vamvatsikos and Cornell, 2002), the demand hazard curves ($\lambda_{DM}(y)$) can be used to evaluate the MAF of exceeding a specific limit state (i.e. the annual limit state frequency).

$$\lambda_{LS} = \int G_{LS|DM}(y)\left|d\lambda_{DM}(y)\right| \tag{6.2}$$

In Equation 6.2, λ_{LS} is the MAF of exceeding the limit state LS, $G_{LS|DM}(y)$ is the probability of exceeding the limit state LS given that the DM equals *y*, and is often referred to as the "fragility[1]". For the cases where the limit state is characterized by a random valued capacity (with the same units as the DM), $G_{LS|DM}(y)$ simply corresponds to the probability that this capacity is less than *y*. For a deterministic representation of the limit state, $G_{LS|DM}(y)$ becomes an indicator function equal to one if *y* is greater than the deterministic capacity and zero otherwise, and λ_{LS} becomes equivalent to $\lambda_{DM}(y)$ evaluated at this deterministic capacity.

A closed form solution to the DM hazard in Equation 6.1 can be obtained under the following simplifying assumptions:

- A log-log linear form of the ground motion hazard ($\lambda_{IM}(x)$) as given in Equation 6.3*:*

$$\lambda_{IM}(x) = k_0 \cdot x^{-k} \tag{6.3}$$

  This form of $\lambda_{IM}(x)$ has shown to be a reasonable fit to the hazard curve (Jalayer, 2003) locally around the region of interest (e.g., MAFs between 1/72 or 50% frequency of exceedence in 50 years and 1/2475 or 2% frequency of exceedence in 50 years).

- A log-normal conditional probability distribution of the DM given the IM, leading to the functional form given in Equation 6.4 for $G_{DM|IM}(y|x)$

$$G_{DM|IM}(y|x) = 1 - \Phi\left[\frac{\ln(y) - \ln(\eta_{DM|IM}(x))}{\sigma_{DM|IM}}\right] \tag{6.4}$$

1. The fragility can also be defined as a function of the IM, S_{a1}, enabling the fragility to be convolved with the seismic hazard to obtain a point estimate of risk in a seismic risk assessment.

where Φ is the standard normal cumulative distribution function (CDF), $\eta_{DM|IM}$ and $\sigma_{DM|IM}$ are the median and dispersion of the DM given the IM. This assumption has been confirmed for peak story drift angles ($ISDA_{max}$) and S_{a1} (Shome, 1999; Luco, 2002; among others) and verified for residual story drift angles ($rISDA_{max}$) and S_{a1} based on the results obtained in Chapter 5. While $\eta_{DM|IM}$ is a function of the IM, $\sigma_{DM|IM}$ is assumed to be constant and independent of the IM.

- A log-log linear form of the relationship between the median DM and the IM ($\eta_{DM|IM}(x)$) as given in Equation 6.5:

$$(\eta_{DM|IM}(x) = a \cdot x^{b}) \Leftrightarrow (\ln(\eta_{DM|IM}(x)) = \ln(a) + b \cdot \ln(x)) \tag{6.5}$$

The parameters *a* and *b* in Equation 6.5 are commonly estimated from a log-log linear least-squares regression of the DM on IM for a suite of acceleration records, given by Equation 6.6. In the regression model, ε is the random error, assumed to be log-normally distributed with a median of one and a dispersion of σ.

$$(DM = a \cdot IM^{b} \cdot \varepsilon) \Leftrightarrow (\ln(DM) = \ln(a) + b \cdot \ln(IM) + \ln(\varepsilon)) \tag{6.6}$$

Finally, σ is estimated by the mean squared deviation of the residuals about the fit (Equation 6.5) from *n* number of (DM, IM) data points, as expressed in Equation 6.7.

$$\sigma_{DM|IM} = \sqrt{\frac{1}{n-2}\sum[\ln(DM) - \ln(a \cdot IM^{b})]^{2}} \tag{6.7}$$

Under the assumptions detailed above, the hazard curve for any DM & IM pair can be expressed as the multiplication of two factors:

$$\lambda_{DM}(y) = \lambda_{IM}(IM(y)) \cdot CF_{\sigma} \tag{6.8}$$

In Equation 6.8, *IM(y)* is the IM corresponding to the demand *y*, and can be obtained from the solution of Equation 6.6 for the IM. The first factor, $\lambda_{IM}(IM(y))$, can be interpreted as a "first order" estimate of the DM hazard since it corresponds to the DM hazard with zero

dispersion. The second factor, CF_{σ}, can be interpreted as a correction factor accounting for the variability of the DM at a given IM, and is expressed by

$$CF_{\sigma} = \exp\left[\frac{1}{2}(k(\sigma_{DM|IM}/b))^2\right] \tag{6.9}$$

6.2.2. Uncertainty Modeling

The process of performance evaluation of structures subjected to ground accelerations entails significant uncertainties. Some of these uncertainties originate from factors that are inherently random at the scale of understanding (e.g. earthquake occurrence on a known fault, record-to-record variability in acceleration records, etc.) and are often denoted as aleatory uncertainty, or randomness. Others stem from assumptions or limited knowledge in representing the physical phenomena such as two-dimensional mathematical idealizations of structures, modeling of structural components in the highly nonlinear range, etc., and are often denoted as epistemic uncertainty or knowledge-based uncertainty. While aleatory uncertainty is irreducible, epistemic uncertainty can be reduced by acquiring additional data or information.

The probabilistic framework defined by Equation 6.8 assumes that the randomness is the only source of uncertainty in the seismic demand assessment. It can further be extended to explicitly distinguish between aleatory and epistemic uncertainties in the demand/ capacity estimation and in the seismic hazard (e.g. Cornell et al., 2002; Kinali and Ellingwood, 2007), and to incorporate structural capacity information (e.g. Vamvatsikos and Cornell, 2002) to obtain annual limit state probabilities. On the other hand, what is of interest here is a comparative analysis of controlled and uncontrolled structural systems, and the probabilistic seismic demand curves developed in this chapter are likely to

provide a correct ordinal ranking of the SMA systems investigated since the uncertainties are modeled consistently.

6.2.3. Accounting for "Collapses"

PSDA needs to be extended to account for collapses (i.e. the cases where the predicted DM is unrealistically large or the numerical algorithm fails to converge to a solution) since the $ISDA_{max}$/$rISDA_{max}$ and S_{a1} data for ground motions that cause a dynamic instability on the model structure cannot be included in the regression model defined by Equation 6.6. This can be achieved by using the Theorem of Total Probability (Benjamin and Cornell, 1970) to express $G_{DM|IM}(y|x)$ as the probability of collapse (given $S_{a1}=x$) plus the probability of the joint event of non-collapse and DM exceeding y (also given $S_{a1}=x$). Usually, a type of binary distribution is used to model the probability of collapse conditioned on the IM (Shome, 1999; Baker, 2005).

For the three- and nine-story uncontrolled PR structures investigated as a part of this study, the ground motion data sets (2%, 10%, and 50% in 50 yr.) mostly consist of records that do not cause collapse, and one or two records that cause collapse (LA38 for model structure LA3DPR; SE21 and SE36 for model structure SE9PR). For such cases, the binary regression is found to be strongly influenced by the very limited number of collapses, and may indicate a different trend that what exists (Baker, 2005). As a result, the acceleration records leading to dynamic instability on the uncontrolled model structures are excluded from the data set for all structures on which the regression analysis is performed. Consequently, the demand hazard curves developed for the uncontrolled structures do not account for the probability of collapse and can be interpreted as an upper bound for the demand hazard. Recall that the martensitic

(LA3M10 and SE9M10) and superelastic (LA3S00 and SE9S10) SMA systems investigated in this chapter did not encounter dynamic instability (see sections 5.5.4.1 and 5.6.4.1).

6.3. Spectral Acceleration Hazard

A site hazard curve for an IM provides the annual probability of exceeding any particular intensity, for a given period and damping ratio. An efficient IM for ground acceleration records is one which the dispersion of the DM given an intensity is relatively small with respect to any other ground motion characteristics, such as magnitude and/or source-to-site distance, and for which a hazard analysis is available (Luco and Cornell, 1998). The most frequently used IM is the spectral acceleration at the fundamental period of the structure (S_{a1}). S_{a1} is a structure-specific IM, hence it may better capture the demands imposed on a specific structure by the earthquake, when compared to non-structure-specific IMs such as peak ground acceleration (PGA). Using an IM that is closely related to structural demands also reduces the number of NTHAs under different earthquake records that are necessary for PSDA (Shome et al., 1998). Another advantage of S_{a1} as an IM is that the hazard curves are readily available (e.g. from the U.S. Geological Survey) to be used in a PSDA. S_{a1} has been found to be "efficient" (i.e. low scatter of the DM) and "sufficient" (i.e. independence of the DM from the magnitude and the distance of the excitation) for short and moderate-period structures (Shome, 1999). Considering the fundamental periods of the structures investigated (1.27 and 3.07 sec. for three- and nine- story PR buildings), S_{a1} is selected as the IM to be used in this study.

The S_{a1} hazard curves for the three and nine-story model structures shown in Figure 6.1 are obtained by fitting a line in log-log space (Equation 6.3) to the points defined by the

median values of S_{a1} (for a damping ratio of 2%) and the corresponding annual probabilities of exceedence (2%, 10%, and 50% in 50 years). The least-squares regression estimates of k and k_0 are also presented in Figure 6.1. Note that the S_{a1} hazard curves shown in Figure 6.1 are for a damping ratio of 2% rather than for the 5% value typically reported by USGS. Further more, the hazard curves developed here are representative of a firm soil site rather than the soft rock site used as a basis by USGS since the SAC earthquake record sets reflect firm soil conditions (Somerville, 1997). Finally, recall that the presence of SMA connections do not change the first mode period or the viscous damping of the PR buildings (the additional damping provided is in the form of hysteretic damping); hence the same hazard curve can be used for both the uncontrolled and the controlled model structures.

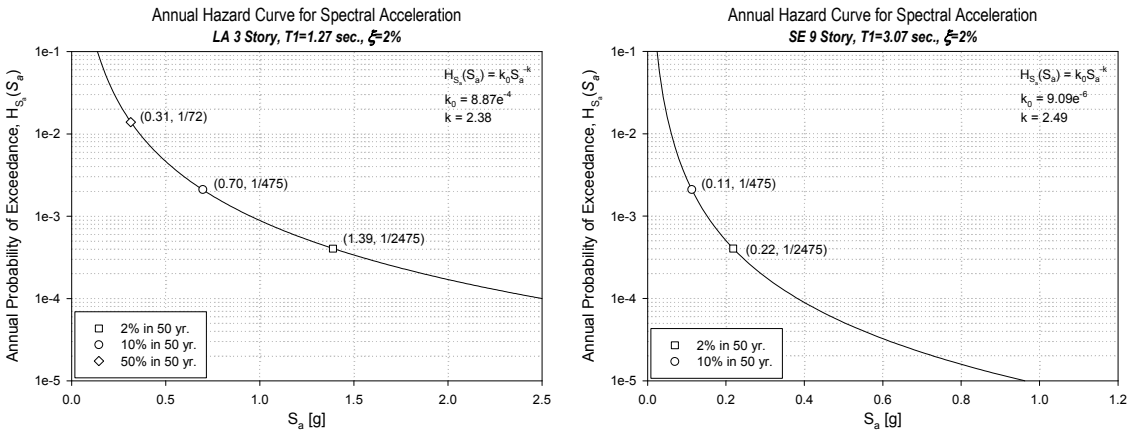

Figure 6.1 Annual spectral acceleration hazard curves for LA 3 story (left) and SE 9 story (right) model structures.

6.4. Median Seismic Demand vs. Ground Motion Intensity

Among the DMs investigated in Chapter 5, normalized hysteretic energy (NHE) and peak base shear (BS) do not have definite limit states that can be related to a structural performance level. They were investigated aiming at a better understanding of how the SMA connections altered the behavior of a structure. A correlation between the connection rotations and the story drifts was also observed (and reported by Maison and Kasai, 2000). Consequently, only the peak and residual story drifts are investigated within the probabilistic framework reviewed in Section 6.2.

The median relationship between the ground motion IM (as measured by S_{a1}) and the structural DM (as measured by $ISDA_{max}$ and $rISDA_{max}$) is established by using the results of the NTHAs of the finite element models for numerous ground motions at different levels of intensity. The S_{a1} is obtained from the elastic response spectrum of the acceleration record for 2% damping. The response of the finite element model subjected to each ground excitation provides the corresponding DM. For a set of S_{a1} versus DM data points, a simple power law relationship given by Equation 6.5 is assumed between the median values of the DM and S_{a1}. The benefits of the SMA connections as a passive control system should be reflected statistically through reduced values of the regression parameters *a* and/or *b* with respect to the corresponding values that describe the uncontrolled system. Once the median relationship between the IM and the DM and the dispersion of the DM given an IM are known, the IM hazard curve can be used to obtain a DM hazard curve (Equation 6.1). The resulting DM hazard curves provide a basis for comparison between the SMA passive control systems and the uncontrolled structures.

6.5. PSDA for the Los Angeles Three-Story Model Structures

6.5.1. Estimate of Peak and Residual Story Drift Demands

The S_{a1} versus $ISDA_{max}$ results (Table 6.1) for the Los Angeles ground acceleration records are plotted in Figure 6.2 for the three-story model structure with PR, martensitic SMA and superelastic SMA connections. The least-squares regression estimates of *a*, *b* and σ (Equation 6.7) are also presented in Figure 6.2.

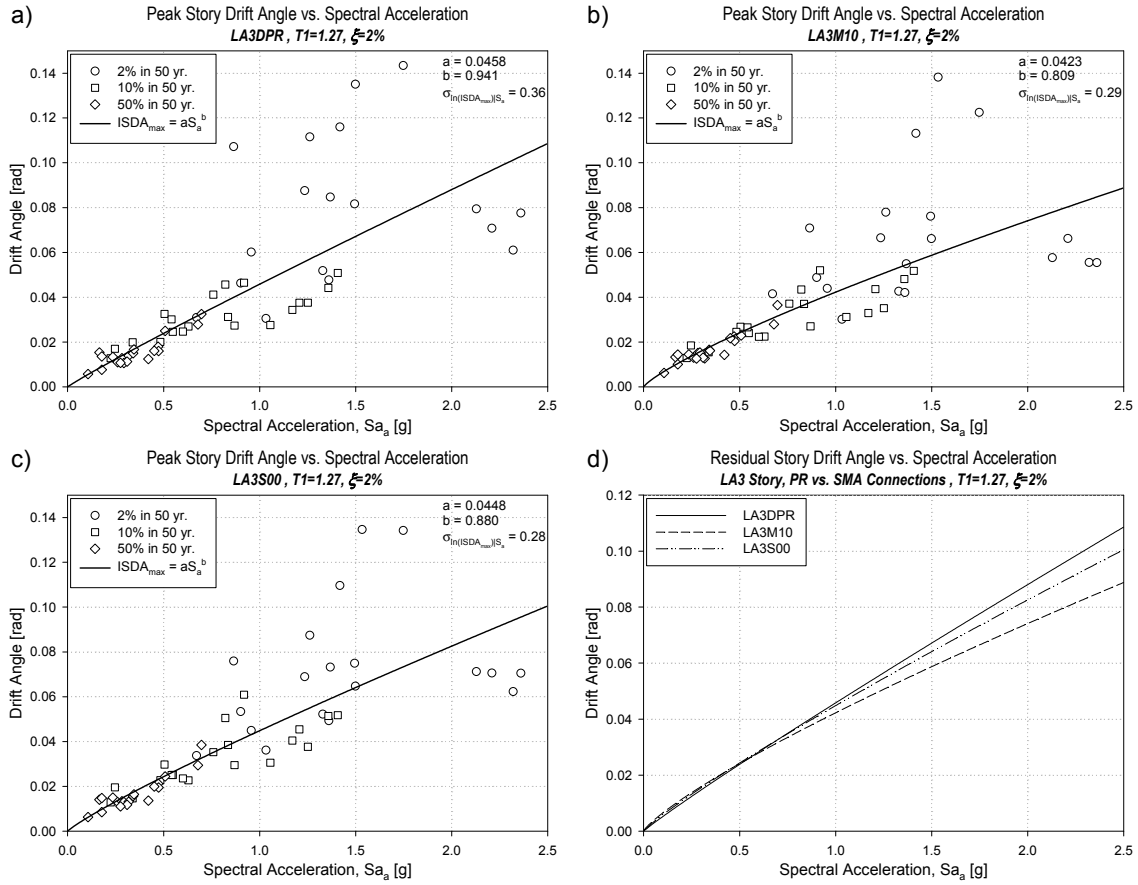

Figure 6.2 Peak story drift angle vs. spectral acceleration and least-squares regression results for LA 3 story model structure with PR (a), martensitic SMA (b) and superelastic SMA (c) connections and a comparison of their medians (d).

The plot of $ISDA_{max}$ for the uncontrolled three-story model structure displays significant amount of scatter, as apparent from the 36% dispersion, with most of the scatter stemming from the responses to the 2% in 50 yr. set of ground motions. Recall that failing PR connections were found to lead to significant increases in $ISDA_{max}$ demands (when compared to ductile PR connections) under the 2% in 50 yr. set (Section 5.5.1) which may explain the unusually high scatter. The uncontrolled $ISDA_{max}$ response shows very little hardening with increasing ground motion intensity, as apparent from the regression parameter *b* being smaller than (but still close to) unity. The implementation of both martensitic and superelastic SMA systems reduces the dispersion (to 29% and 28%, respectively) by means of controlling the $ISDA_{max}$ demand under high levels of seismic intensity. Reduced $ISDA_{max}$ demands also lead to smaller values for parameter *b* (0.809 for LA3M10 and 0.880 for LA3S00 compared to 0.940 for LA3DPR), introducing more hardening to the system and improving performance under seismic events with lower return periods. The pronounced hardening behavior observed in the model structures with SMA connections can be explained by a switch in the direction or a shift in the story in which the maximum drift is observed (Vamvatsikos and Cornell, 2002), as it was observed for the Los Angeles three-story structure (Section 5.5.4.1). The effect of both SMA systems on the $ISDA_{max}$ demand becomes apparent for ground motions with S_{a1} greater than 0.5 g, and increases with increasing seismic intensity. One observation that is common to all three systems is the reduced drift demands for S_{a1} values greater than 2.0 g. A possible explanation is that a stronger ground motion may lead to earlier yielding of a lower floor, which in turn acts as a fuse to reduce the demands on a higher floor, leading to a smaller $ISDA_{max}$ demand for the whole structure. Similar behavior was also observed in a three-story SMRF by Vamvatsikos and Cornell (2002).

Table 6.1 Record-by-record spectral acceleration and peak and residual story drift results for LA 3 story structure with PR and SMA connections.

Earthquake Record		S_{a1} (g)	Max. Peak Story Drift (rad)			Max. Residual Story Drift (rad)		
			LA3DPR	LA3M10	LA3S00	LA3DPR	LA3M10	LA3S00
10% in 50 yr. Set	LA01	0.87	0.0273	0.0270	0.0295	0.0010	0.0029	0.0031
	LA02	0.63	0.0269	0.0224	0.0227	0.0032	0.0017	0.0006
	LA03	0.50	0.0325	0.0269	0.0297	0.0019	0.0026	0.0006
	LA04	0.34	0.0199	0.0154	0.0147	0.0023	0.0016	0.0000
	LA05	0.55	0.0246	0.0240	0.0251	0.0025	0.0007	0.0004
	LA06	0.22	0.0128	0.0129	0.0129	0.0008	0.0004	0.0000
	LA07	0.48	0.0200	0.0245	0.0227	0.0013	0.0031	0.0001
	LA08	0.60	0.0247	0.0224	0.0235	0.0021	0.0025	0.0001
	LA09	1.41	0.0508	0.0517	0.0518	0.0126	0.0123	0.0079
	LA10	1.06	0.0276	0.0312	0.0305	0.0028	0.0026	0.0016
	LA11	0.82	0.0457	0.0434	0.0505	0.0074	0.0063	0.0012
	LA12	0.25	0.0170	0.0185	0.0195	0.0013	0.0007	0.0002
	LA13	1.25	0.0376	0.0351	0.0377	0.0072	0.0057	0.0014
	LA14	1.17	0.0344	0.0329	0.0404	0.0023	0.0077	0.0052
	LA15	0.84	0.0312	0.0370	0.0385	0.0013	0.0092	0.0040
	LA16	1.36	0.0442	0.0481	0.0514	0.0121	0.0072	0.0035
	LA17	0.76	0.0412	0.0371	0.0352	0.0039	0.0031	0.0015
	LA18	0.92	0.0465	0.0520	0.0609	0.0189	0.0113	0.0049
	LA19	0.54	0.0301	0.0266	0.0251	0.0036	0.0016	0.0003
	LA20	1.21	0.0376	0.0436	0.0455	0.0007	0.0018	0.0006
2% in 50 yr. Set	LA21	2.32	0.0610	0.0555	0.0623	0.0165	0.0153	0.0008
	LA22	1.33	0.0519	0.0426	0.0522	0.0053	0.0079	0.0005
	LA23	0.67	0.0309	0.0415	0.0337	0.0077	0.0037	0.0012
	LA24	1.50	0.1350	0.0661	0.0647	0.1121	0.0095	0.0005
	LA25	1.36	0.0477	0.0421	0.0493	0.0082	0.0109	0.0036
	LA26	2.21	0.0708	0.0662	0.0706	0.0025	0.0011	0.0018
	LA27	1.23	0.0875	0.0665	0.0689	0.0571	0.0115	0.0009
	LA28	1.49	0.0817	0.0761	0.0749	0.0069	0.0134	0.0031
	LA29	1.03	0.0305	0.0301	0.0361	0.0025	0.0037	0.0043
	LA30	0.96	0.0601	0.0440	0.0450	0.0238	0.0080	0.0047
	LA31	2.13	0.0794	0.0576	0.0712	0.0251	0.0143	0.0015
	LA32	2.36	0.0775	0.0554	0.0705	0.0193	0.0139	0.0039
	LA33	0.86	0.1072	0.0708	0.0759	0.0899	0.0164	0.0034
	LA34	1.37	0.0847	0.0549	0.0732	0.0497	0.0089	0.0042
	LA35	1.53	0.1546	0.1382	0.1346	0.1276	0.0550	0.0222
	LA36	1.75	0.1434	0.1224	0.1342	0.1324	0.0173	0.0168
	LA37	1.26	0.1116	0.0779	0.0874	0.0931	0.0158	0.0019
	LA38	1.65	“collapse”	0.1301	0.1388	“collapse”	0.0591	0.0275
	LA39	0.90	0.0463	0.0488	0.0533	0.0065	0.0197	0.0038
	LA40	1.42	0.1160	0.1131	0.1096	0.0810	0.0515	0.0074
50% in 50 yr. Set	LA41	0.68	0.0279	0.0279	0.0294	0.0030	0.0062	0.0040
	LA42	0.24	0.0134	0.0145	0.0150	0.0006	0.0002	0.0000
	LA43	0.26	0.0110	0.0131	0.0130	0.0001	0.0005	0.0000
	LA44	0.11	0.0057	0.0062	0.0063	0.0003	0.0001	0.0000
	LA45	0.28	0.0128	0.0152	0.0133	0.0006	0.0000	0.0000
	LA46	0.29	0.0106	0.0153	0.0130	0.0001	0.0032	0.0000
	LA47	0.17	0.0154	0.0133	0.0141	0.0016	0.0009	0.0000
	LA48	0.18	0.0076	0.0101	0.0085	0.0002	0.0003	0.0000
	LA49	0.32	0.0139	0.0127	0.0131	0.0009	0.0004	0.0000
	LA50	0.31	0.0112	0.0130	0.0118	0.0003	0.0002	0.0000
	LA51	0.47	0.0179	0.0225	0.0212	0.0012	0.0019	0.0012
	LA52	0.18	0.0136	0.0144	0.0148	0.0009	0.0007	0.0000
	LA53	0.42	0.0124	0.0143	0.0136	0.0012	0.0008	0.0000
	LA54	0.34	0.0150	0.0165	0.0157	0.0010	0.0021	0.0010
	LA55	0.35	0.0167	0.0161	0.0164	0.0005	0.0004	0.0000
	LA56	0.47	0.0160	0.0205	0.0195	0.0003	0.0005	0.0000
	LA57	0.28	0.0108	0.0127	0.0110	0.0009	0.0000	0.0000
	LA58	0.45	0.0161	0.0217	0.0199	0.0011	0.0014	0.0000
	LA59	0.70	0.0325	0.0364	0.0385	0.0021	0.0024	0.0005
	LA60	0.51	0.0249	0.0229	0.0244	0.0008	0.0023	0.0009

The median relationship between the residual drift ($rISDA_{max}$) and S_{a1} and the least-squares regression estimates (*a*, *b* and σ) for the three-story model structure with PR, martensitic SMA and superelastic SMA connections subjected to Los Angeles ground acceleration records are presented in Figure 6.3. The results of the 50% in 50 yr. set are negligible when compared to the results of the 2% and 10% in 50 yr. sets (see Table 6.1), and are excluded from the data set on which the regression of $rISDA_{max}$ on S_{a1} is performed.

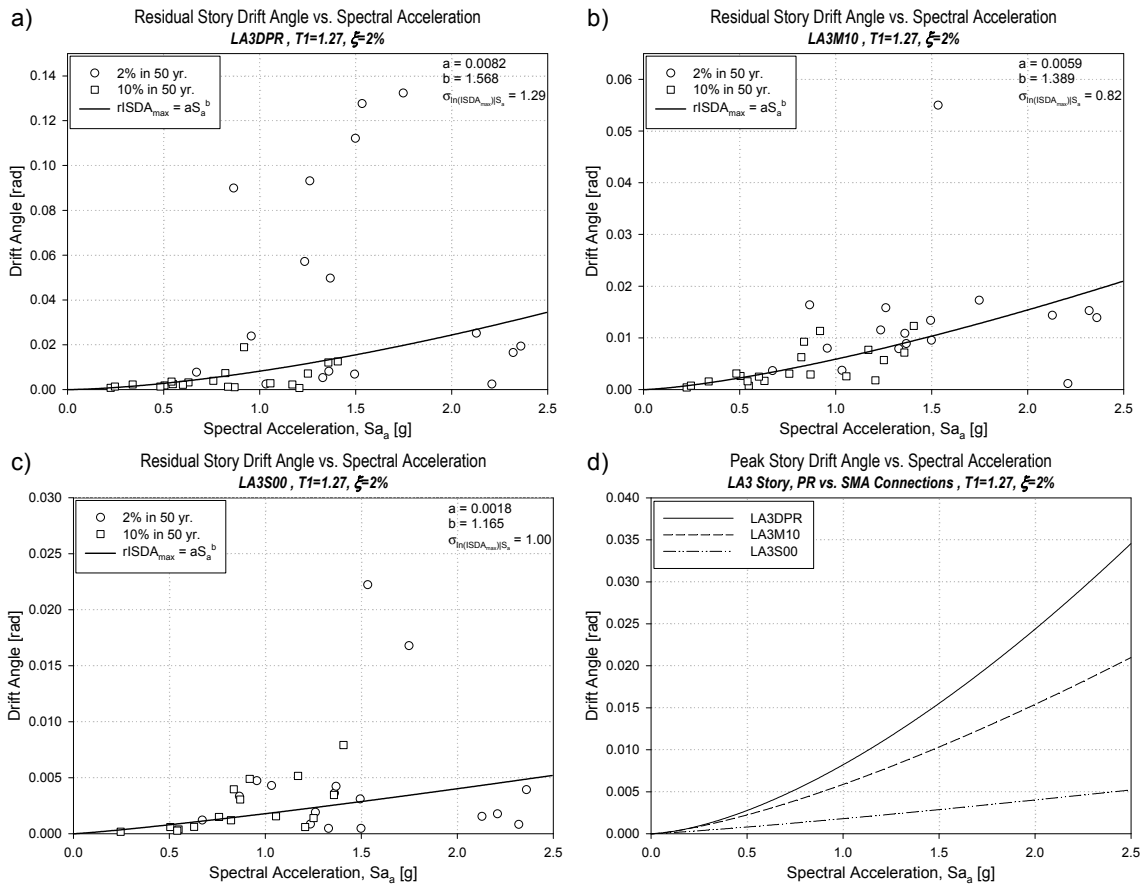

Figure 6.3 Residual story drift angle vs. spectral acceleration and least-squares regression results for LA 3 story model structure with PR (a), martensitic SMA (b) and superelastic SMA (c) connections and a comparison of their medians (d).

The regression of the predicted $rISDA_{max}$ demand on S_{a1} for the uncontrolled three-story structure is very poor, as is apparent from the 129% dispersion. As for the $ISDA_{max}$ regression, most of the scatter is due to the large residual drifts caused by the acceleration records in the 2% in 50 yr. set. Recall that the $rISDA_{max}$ response was found to be highly sensitive to PR connection failure under the 2% in 50 yr. ground motions, while being insensitive to PR connection failure under the 10% in 50 yr. set (see Section 5.5.1), which eventually leads to the observed high dispersion. The regression parameter *b* is estimated to be 1.568 which represents an undesirable softening behavior in which increases in S_{a1} produces correspondingly larger increases in the uncontrolled $rISDA_{max}$ demand. Both SMA systems reduce the dispersion in residual story drift (to 82% for LA3M10 and to 100% for LA3S00), but not to a level comparable to the dispersion observed in the controlled $ISDA_{max}$ response (28% for LA3M10 and 29% for LA3S00). Both SMA systems also reduce the softening observed in the uncontrolled $rISDA_{max}$ response and effectively control residual drifts under seismic events with low return periods.

6.5.2. Peak and Residual Drift Demand Hazards

Using the S_{a1} hazard (defined by the parameters *k* and k_0, see Figure 6.1), and the distribution of $ISDA_{max}$ and $rISDA_{max}$ demands given S_{a1} (defined by the parameters *b*, *a*, and σ, see Figures 6.2 and 6.3), the peak ($\lambda_{ISDAmax}$) and the residual ($\lambda_{rISDAmax}$) drift demand hazard curves are calculated according to Equation 6.9 and plotted in Figure 6.4 for the Los Angeles three-story model structure with PR and SMA connections. Also given in Table 6.2 are $ISDA_{max}$ and $rISDA_{max}$ demands corresponding 2% and 10% annual probabilities of exceedence.

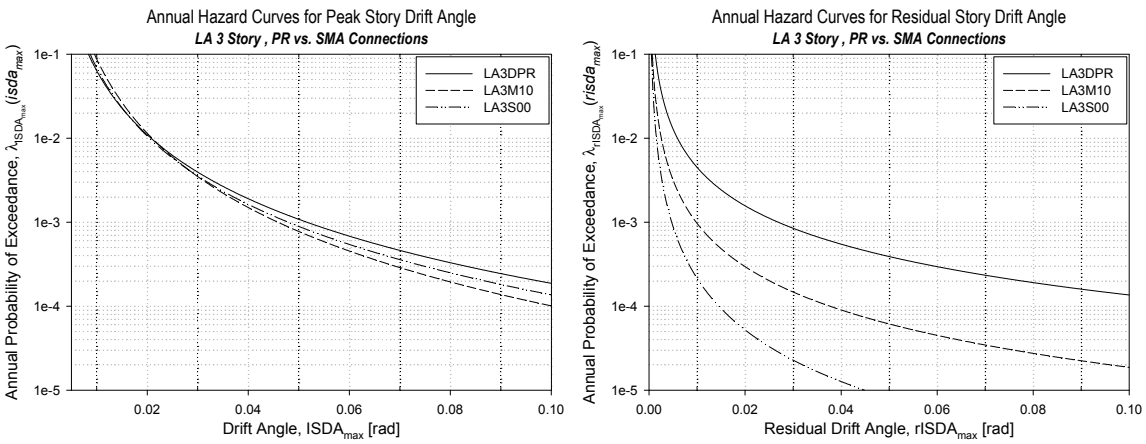

Figure 6.4 Annual hazard curves for peak (left) and residual (right) story drift demands for LA 3 story model structure with PR and SMA connections.

Table 6.2 Max. peak and residual story drift demands corresponding to different mean recurrence intervals for LA 3 story model structure with PR and SMA connections.

Mean Recurrence Interval	Max. Peak Story Drift (rad)			Max. Residual Story Drift (rad)		
	LA3DPR	LA3M10	LA3S00	LA3DPR	LA3M10	LA3S00
2,475 yr. (2% in 50 yr.)	0.074	0.062	0.067	0.0488	0.0166	0.0073
475 yr. (10% in 50 yr.)	0.039	0.036	0.036	0.0165	0.0064	0.0033

Both control strategies utilizing martensitic (LA3M10) and superelastic (LA3S00) SMA connections result in favorable reductions in $ISDA_{max}$ hazard when compared to the uncontrolled system (LA3DPR). For example, $ISDA_{max}$ demands corresponding to 2% annual probability of exceedence (or a 2,475 year mean recurrence interval) for the LA3DPR model structure are 19% and 10% greater than the LA3M10 and LA3S00 model structures, respectively (Table 6.2). However, no single SMA system proves to be most effective over the complete range of drift demands considered. The three hazard curves cross each other at an $ISDA_{max}$ of approximately 0.021 rad., leading to higher drift

demands at low return periods and lower drift demands at high return periods for both SMA systems when compared to the uncontrolled structure. This condition reflects the fact that SMA connections as passive control systems only impact the structural response if the deformation demands are sufficiently large. The $ISDA_{max}$ hazard for the martensitic and the superelastic SMA systems are similar for drift demands larger than 0.021 rad, the martensitic SMA system being the one with a smaller $ISDA_{max}$ hazard.

As is the case for $ISDA_{max}$, both SMA systems cause a decrease (over the uncontrolled system) in the MAF of exceeding a specified $rISDA_{max}$ demand (or, similarly, an decrease in $rISDA_{max}$ demand for a given hazard level). This beneficial effect, which is more pronounced for the superelastic SMA system, is a consequence of both the smaller median and the smaller dispersion of $rISDA_{max}$ given S_{a1} (Figure 6.3) observed in the controlled structures. The differences in $rISDA_{max}$ hazard between the martensitic and superelastic SMA systems and the uncontrolled system are greater at larger levels of $rISDA_{max}$ demand, which is apparent from the significant downward shift observed in the hazard curves. For example, the $rISDA_{max}$ demand corresponding to 2% annual probability of exceedence for the LA3DPR model structure is more than 2.9 and 6.6 times the $rISDA_{max}$ demands for the LA3M10 and LA3S00 model structures, respectively (Table 6.2).

6.6. PSDA for the Seattle Nine-Story Model Structures

6.6.1. Estimate of Peak and Residual Story Drift Demands

The S_{a1} versus $ISDA_{max}$ results (Table 6.3) for the Seattle ground acceleration records are plotted in Figure 6.5 for the nine-story model structure with PR, martensitic SMA and

superelastic SMA connections. The least-squares regression estimates of *a*, *b* and σ (Equation 6.7) are also presented in Figure 6.5.

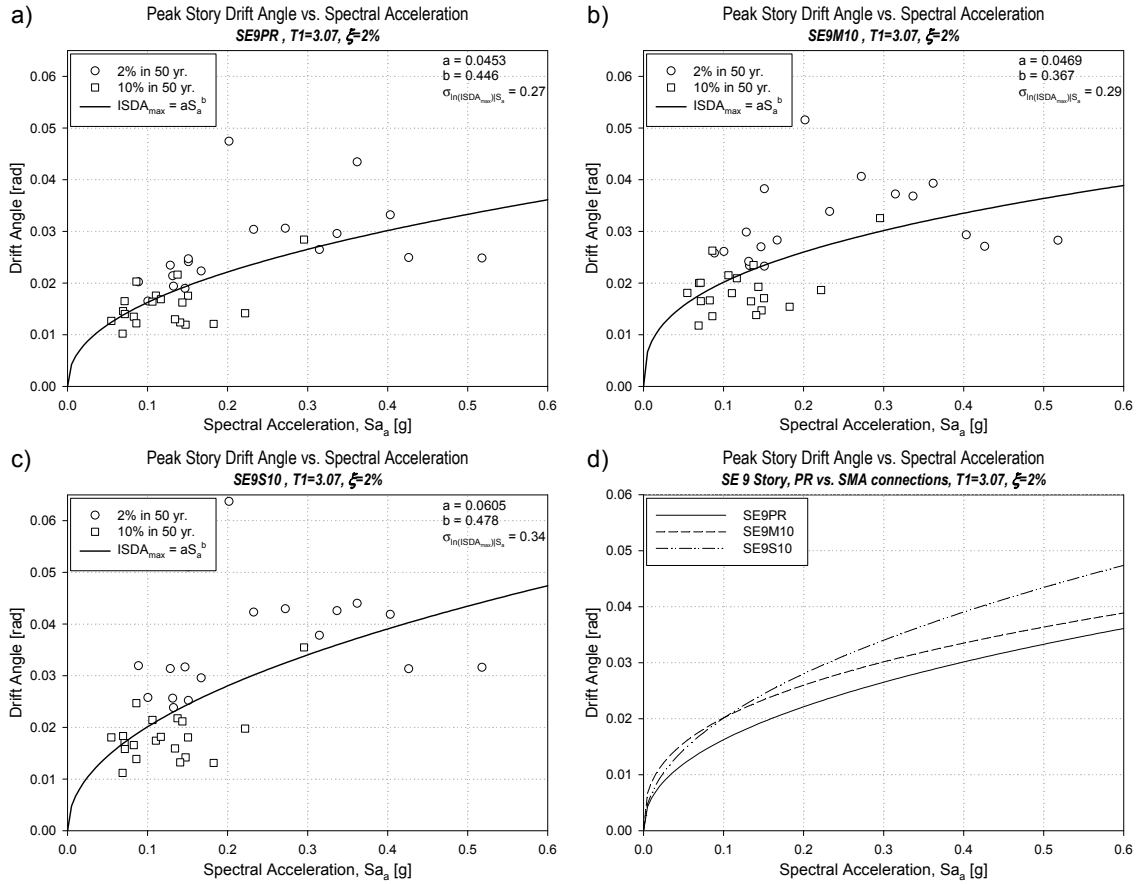

Figure 6.5 Peak story drift angle vs. spectral acceleration and least-squares regression results for SE 9 story model structure with PR (a), martensitic SMA (b) and superelastic SMA (c) connections and a comparison of their medians (d).

Even though the martensitic SMA system exhibits slightly stronger hardening behavior than the uncontrolled structure (*b* parameter of 0.367 for SE9M10 vs. 0.446 for SE9PR), it results in larger $ISDA_{max}$ demand over the range of S_{a1} values considered (0 to 0.6 g). This is also apparent from the regression parameter *a*, which can be interpreted as the

DM corresponding to unit IM (*a* parameter of 0.0469 for SE9M10 vs. 0.0453 for SE9PR). The stronger hardening observed in the martensitic SMA system reduces the $ISDA_{max}$ response at higher levels of S_{a1} that are associated with very long return periods, rendering it ineffective in controlling the $ISDA_{max}$ demand in the nine-story structure. The superelastic SMA system not only exhibit the smallest amount of hardening (*b* parameter of 0.478), it also has the largest dispersion (34% for SE9S10 vs. 29% for SE9M10 and 27% for SE9PR), making it the least favorable choice for controlling the $ISDA_{max}$ demand. Note that the *b* parameter for all three systems is significantly smaller than unity[1], indicating a hardening behavior which is different than what has been observed for the FR SMRFs investigated in the SAC project (approximately *b*=1, e.g. Luco and Cornell, 1998, 2000). This hardening behavior, where increases in S_{a1} produce correspondingly smaller changes in $ISDA_{max}$, can be attributed to the flexibility of the nine-story PR frame, which leads to reduction of the inertial forces.

1. Note that b=1 implies that the total displacement is equal to the elastic displacement, regardless of nonlinear action, which is the "equal displacement rule" first advanced by Veletsos and Newmark (1960).

Table 6.3 Record-by-record spectral acceleration and peak and residual story drift results for SE 9 story structure with PR and SMA connections.

Earthquake Record		S_{a1} (g)	Max. Peak Story Drift (rad)			Max. Residual Story Drift (rad)		
			SE9PR	SE9M10	SE9S10	SE9PR	SE9M10	SE9S10
10% in 50 yr. Set	SE01	0.30	0.0284	0.0326	0.0355	0.0091	0.0073	0.0004
	SE02	0.15	0.0176	0.0171	0.0181	0.0022	0.0021	0.0003
	SE03	0.08	0.0135	0.0167	0.0166	0.0027	0.0024	0.0003
	SE04	0.15	0.0119	0.0147	0.0142	0.0013	0.0014	0.0002
	SE05	0.18	0.0121	0.0154	0.0131	0.0021	0.0022	0.0004
	SE06	0.22	0.0142	0.0186	0.0198	0.0018	0.0009	0.0000
	SE07	0.07	0.0146	0.0200	0.0183	0.0014	0.0013	0.0000
	SE08	0.07	0.0165	0.0201	0.0170	0.0018	0.0015	0.0001
	SE09	0.07	0.0102	0.0118	0.0112	0.0008	0.0010	0.0002
	SE10	0.11	0.0176	0.0180	0.0174	0.0071	0.0038	0.0002
	SE11	0.12	0.0169	0.0209	0.0182	0.0048	0.0030	0.0003
	SE12	0.07	0.0140	0.0165	0.0158	0.0019	0.0012	0.0002
	SE13	0.09	0.0122	0.0136	0.0139	0.0015	0.0011	0.0002
	SE14	0.14	0.0124	0.0138	0.0132	0.0018	0.0012	0.0003
	SE15	0.11	0.0164	0.0215	0.0214	0.0025	0.0019	0.0003
	SE16	0.14	0.0216	0.0235	0.0217	0.0072	0.0046	0.0001
	SE17	0.13	0.0130	0.0165	0.0159	0.0015	0.0004	0.0001
	SE18	0.14	0.0162	0.0193	0.0212	0.0007	0.0006	0.0003
	SE19	0.09	0.0203	0.0263	0.0247	0.0036	0.0014	0.0004
	SE20	0.05	0.0127	0.0181	0.0181	0.0008	0.0003	0.0002
2% in 50 yr. Set	SE21	0.49	"collapse"	0.0683	0.0689	"collapse"	0.0341	0.0015
	SE22	0.13	0.019	0.0234	0.0238	0.005	0.0039	0.0000
	SE23	0.40	0.033	0.0293	0.0419	0.012	0.0045	0.0009
	SE24	0.36	0.043	0.0393	0.0440	0.026	0.0115	0.0009
	SE25	0.43	0.025	0.0271	0.0313	0.006	0.0030	0.0008
	SE26	0.52	0.025	0.0282	0.0316	0.001	0.0038	0.0011
	SE27	0.27	0.031	0.0406	0.0429	0.010	0.0067	0.0010
	SE28	0.17	0.022	0.0283	0.0296	0.007	0.0036	0.0004
	SE29	0.31	0.026	0.0372	0.0378	0.006	0.0109	0.0005
	SE30	0.34	0.030	0.0368	0.0426	0.008	0.0020	0.0005
	SE31	0.20	0.047	0.0516	0.0637	0.018	0.0054	0.0004
	SE32	0.13	0.023	0.0298	0.0314	0.004	0.0043	0.0007
	SE33	0.15	0.024	0.0383	0.0510	0.004	0.0033	0.0005
	SE34	0.10	0.017	0.0261	0.0258	0.002	0.0011	0.0004
	SE35	0.09	0.020	0.0258	0.0319	0.002	0.0012	0.0001
	SE36	0.26	"collapse"	0.0508	0.0511	"collapse"	0.0271	0.0020
	SE37	0.15	0.019	0.0270	0.0317	0.001	0.0010	0.0001
	SE38	0.23	0.030	0.0338	0.0423	0.013	0.0066	0.0006
	SE39	0.15	0.025	0.0232	0.0252	0.002	0.0017	0.0003
	SE40	0.13	0.021	0.0242	0.0256	0.004	0.0005	0.0001

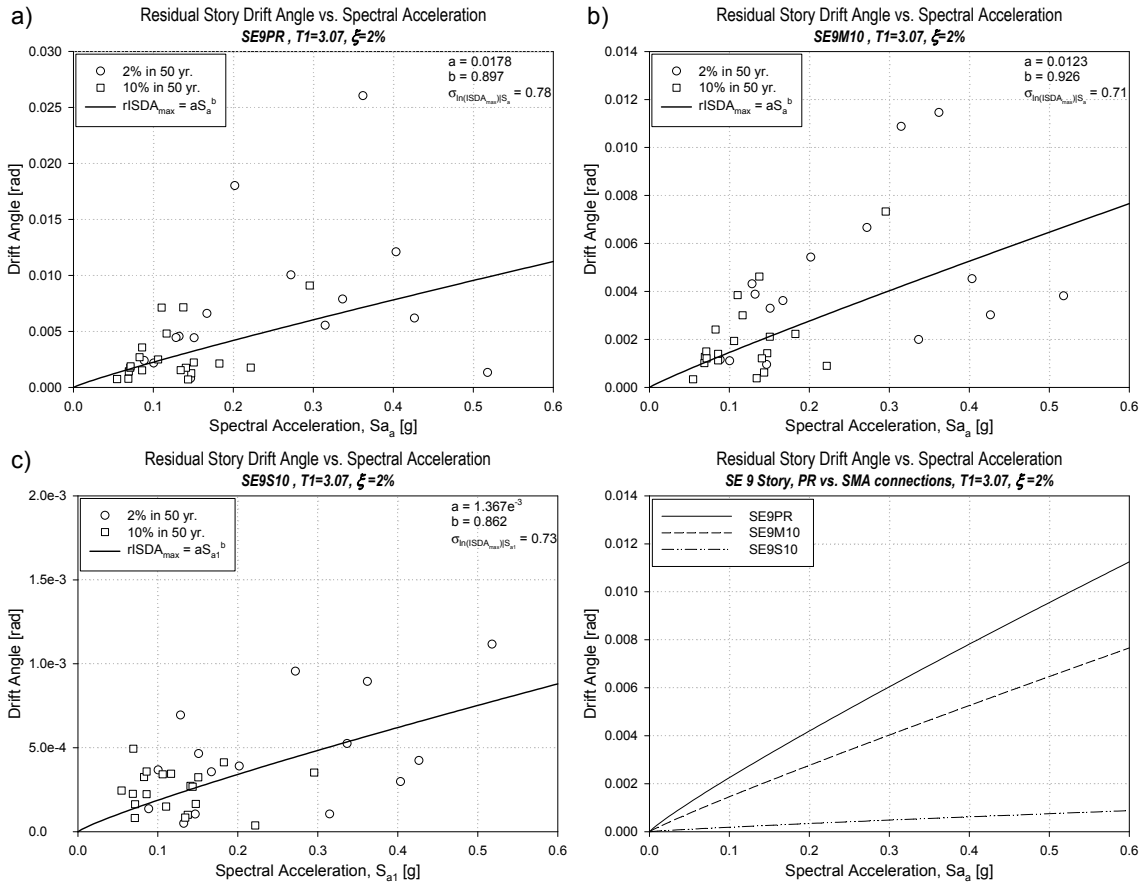

Figure 6.6 Residual story drift angle vs. spectral acceleration and least-squares regression results for SE 9 story model structure with PR (a), martensitic SMA (b) and superelastic SMA (c) connections and comparison of their medians (d).

The regression of the predicted rISDA$_{max}$ demand on S_{a1} for the uncontrolled nine-story structure exhibits a slight hardening behavior (*b* parameter of 0.897) along with significant dispersion (78%). The martensitic SMA system not only reduces the rISDA$_{max}$ demand with increasing S_{a1} values, but also reduces the dispersion observed in the uncontrolled system (to 71%). Among the two SMA systems considered, the superelastic SMA system is the most effective controlling the rISDA$_{max}$ demand, virtually eliminating permanent drifts within the range of S_{a1} considered (0 to 0.6g).

6.6.2. Peak and Residual Drift Demand Hazards

Using the S_{a1} hazard (defined by the parameters k and k_0, see Figure 6.1), and the distribution of $ISDA_{max}$ and $rISDA_{max}$ demands given S_{a1} (defined by the parameters b, a, and σ, see Figures 6.5 and 6.6), the peak ($\lambda_{ISDAmax}$) and the residual ($\lambda_{rISDAmax}$) drift demand hazard curves are calculated according to Equation 6.9 and are plotted in Figure 6.7 for the Seattle nine- story model structure with PR and SMA connections. Also given in Table 6.4 are $ISDA_{max}$ and $rISDA_{max}$ demands corresponding to 2% and 10% annual probabilities of exceedence.

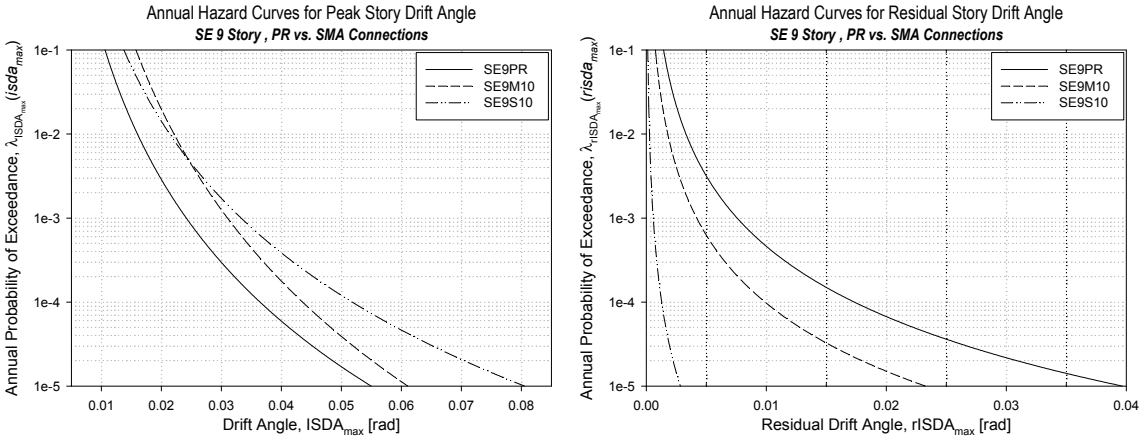

Figure 6.7 Annual hazard curves for peak (left) and residual (right) story drift demands for SE 9 story model structure with PR and SMA connections.

Table 6.4 Max. peak and residual story drift demands corresponding to different mean recurrence intervals for SE 9 story model structure with PR and SMA connections.

Mean Recurrence Interval	Max. Peak Story Drift (rad)			Max. Residual Story Drift (rad)		
	SE9PR	SE9M10	SE9S10	SE9PR	SE9M10	SE9S10
2,475 yr. (2% in 50 yr.)	0.028	0.034	0.040	0.0105	0.0059	0.0008
475 yr. (10% in 50 yr.)	0.021	0.028	0.029	0.0058	0.0032	~0

The martensitic SMA system produces a fairly even shift upwards of the $ISDA_{max}$ hazard over the range of return periods considered. The superelastic SMA system results in a smaller $ISDA_{max}$ hazard for demands greater than approximately 0.025 rad. when compared to the martensitic SMA system. As was observed in Section 5.6.4.1, the connection rotation demands in the nine-story structure are not large enough for the two SMA systems to be effective, leading to the amplified $ISDA_{max}$ hazard observed for the two SMA systems. For example, $ISDA_{max}$ demands corresponding to 2% annual probability of exceedence for the SE9PR model structure are 18% and 30% less than the SE9M10 and SE9S10 model structures, respectively (Table 6.4) On the other hand, a significant reduction in the $rISDA_{max}$ hazard is achieved with the help of the SMA systems, which is apparent from the downward shift of the hazard curves when the SMA connections are employed. The superelastic SMA system (SE9S10) virtually eliminates $rISDA_{max}$ demand while the martensitic SMA system results in an average 44% reduction for the 2% in 50 yr. event (Table 6.4).

6.7. Conclusions

The peak and residual drift demand hazard curves for the Los Angeles three-story and the Seattle nine-story frames provide a concise way to summarize the effects of the SMA

connections that were also investigated in Chapter 5 in a probabilistic format. By either means, it is observed that the benefits of the SMA connections depend on the demand level and the type of structure they are implemented in.

A comparative analysis of the hazard curves indicates that no single strategy is the most effective for controlling the $ISDA_{max}$ demand at all hazard levels. While the martensitic SMA system is the most effective strategy for the three-story structure subjected to ground motions with longer return periods, the reduction in the $ISDA_{max}$ hazard is still not substantial. On the other hand, the hazard curves developed for $rISDA_{max}$ indicate that the superelastic SMA system is the most effective strategy for reducing the $rISDA_{max}$ demands for the three- and the nine-story structures at all hazard levels. The martensitic SMA system is also effective in reducing the $rISDA_{max}$ hazard, although this effect is less pronounced. For both martensitic and superelastic SMA systems, the reduction in the $rISDA_{max}$ hazard is obtained at the expense of increase in the $ISDA_{max}$ hazard for the nine-story structure, indicating that the selection of a particular system must be based on a specific performance objective.

CHAPTER 7

SUMMARY, CONCLUSIONS, AND FUTURE RESEARCH

7.1. Summary

Shape Memory Alloys (SMAs) exhibit the ability to undergo large deformations but can recover permanent strains via heating (shape memory effect) or when stress is removed (superelastic effect). This study has evaluated the comparative seismic performance of steel moment resisting frames (SMRFs) with innovative beam-to-column connections that use SMA bars as connecting elements.

The performance evaluation studies are based on two types of SMA beam-to-column connections: (1) superelastic SMA connections with recentering capability; (2) martensitic SMA connection with high energy dissipation capacity. Fiber models for these SMA connections are implemented in the OpenSees finite element framework, and are verified against data from full-scale experimental tests that were performed on a prototype SMA connection in previous research at Georgia Tech. Three- and nine-story model buildings with partially restrained (PR) moment frames are selected from the SAC Phase II Project as case studies. Nonlinear time history analyses on these model buildings, with and without SMA connections, are conducted using suites of ground acceleration records from the SAC Phase II project that represent different seismic hazard levels. The effects of SMA connections on peak and residual inter-story drift angles, connection rotations, and normalized dissipated hysteretic energy demands and the sensitivity of the demand measures to variations in SMA connection design are quantified.

The seismic demands on the model buildings with conventional PR and selected SMA connections are evaluated in a probabilistic framework. The resulting seismic demand relationships are used to assess the effectiveness of the SMA connections in enhancing the building performance over a range of demand levels. The results of this performance evaluation show that the SMA connections are most effective in controlling structural response under high levels of seismic intensity leading to large deformation demands. In particular, the energy dissipating SMA connections are effective in reducing maximum deformation demands, while the recentering SMA connections are more suitable for controlling residual deformations in the structure.

7.2. Conclusions

Some of the specific conclusions that can be drawn from this dissertation for the comparative seismic performance SMRFs with SMA connections are as follows:

- Explicit modeling of limited ductility of PR connections may be necessary for PR frames located at regions of high seismicity: Failure of PR connections affected the predicted peak and residual deformation demands considerably on the three-story structure, albeit only for seismic events with high return periods. This was not the case for the nine-story structure, even for the high seismic hazard, mainly because the observed connection rotation demands were within the ductile range. Both structures were found to be prone to dynamic instability.

- Martensitic SMA connections are most effective in controlling peak deformation demands: Post-yield stiffness and energy dissipation capacity provided by the martensitic SMA connections lessened the instances of dynamic instability in the three- and nine-story structures and reduced the peak and residual deformation demands in the three-story structure considerably. This was not the case for the nine-story structure for the peak deformation demands. Most of the benefits of using

martensitic SMA connections were observed under high seismic hazard, and were less apparent at lower levels of seismicity.

- Superelastic SMA connections are most effective in controlling residual deformation demands: The self-recentering capability of superelastic SMA connections significantly reduced (for the three-story structure), and virtually eliminated (for the nine-story structure) the residual deformation demands over a range of seismic hazard. Even though the reduction of the residual deformation demands was obtained at the expense of increased peak deformation demands for the nine-story structure, the instances of dynamic instability were effectively mitigated in both the three- and the nine-story structures.

- No single passive control strategy utilizing SMA connections is most effective for reducing seismic demands over a range of hazard levels; hence, the selection of a particular system must be based on a specific performance objective. In general, both martensitic and superelastic SMA connections required a certain amount of connection rotation demand to be effective in reducing peak deformation demands. On the contrary, superelastic SMA connections effectively reduced residual deformation demands regardless of the rotation demand imposed on the connections.

7.3. Future Research

This work presents a probabilistic seismic assessment of the comparative performance SMRFs with SMA connections. The performance assessment procedure involves development of mathematical models to represent physical phenomena, performing of nonlinear dynamic analyses to estimate seismic demands, and processing of the results in order to perform probabilistic seismic demand assessments. At every step, certain assumptions were made, which define the limitations of this work as well as possible suggestions for future research:

- A more accurate assessment of seismic demands can be made by means of more refined modeling techniques, such as utilization of three-dimensional finite element models instead of two-dimensional frames, consideration of possible nonlinearity in girders and panel zones, and more refined force-deformation models to represent the SMA stress-strain and SMA and PR connection moment-rotation behaviors.

- The two case studies investigated in this dissertation may not be the most appropriate candidates for implementation of SMA connections: Highly flexible PR connection designs utilized in the two PR frames required rather large connection rotations to dissipate significant energy, limiting the effectiveness of the SMA systems. The information obtained in Chapter 5 can be used to design alternate case studies to be investigated along with hybrid SMA connection systems consisting of superelastic and martensitic SMA connections.

- Through this dissertation, the relative performance of SMRFs with PR and SMA connections are assessed by the changes (reduction/increase) in the predicted seismic demands (Chapter 5) and by comparing the demand hazard curves over a range of demand levels (Chapter 6). This approach can be extended to a complete seismic performance evaluation by means of determining performance limits specific to each frame and relating seismic response of the frames to multiple performance levels.

- The probabilistic framework utilized to develop the demand hazard curves considers the randomness as the only source of uncertainty in the seismic demand assessment. It can further be extended to explicitly distinguish between aleatory and epistemic uncertainties in the demand/capacity estimation and in the seismic hazard. Along with structure specific limit states, the demand hazard curves can be convolved with fragility relationships to obtain a point estimate for annual limit state probabilities that account for all sources of uncertainty.

- Finally, the experimental data used to validate the fiber SMA connection model is from a proof-of-concept specimen rather than a typical connection design. The promising results presented in this dissertation along with the tools implemented to

facilitate parametric studies can stimulate further experimental work on design, testing and pre-qualification of practical SMA connection details.

CHAPTER III

EXTENSIONS TO THE FINITE ELEMENT PLATFORM

A.1. Introduction

The OpenSees finite element framework is designed using an object-oriented architecture that promotes using the existing classes to develop new components. This chapter presents the user information for the new features implemented to OpenSees as a part of this research. A detailed explanation of OpenSees object-oriented architecture can be found in McKenna (1997).

A.2. Uniaxial Force-Deformation Models

A.2.1. PRConnection Model

The `PRConnection`[1] uniaxial force-deformation model is an implementation of the PR connection moment-rotation algorithm used in the SAC study (Maison and Kasai, 2000) that is extended to account for connection failure. The corresponding OpenSees command and arguments are given in Table A.1.

1. OpenSees commands/classes corresponding to a certain feature are presented with a different style, e.g. `PRConnection`.

Table A.1 PRConnection uniaxial material syntax.

uniaxialMaterial PRConnection $matTag $pUA $pMA $pUB $pMB $pShr $pN $pMU $pMApinch $pMBpinch $nMA $nUB $nMB $nShr $nN $nMU $nMApinch $nMBpinch	
$matTag	Unique material object integer tag
$pUA	(+) control deformation that defines the linear elastic portion of the envelope
$pMA	(+) force corresponding the control deformation $pUA
$pUB	(+) control deformation that defines the end of curved portion of the envelope
$pMB	(+) force corresponding the control deformation $pUB
$pShr	Strain hardening stiffness for the envelope on (+) quadrant, as a ratio of initial stiffness ($pMA / $pUA)
$pN	Power used to define the curve between ($pUA, $pMA) and ($pUB, $pMB) on (+) quadrant
$pMU	(+) limiting moment for the envelope
$pMApinch	(+) control moment corresponding to $pUA that lies on the pinching envelope. $pMApinch < $pMA
$pMBpinch	(+) control moment corresponding to $pUB that lies on the pinching envelope. $pMBpinch < $pMB
$nMA	(-) control deformation that defines the linear elastic portion of the envelope
$nUB	(-) control deformation that defines the end of curved portion of the envelope
$nMB	(-) force corresponding the control deformation $nUB
$nShr	Strain hardening stiffness for the envelope on (-) quadrant, as a ratio of initial stiffness ($pMA / $pUA)
$nN	Power used to define the curve between ($nUA, $nMA) and ($nUB, $nMB) on (-) quadrant
$nMU	(-) limiting moment for the envelope
$nMApinch	(-) control moment corresponding to $nUA that lies on the pinching envelope. \|$nMApinch| < |$nMA|
$nMBpinch	(-) control moment corresponding to $nUB that lies on the pinching envelope. \|$nMBpinch| < |$nMB|

A.2.2. SuperelasticSMA Model

The `SuperelasticSMA` uniaxial force-deformation model is an implementation of the phenomenological force-displacement relationship developed by DesRoches et al. (2004). was chosen for this purpose. The corresponding OpenSees command and arguments are given in Table A.2.

Table A.2 SuperelasticSMA uniaxial material syntax.

uniaxialMaterial SuperelasticSMA $matTag $elasticStiffness $pLoadingPlateauStress $pUnloadingPlateauStress $pLoadingPlateauStiffnessRatio $pTransformationStrain $pMartensiteStiffnessRatio $nLoadingPlateauStress $nUnloadingPlateauStress $nLoadingPlateauStiffnessRatio $nTransformationStrain $nMartensiteStiffnessRatio	
$matTag	Unique material tag
$elasticStiffness	Initial modulus of elasticity of the material in Austenite state
$pLoadingPlateauStress	(+) stress where transformation from Austenite to Martensite starts
$pUnloadingPlateauStress	(+) stress where transformation from Martensite to Austenite ends
$pLoadingPlateauStiffness	Loading plateau stiffness on (+) quadrant, as a ratio of initial stiffness
$pTransformationStrain	(+) strain where transformation from Austenite to Martensite ends
$pMartensiteStiffnessRatio	Elastic stiffness of fully-transformed Martensite on (+) quadrant, as a ratio of initial stiffness
$nLoadingPlateauStress	(-) stress where transformation from Austenite to Martensite starts
$nUnloadingPlateauStress	(-) stress where transformation from Martensite to Austenite ends
$nLoadingPlateauStiffness	Loading plateau stiffness on (-) quadrant, as a ratio of initial stiffness
$nTransformationStrain	(-) strain where transformation from Austenite to Martensite ends
$nMartensiteStiffnessRatio	Elastic stiffness of fully-transformed Martensite on (-) quadrant, as a ratio of initial stiffness

A.3. Recorders

A.3.1. Energy Recorder

The `Energy` recorder makes is possible to calculate the strain, damping, kinetic, and total energy stored in an element or a group of elements at any instant of a transient analysis. The elements that can be monitored with an `Energy` recorder are of type `ElasticBeamColumn`, `NonlinearBeamColumn`, or `ZeroLengthSection`. The corresponding OpenSees command and arguments are given in Table A.3.

Table A.3 Energy recorder syntax.

recorder Energy <-file $fileName> <-time> <-ele ($ele1 $ele2 ...)> <-node ($node1 $node2 ...)> <-eleRange $startEle $endEle> <-nodeRange $startNode $endNode> <-elementRegion $regTag> <-nodeRegion $regTag> <-ele all> <-node all> <-cumulative> $energyType	
$fileName	File where results are stored. Each line of the file contains the result for a converged state (optional, default screen output)
-time	Puts the pseudo time as the first entry in the line (optional)
$ele1 $ele2 ...	Tags of elements whose response is being recorded -- selected elements in domain (optional)
$node1 $node2 ...	Tags of nodes whose response is being recorded (optional)
$startEle $endEle	Tags for start and end elements whose response is being recorded -- range of selected elements in domain (optional, default all)
$startNode $endNode	Tags for start and end nodes whose response is being recorded -- range of selected elements in domain (optional, default all)
$regTag	previously defined tag of region of elements/nodes in domain (optional)
all	elements/nodes whose response is being recorded -- all elements/nodes in domain (optional & default)
-cumulative	Sums up the responses of elements/nodes which are being monitored (optional)
$energyType	Options: strainEnery, DampingEnergy, KineticEnergy, TotalEnergy

REFERENCES

“OpenSees - Open System for Earthquake Engineering Simulation.” (2007). June 1, <http://opensees.berkeley.edu/>

“Post-tensioned connection systems for seismic-resistant steel frames.” (2005). June 1, <http://www.u.arizona.edu/~asumer/>

“USGS National Seismic Hazard Mapping Project.” (2007).June 1, <http://eqhazmaps.usgs.gov>

Abdalla, K. M. and Chen, W. F. (1995). "Expanded database of semi-rigid steel connections ." Computers & Structures, 56(4), 553-564.

Aizawa, S., Kakizawa, T., and Higasino, M. (1998). "Case studies of smart materials for civil structures." Smart Materials and Structures, 7(5), 617-26.

Andrawes, B., McCormick, J., and Desroches, R. (2004). "Effect of cyclic modeling parameters on the behavior of shape memory alloys for seismic applications." Smart Structures and Materials 2004 - Smart Structures and Integrated Systems, International Society for Optical Engineering, Bellingham, WA, p 324-334.

Astaneh-Asl, A. and Nader, M. N. (1990). "Experimental studies and design of steel tee shear connections." Journal of Structural Engineering, 116(10), 2882-2902.

Astaneh-Asl, A., Nader, M. N., and Malik, L. (1989). "Cyclic behavior of double angle connections ." Journal of Structural Engineering, 115(5), 1101-1118.

Azizinamini, A. and Radziminski, J. B. (1989). "Static and cyclic performance of semirigid steel beam-to-column connections." Journal of Structural Engineering, 115(12), 2979-2997.

Baber, T.T. and Wen, Y.K. (1981). "Random vibration of hysteretic degrading systems." Journal of Engineering Mechanics, 107(6), 1069-1086.

Baker, J. W. (2005). "Vector-Valued Ground Motion Intensity Measures for Probabilistic Seismic Demand Analysis." Stanford University.

Barroso, L. R. and Winterstein, S. (2002). "Probabilistic seismic demand analysis of controlled steel moment-resisting frame structures." Earthquake Engineering and Structural Dynamics, 31(12), 2049-2066.

Benjamin J. R., Cornell C. A. (1970). “Probability, Statistics, and Decision for Civil Engineers.” McGraw Hill, Inc., New York.

Bernuzzi, C., Zandonini, R., and Zanon, P. (1996). "Experimental Analysis and Modelling of Semi-rigid Steel Joints under Cyclic Reversal Loading ." Journal of Constructional Steel Research, 38(2), 95-123.

Bursi, O. S., Ballerini M., Nemati, N., and Zandonini, R. (1996). "Quasi-static monotonic and low-cycle behaviour of steel isolated tee stub connections." Stessa '97: Second International Conference on the Behaviour of Steel Structures in Seismic Areas.

Calado, L. (2003). "Non-linear cyclic model of top and seat with web angle for steel beam-to-column conections." Engineering Structures, 25(9), p 1189-1197.

Calado, L., De Matteis, G., Lanfoldo, R., and Mazzolani, F. M. (1999). "Cyclic behavior of steel beam-to-column connections : Interpretation of experimental results." Stability and ductility of steel structures : Proceedings of the 6th International Colloquium, first session, SDSS'99, Elsevier, Amsterdam; New York, p 211-220.

CEN (1997). "Eurocode 3, Part 1.1: Joints in Building Frames (Annex J)." Rep. No. CEN/ TC250/SC3-PT9, Comite Europeen de Normalisation.

Chen, W. F. and Kishi, N. (1989). "Semi-rigid steel beam-to-column connections: Data base and modeling." Journal of Structural Engineering, 115(1), 105-119.

Chen, P. F.-S. and Powell, G. H. (1982). "Generalized plastic hinge concepts for 3D beam-column elements." Rep. No. UCB/EERC-82/20 , Earthquake Engineering Research Center, University of California, Berkeley.

Chen, S. J., Yeh, C. H., and Chu, J. M. (1996). "Ductile Steel Beam-to-Column Connections for Seismic Resistance." Journal of Structural Engineering, 122(11), 1292-1299.

Chen, S. J., Yeh, C. H., and Chu, J. M. (1997). "Dynamic Behavior of Steel Frames with Beam Flanges Shaved Around Connection ." Journal of Constructional Steel Research, 42(1), 49-70.

Chen, S. J., Tsao, Y. C., and Chao, Y. C. (2001). "Enhancement of ductility of existing seismic steel moment connections." Journal of Structural Engineering, 127(5), 538-545 .

Civjan, S. A., Engelhardt, M. D., and Gross, J. L. (2000). "Retrofit of Pre-Northridge Moment-Resisting Connections." Journal of Structural Engineering, 126(4), 445-4452.

Cornell, C. A. (1996). "Calculating building seismic performance reliability: a basis for multi-level design norms." Proceedings of the 11th World Conference on Earthquake Engineering, Paper No. 2122, Acapulco, Mexico.

Cornell, C. A., Jalayer, F., Hamburger, R. O., and Foutch, D. A. (2002). "Probabilistic Basis for 2000 SAC Federal Emergency Management Agency Steel Moment Frame Guidelines." Journal of Structural Engineering, 128(4), 526-533.

Delemont, M. (2001), "Seismic Retrofit of Bridges Using Shape Memory Alloys." Department of Civil and Environmental Engineering, Georgia Institute of Technology.

Della Corte, G., De Matteis, G., and Lanfoldo R. (2000). "Influence of connection modeling on seismic response of moment resisting steel frames." Moment resistant connections of steel frames in seismic areas : Design and reliability, E & FN Spoon, London and New York, p 485-512.

Della Corte, G., De Matteis, G., Landolfo, R., and Mazzolani, F. M. (2002). "Seismic analysis of MR steel frames based on refined hysteretic models of connections." Journal of Constructional Steel Research, 58(10), p 1331-1345.

De Matteis, G., Lanfoldo, R., and Calado, L. (2000). "Cyclic behavior of semi-rigid angle connections: A comperative study on tests and modeling." Behaviour of Steel Structures in Seismic Areas: STESSA 2000, A. A. Balkema, Rotterdam, p 165-174.

Deng, C. G., Bursi, O. S., and Zandonini, R. (2000). "A hysteretic connection element and its applications ." Computers & Structures, 78(1-3), 93-110.

DesRoches, R. and Delemont, M. (2002). "Seismic retrofit of simply supported bridges using shape memory alloys." Engineering Structures, 24(3), 325-332.

DesRoches, R., McCormick, J., and Delemont, M. (2004). "Cyclic properties of superelastic shape memory alloy wires and bars." Journal of Structural Engineering, 130(1), 38-46.

De Stefano, M., De Luca, A., and Astaneh-Asl, A. (1994). "Modeling of cyclic moment-rotation response of double-angle connections." Journal of Structural Engineering, 120(1), 212-229.

Duerig, T. W., Melton, K. N., Stoeckel D., and Wayman, C. M. (1990). Engineering aspects of shape memory alloys, Butterworth-Heinemann Ltd., London.

Ellingwood, B. R. (1998). "Reliability-Based Performance Concept for Building Construction." Structural Engineering World Wide 1998, Elsevier Science Ltd., Oxford, England, T178-4.

Ellingwood, B. R. (2000). "LRFD: implementing structural reliability in professional practice." Engineering Structures, 22(2), 106-115 .

Ellingwood, B. R. (2001). "Earthquake risk assessment of building structures." Reliability Engineering and System Safety, 74(3), 251-262 .

Elnashai, A. S. and Elghazouli, A. Y. (1994). "Seismic behaviour of semi-rigid steel frames." Journal of Constructional Steel Research, 29(1-3), 149-174.

Elnashai, A. S., Elghazouli, A. Y., and Denesh-Ashtiani, F. A. (1998). "Response of Semirigid Steel Frames to Cyclic and Earthquake Loads." Journal of Structural Engineering, 124(8), 857-867.

Faella, C., Piluso, V., and Rizzano, G. (2000). "Cyclic behaviour of bolted T-stubs: experimental analysis and modelling ." Behaviour of Steel Structures in Seismic Areas: STESSA 2000, A. A. Balkema, Rotterdam, pages 183-190.

Faella, C., Piluso, V., and Rizzano, G. (1997a). "Plastic deformation capacity of bolted T-stubs." Stessa '97: Second International Conference on the Behaviour of Steel Structures in Seismic Areas.

Faella, C., Piluso, V., and Rizzano, G. (1997b). "Prediction of bolted connection ductility." Stessa '97: Second International Conference on the Behaviour of Steel Structures in Seismic Areas.

FEMA (1995). "NEHRP guidelines for the seismic rehabilitation of buildings." Rep. No. FEMA 273, Washington, D. C.

FEMA (1997). "Interim guidelines : Evaluation, repair, modification and design of welded steel moment frame structures." Rep. No. FEMA 267, Washington, D. C.

FEMA (2000a). "Recommended seismic design criteria for new steel moment-frame buildings." Rep. No. FEMA 350, Washington, D. C.

FEMA (2000b). "Recommended Seismic Evaluation and Upgrade Criteria for Existing Welded Steel Moment-Frame Buildings." Rep. No. FEMA 351, Washington, D. C.

FEMA (2000c). "Recommended Specifications and Quality Assurance Guidelines for Steel Moment-Frame Construction for Seismic Applications." Rep. No. FEMA 353, Washington, D. C.

FEMA (2000d). "State of the art report on connection performance." Rep. No. FEMA 355D, Washington, D. C.

FEMA (2000e). "State of the Art Report on Performance Prediction and Evaluation of Steel Moment-Frame Buildings." Rep. No. FEMA 355F, Washington, D. C.

FEMA (2000f). "State of the Art Report on Systems Performance of Steel Moment Frames Subject to Earthquake Ground Shaking." Rep. No. FEMA 355C, Washington, D. C.

FEMA (2000g). "Prestandard and Commentary for the Seismic Rehabilitation of Buildings." Rep. No. FEMA 356, Washington, D. C.

Foutch, D. A. and Shi, S. (1997). "Connection element (type 10) for DRAIN-2DX." Internal Report, University of Illinois at Urbana-Champaign.

Foutch, D. A. and Yun, S.-Y. (2002). "Modeling of steel moment frames for seismic loads." Journal of Constructional Steel Research, 58(5-8), 529-564.

Frye, M. J. and Morris, G. A. (1975). "Analysis of flexibly connected braced steel frames." Canadian Journal of Civil Engineering, 2(3), 280-291.

Green, T. P., Leon, R. T., and Rassati, G. A. (2004). "Bidirectional tests on partially restrained, composite beam-to-column connections." Journal of Structural Engineering, 130(2), 320-327.

Gross, J. L. (1998). "A Connection model for the seismic analysis of welded steel moment frames." Engineering Structures, 20 (4-6), 390-397.

Gross, J. L., Engelhardt, M. D., Uang, C.-M., Kasai, K., and Iwankiw, N. R. (1999). "Modification of existing welded steel moment frame connections for seismic resistance." Rep. No. Design Guide 12, American Institute of Steel Construction, Chicago, IL.

Gupta, A. and Krawinkler, H. (1999). "Seismic demands for performance evaluation of steel moment resisting frame structures." Rep. No. BLUME-132, The John A. Blume Earthquake Engineering Center, Stanford, CA.

Gupta, A. and Krawinkler, H. (2000a). "Behavior of Ductile SMRFs at Various Seismic Hazard Levels." Journal of Structural Engineering, 126(1), 98-107.

Gupta, A. and Krawinkler, H. (2000b). "Dynamic P-Delta Effects for Flexible Inelastic Steel Structures." Journal of Structural Engineering, 126(1), 145-154.

Hamburger, R. O. (1998). "A Reliability Basis for Design Performance Objectives." Structural Engineering World Wide, Elsevier Science Ltd., Oxford, England, T166-1.

Harper, W. L. and Radziminski, J. B. (1990). "Comparison of the static and cyclic behavior of all-bolted and bolted/welded semi-rigid steel connections." Proceedings of the 4th US National Conference on Earthquake Engineering, EERI, Oakland, CA, p 595-604.

Huber, G. and Tschemmernegg, F. (1998). "Modelling of Beam-to-Column Joints." Journal of Constructional Steel Research, 45(2), 199-216.

ICBO (1994). "Uniform Building Code." International Conference of Building Officials (ICBO), Whittier, CA.

ICC (2003). "International Building Code." International Code Counsil, Falls Curch, VA.

Jalayer, F. (2003). "Direct Probabilistic Seismic Anaysis: Implementing Non-linear Dynamic Assessments." Stanford University.

Kasai, K., Maison B. F., and Mayangarum, A. (1999). "Effects of partially restrained connection stiffness and strength on frame seismic performance." Rep. No. SAC/ BD-99/17, SAC Joint Venture, Sacramento, CA.

Kattner, M. and Crisinel, M. (2000). "Finite element modelling of semi-rigid composite joints ." Computers and Structures , 78(1), 341-353 .

Kinali, K. and Ellingwood, B. R. (2007). "Seismic fragility assessment of steel frames for consequence-based engineering: A case study for Memphis, TN." Engineering Structures, 29(6), 1115-1127.

Kishi, N. and Chen, W. F. (1986). Rep. No. CE-STR-86-18, School of Civil Engineering, Purdue University.

Kishi, N. and Chen, W. F. (1987). "Moment-rotation relation of top-and seat-angle connections." Rep. No. CE-STR-87-4, School of Civil Engineering, Purdue University.

Kishi, N. and Chen, W. F. (1990). "Moment-rotation relations of semi-rigid connections with angles." Journal of Structural Engineering, 116(7), 1813-1834.

Kishi, N., Chen, W. F., Matsouka, K. G., and Nomachi, S. G. (1988). "Moment-rotation relation of top and seat angle with double web angle connections." Connections in Steel Structures: Behavior, Strength and Design, Elsevier Apllied Science Publishers, London, England, 121-134.

Krawinkler, H. (1978). "Shear in beam-column joints in seismic design of steel frames." Engineering Journal, 15(3), 82-91.

Krawinkler, H. and Gupta, A. (1998). "Story drift demands for steel moment frame structures in different seismic regions." Proceedings, Sixth U.S. National Conference on Earthquake Engineering , Earthquake Engineering Research Institute, Oakland, CA.

Krawinkler, H. and Seneviratna, G. D. P. K. (1998). "Pros and cons of a pushover analysis of seismic performance evaluation." Engineering Structures, 20(4-6), 452-464.

Kukreti, A. R. and Abolmaali, A. S. (1999). "Moment-rotation hysteresis behavior of top and seat angle steel frame connections." Journal of Structural Engineering, 125 (8), 810-820.

Lafortune, P., McCormick, J., DesRoches, R., and Terriault, P. (2007). "Testing of Superelastic Recentering Pre-Strained Braces for Seismic Resistant Design." Journal of Earthquake Engineering, 11(3), 383-399.

Leon, R. T. (1997). "Seismic performance of bolted and riveted connections." Rep. No. FEMA 288 (Sac Rep. No. 95-09), SAC Joint Venture, Sacramento, CA.

Leon, R. T. (1998). "Analysis and design problems for PR composite frames subjected to seismic loads." Engineering Structures, 20(4-6), 364-371.

Leon, R. T., Forcier, G. P., Roeder, C. W., and Preece, R. F. (1994). "Cyclic performance of riveted connections." Proceedings of the Structures Congrees '94, ASCE, New York, NY, p 1490-1495.

Leon, R. T., Hoffman, J. J., and Stager, T. (1996). "Partially Restrained Composite Connections." Rep. No. Steel Design Guide Series 8, American Institute of Steel Construction, Chicago, IL.

Leon R. T. and Shin K. J. (1995). "Performance of semi-rigid frames." Restructuring--America and beyond : Proceedings of Structures Congress XIII, American Society of Civil Engineers, New York, p 1020-1035.

Leon, R. T. and Swanson, J. A. (2000). "Cyclic modeling of T-stub bolted connections." Behaviour of Steel Structures in Seismic Areas: STESSA 2000, A. A. Balkema, Rotterdam, p 703-710.

Luco, N. (2002). "Probabilistic Seismic Demand Analysis, SMRF Connection Fractures, and Near-Source Effects." Stanford University.

Luco, N. and Cornell, C. A. (1998). "Effects of random connection fractures on the demands and reliability for a 3-story pre-Northridge SMRF structure ." Sixth U.S. National Conference on Earthquake Engineering , Earthquake Engineering Research Institute, Oakland, CA, Paper no: 244.

Luco, N. and Cornell, C. A. (2000). "Effects of connection fractures on SMRF seismic drift demands." Journal of Structural Engineering, 126(1), 127-136.

Madas, P. J. and Elnashai, A. S. (1992). "A component-based model for beam-column connections." Earthquake Engineering, Tenth World Conference.

Maison, B. F. (1992). PC-ANSR: A computer program for nonlinear structural analysis. National Information Service for Earthquake Engineering-NISEE/Computer Applications, University of California, Berkeley.

Maison, B. F. and Bonowitz, D. (1999). "How safe are pre-Northridge WSMFs? A case study of the SAC Los Angeles nine-story building." Earthquake Spectra, 15(4), 765-789.

Maison, B. F. and Kasai, K. (2000). "Seismic performance of 3 and 9 story partially restrained moment frame buildings." Rep. No. SAC/BD-99/16, SAC Joint Venture, Sacramento, CA.

Maison, B. F., Kasai, K., Dexter, R., Ingraffea, A. R., and Deierlein, G. G. (1996). "Selected Results from the SAC Phase I Beam-Column Connection Pre-Test Analyses." Rep. No. SAC/BD-96/01, SAC Joint Venture, Sacramento, CA.

Maison, B. F., Rex, C. O., Lindsey, S. D., and Kasai , K. (2000). "Performance of PR Moment Frame Buildings in UBC Seismic Zones 3 and 4." Journal of Structural Engineering, 126(1), 108-116.

Mander, J. B., Chen, S. S., and Pekcan, G. (1994). "Low-cycle fatigue behavior of semi-rigid top-and-seat angle connections." Engineering Journal, 31(3), 111-122.

MANSIDE (1998). "Memory Alloys for New Structural Vibrations Isolating Devices." MANSIDE Third Twelve Monthly Process Report.

Mayangarum, A. (1996). "Design, analysis, and application of bolted semi-rigid connections for moment resisting frames." MS Thesis. Lehigh University.

Mazzoni, S., McKenna, F. T., Scott, M. H. and Fenves, G. L. (2007). “Open System for Earthquake Engineering Simulation User Manual”. <http://peer.berkeley.edu/~silvia/OpenSees/manual/html/>

McCormick, J. (2006). "Cyclic Behavior of Shape Memory Alloys: Material Characterization and Optimization." Georgia Institute of Technology.

McCormick, J., Barbero, L., and Desroches, R. (2005). "Effect of mechanical training on the properties of superelastic shape memory alloys for seismic applications." Smart Structures and Materials 2005 - Smart Structures and Integrated Systems, International Society for Optical Engineering, Bellingham, WA, p 430-439.

McKenna, F. T. (1997). “Object-oriented finite element programming: Frameworks for analysis, algorithms and parallel computing”. Ph.D. thesis, University of California, Berkeley.

Medina, R. A. and Krawinkler, H. (2005). "Evaluation of Drift Demands for the Seismic Performance Assessment of Frames." Journal of Structural Engineering, 131(7), 1003-1013.

Moncarz, D. and Gerstle, H. (1981). "Steel frames with nonlinear connections." ASCE Journal Structural Divison, 107(8), 1427-1441.

Nader, M. N. and Astaneh-Asl, A. (1991). "Dynamic behavior of flexible, semirigid and rigid steel frames." Journal of Constructional Steel Research, 18(3), 179-192.

Nader, M. N. and Astaneh-Asl, A. (1996). "Shaking Table Tests of Rigid, Semirigid, and Flexible Steel Frames." Journal of Structural Engineering, 122(6), 579-719.

Naeim, F., Skliros, K., Reinhorn, A. M., and Sivaselvan. M. V. (2000). "Effects of Hysteretic Deterioration Characteristics on Seismic Response of Moment Resisting Steel Structures." Rep. No. SAC/BD-99/18, SAC Joint Venture, Sacramento, CA.

Nemati, N., Le Houedec, D., and Zandonini, R. (2000). "Numerical modelling of the cyclic behaviour of the basic components of steel end plate connections." Advances in Engineering Software, 31(11), 837-849.

Neuenhofer, A. and Filippou, F. C. (1997). "Evaluation of nonlinear frame finite-element models." Journal of Structural Engineering, 123(7), 958-966.

Ocel, J. M. (2002). "Cyclic Behavior of Steel Beam-Column Connections with Shape Memory Alloy Connecting Elements." Georgia Institute of Technology.

Ocel, J., DesRoches, R., Leon, R. T., Hess, W. G., Krumme, R., Hayes, J. R., and Sweeney, S. (2004). "Steel beam-column connections using shape memory alloys." Journal of Structural Engineering, 130(5), 732-740.

Prakash, V., Powell, G. H., and Campbell, S. D. (1993). "DRAIN-2DX base program description and user guide: version 1.10." Rep. No. UCB/SEMM-1993/17 , Dept. of Civil Engineering, University of California, Berkeley.

Rassati, G. A., Noe, S., and Leon, R. T. (2000). "PR Composite Joints Under Cyclic and Dynamic Loading Conditions - A Component Modeling Approach." International Workshop on Connections in Steel Structures IV.

Rassati, G. A., Leon, R. T., and Noe, S. (2004a). "Component modeling of PR composite frames under cyclic and dynamic loading: Numerical analyses." International Journal of Steel Structures, 4(3), 131-140.

Rassati, G. A., Leon, R. T., and Noe, S. (2004b). "Component modeling of partially restrained composite joints under cyclic and dynamic loading." Journal of Structural Engineering, 130(2), 343-351.

Richard, R. M. and Abbot, B. J. (1975). "Versatile elastic-plastic stress-strain formula." Journal of Engineering Mechanics, 101, 511-515.

Richard, R. M. and Abbot, B. J. (1975). "Versatile elastic-plastic stress-strain formula." Journal of Engineering Mechanics, 101, 511-515.

Sakurai, S., Ellingwood, B. R., and Kushiyama, S. (2001). "Probabilistic study of the behavior of steel frames with partially restrained connections." Engineering Structures, 23(11), 1410-1417.

Salazar, A. R. and Haldar, A. (2001). "Energy dissipation at PR frames under seismic loading." Journal of Structural Engineering, 127(5), 588-593.

Serneels, A. (1999). "Shape memory alloy characterisation and optimisation." Proceedings of the First European Conference on Shape Memory and Superelastic Technologies: SMST-99, SMST Europe, Lubbeek, Belgium, p 6-23.

Shen, J. and Astaneh-Asl, A. (1999). "Hysteretic behavior of bolted-angle connections." Journal of Constructional Steel Research, 51(3), 201-218.

Shen, J. and Astaneh-Asl, A. (2000). "Hysteresis model of bolted-angle connections." Journal of Constructional Steel Research, 54(3), 317-343.

Shin, K. J. (1992). "Seismic response of semi-rigid composite frames ." Structures Congress '92, American Society of Civil Engineers, p 645-648.

Shome, N., Cornell, C. A., Bazzurro, P., and Carballo, J. E. (1998). "Earthquakes, records, and nonlinear responses." Earthquake Spectra, 14(3), 469-500.

Shome, N. (1999). "Probabilistic Seismic Demand Analysis of Nonlinear Structures." Ph.D. Dissertation, Stanford Universtity.

Somerville, P. G. (1997). "Development of Ground Motion Time Histories for Phase 2 of the FEMA/SAC Steel Project." Rep. No. SAC/BD-97/04, SAC Joint Venture, Sacramento, CA.

Song, J. and Ellingwood, B. R. (1999a). "Seismic reliability of special moment steel frames with welded connections: I." Journal of Structural Engineering, 125(4), 357-371.

Song, J. and Ellingwood, B. R. (1999b). "Seismic reliability of special moment steel frames with welded connections: II." Journal of Structural Engineering, 125(4), 372-384.

Song, J. and Ellingwood, B. R. (1999c). "Probabilistic modeling of steel moment frames with welded connections." Engineering Journal, 36(3), 121-128.

Song, J. and Ellingwood, B. R. (2001). "Risk evaluation of steel frames with welded connections under earthquake." Structural Engineering and Mechanics, 11(6), 663-672.

Swanson, J. A. and Leon, R. T. (2000). "Bolted steel connections: Tests on T-stub components." Journal of Structural Engineering, 126(1), 50-56.

Swanson, J. A. and Leon, R. T. (2001). "Stiffness Modeling of Bolted T-Stub Connection Components." Journal of Structural Engineering, 127(5), 498-505.

Tschemmernegg, F. and Humer, C. (1988). "The Design of structural steel frames under consideration of the nonlinear behaviour of joints." Journal of Constructional Steel Research, 11(2), 73-103.

Tschemmernegg, F. and Querioz, G. (1996). "Mechanical modeling of semi-rigid joints for the analysis of framed steel and composite structures." 3rd International Workshop on Connections in Steel Structures, Elsevier Science.

Vamvatsikos, D. and Cornell, C. A. (2002). "Incremental dynamic analysis." Earthquake Engineering & Structural Dynamics, 31(2), 491-514.

Vamvatsikos, D. and Cornell, C. A. (2004). "Applied incremental dynamic analysis." Earthquake Spectra, 20(2), 523-553.

Veletsos, A. S., Newmark, N. M. (1960). "Effect of Inelastic Behavior on the Response of Simple Systems to Earthquake Motions." Proceedings of the 2nd World Conference on Earthquake Engineering, Japan, p 895-912..

Wales, M. W. and Rossow, E. C. (1983). "Coupled Moment-Axial Force Behavior in Bolted Joints." Journal of Structural Engineering, 109(5), 1250-1266.

Wang, C.-H. and Wen, Y.-K. (2000a). "Evaluation of Pre-Northridge Low-Rise Steel Buildings. I: Modeling." Journal of Structural Engineering, 126(10), 1160-1168.

Wang, C. H. W. Y. K. (2000b). "Evaluation of Pre-Northridge Low-Rise Steel Buildings. II: Reliability." Journal of Structural Engineering, 126(10), 1169-1176.

Welch, B., Jones, K., and Hobbs, J. (2003). Practical Programming in Tcl and Tk, Prentice Hall.

Wen, Y. K., Ellingwood, B. R., Veneziano, D., and Bracci, J. (2003). "Uncertainty Modeling in Earthquake Engineering." Rep. No. MAE Center Project FD-2 Report.

White, D. W. and Chen, W. (1996). "Generalized models for semi-rigid connections." 3rd International Workshop on Connections in Steel Structures, Elsevier Science.

Williams, M. S. and Sexsmith, R. G. (1995). "Seismic Damage Indices for Concrete Structures: A State-of-the-Art Review." Earthquake Spectra, 11(2), 319-349.

Yang, T.-S. and Popov, E. P. (1995). Rep. No. UCB/EERC-95/08, Earthquake Engineering Research Center, University of California, Berkeley.

Youssef, N. F. G., Bonowitz, D., and Gross, J. L. (1995). "Survey of Steel Moment-Resisting Frame Buildings Affected by the 1994 Northridge Earthquake." Rep. No. NISTIR 5625, National Institute of Standards and Technology.

Yun, S. Y., Hamburger, R. O., Cornell, C. A., and Foutch, D. A. (2002). "Seismic Performance Evaluation for Steel Moment Frames." Journal of Structural Engineering, 128(4), 534-545.

Zahrah, T. F. and Hall, W. J. (1982). "Seismic energy absorption in simple structures." SRS No.501, University of Illinois at Urbana-Champaign.